APPLICATIONS OF FTIR MICROSPECTROSCOPY TO DISSECT THE CHANGES IN MOLECULAR COMPOSITION OF AGING *Caenorhabditis elegans* OOCYTES.

A Thesis Submitted to the
College of Graduate and Postdoctoral Studies
in Partial Fulfillment of the Requirements
for the degree of Master of Science
in the Department of Biology
University of Saskatchewan
Saskatoon

By

V. Irina Ramanandraitsiory

Permission to Use

In presenting this thesis in partial fulfilment of the requirements for a Postgraduate degree from the University of Saskatchewan, I agree that the Libraries of this University may make it freely available for inspection. I further agree that permission for copying of this thesis in any manner, in whole or in part, for scholarly purposes may be granted by the professor or professors who supervised my thesis work or, in their absence, by the Head of the Department or the Dean of the College in which my thesis work was done. It is understood that any copying or publication or use of this thesis or parts thereof for financial gain shall not be allowed without my written permission. It is also understood that due recognition shall be given to me and to the University of Saskatchewan in any scholarly use which may be made of any material in my thesis.

Requests for permission to copy or to make other use of material in this thesis in whole or part should be addressed to:

Head of the Department of Biology
112 Science Place
W.P. Thompson Building
University of Saskatchewan
Saskatoon, Saskatchewan, S7N 5E5
Canada

OR

Dean
College of Graduate and Postdoctoral Studies
University of Saskatchewan
116 Thorvaldson Building, 110 Science Place
Saskatoon, SK S7N 5C9
Canada

Abstract

The decline in reproductive capacity is one of the first signs of aging and represents a considerable health problem in modern societies such as Canada with an increasing maternal age. To prepare for challenges brought up by older maternity, there is a need to understand the biology of reproductive aging at the molecular level. For instance, what are the biochemical signatures associated with aging oocytes that precede and predict the incipient loss in fertilizing ability in these cells? The simple nematode *C. elegans* has a short reproductive span during which it displays a corresponding drop in oocyte quality overtime thus providing a tractable and relevant model to study germ cell aging. Here, FTIR (Fourier Transform Infrared) microspectroscopy was systematically applied as an imaging platform to address in vivo changes in the macromolecular composition of *C. elegans* oocytes transitioning from reproductive to post-reproductive stages. Using this pioneering experimental approach optimized to image *C. elegans* cells, a marked increase in lipid and protein signatures consistent with an altered mobilization of yolk (lipoprotein) was detected in old wild-type oocytes. These results were corroborated using standard fluorescent and transgenic techniques demonstrating a spike in lipoprotein storage in aged oocytes. Finally, a *bona fide* mutant defective in yolk import served as a proof of method to validate the usefulness and reliability of FTIR microspectroscopy as a mapping tool to quickly and reproducibly draw the biochemical landscape of aging oocytes. Overall, this exploratory study supports a role of lipotoxicity in driving oocyte aging and provides an integrated experimental approach for further studies aimed at dissecting the molecular underpinnings behind reproductive decline in germ cells.

Acknowledgements

I would like to express my deepest gratitude to my first supervisor Dr. Carlos Carvalho, for having given me the opportunity to work on this thesis. I am very grateful to him for all his help and advice throughout my research. This thesis would not have been possible without his valuable advice and constant encouragement.

I gratefully acknowledge the financial support from Canadian Light Source (CLS) in the form of a student fellowship throughout my study. I am thankful to my second supervisor Dr. Thomas Ellis for not only to arrange this financial support but also for his guidance during the course of this thesis work.

I would also like to thank Dr. Bogdan Popescu, Dr. Chris Todd, Dr. Ken Wilson and Dr. Saroj Kumar for serving on my thesis committee. My special gratitude goes to Dr. Saroj Kumar for his advice and feedback whenever I approached him in person or by email.

I wish to extend my appreciation to Dr. Ferenc Bodonrics, Dr. Xia Liu, Dr. Mark Hackett, Dr. Tim May, Dr. Scott Rosendall and Dr. Stuart Read for their help with FTIR data collection and analysis.

I am greatly indebted to my colleagues at Canadian Light Source (especially Dr. Vijayan Perumal, Dr. Lahlali Rachid, Dr. Appathurai, Mr. Willard, Mr. Ahmed, and Samira) and at Biology department for their moral support and guidance, which helped me to complete my thesis. They were always available even during the weekend when I was looking for help and advice.

Finally, I would like to thank my parents, my sister and my Malagasy friends for their understanding, love and encouragement.

Dedication

I lovingly dedicated this thesis to my beloved parents. Without their support, patience, and love; I would not have made it.

Don't lose hope. Everything happens for a reason. You never know what tomorrow may bring. -Unknown-

Contents

List of Tables

List of Figures

List of Abbreviations

apoB-100	Apolipoprotein B-100
ATP	Adenosine triphosphatase
ATR	Attenuated total reflectance
AD	Alzheimer's disease
BaF_2	Barium Fluoride
C. elegans	*Caenorhabitis elegans*
CGC	Caenorhabitis genetics center
C	Carbon
CO	Carbon Monoxide
CARS	Coherent Anti-Stokes Raman Scattering
CaF_2	Calcium Fluoride
CLS	Canadian Light Source
CH_2	methylene
CH_3	methyl
cm^{-1}	Unit of wavenumber
DNA	Deoxyribonucleic acid, a molecule that encodes genetic information
D_2O	Deuterium Oxide
DR	Dietary restriction
Daf	Abnormal dauer formation
DIC	Differential Interference Contrast
DTC	Distal Tip Cell
DMSO	Dimethyl Sulfoxide
E. Coli	*Escherichia Coli*
EMS	Ethyl methanesulphonate
ER	Endoplasmic Reticulum
FFA	Free Fatty Acids
FPA	Focal plane array
FTIR	Fourier Transform Infrared
FOXO	Forkhead box protein O
GFP	Green fluorescent protein
H	Hydrogen
H_2O	Water
IR	Infrared
IGF-1	Insulin-like growth factor-1
IIS	Insulin/IGF-1 signaling
JH	Juvenile hormone
LDL	Low density lipoprotein
LN	Liquid Nitrogen
LRO	Lysosome-related organelles
MCT	Mercury Cadmuim Tellurium

mRNA	Messenger RNA
MIR	Mid Infrared
MSP	Major Sperm Protein
NGM	Nematode growth media
O	Oxygen
PI3K	Phosphoinositide 3-Kinase
PO_2^-	Phosphate
PUFAs	Polyunsaturated fatty acids
RNA	Ribonucleic Acid
RME	Receptor Mediated Endocytosis
RNAi	RNA interference
ROS	Reactive Oxygen Species
SE	Standard error of the mean
TGF-β	Transforming growth factor beta
UV	Ultraviolet
UPR	Unfolded protein response
YP	Yolk Platelets
β-sheet	Beta sheet
α-helix	Alpha-helix
ν	Stretching vibrations
ν_{asym}	Antisymmetric stretch
ν_{sym}	Symmetric stretch
ϵ	Molar Absorption Coefficient

Chapter 1
INTRODUCTION

1.1 Relevance and Rationale

Increasing numbers of young couples tend to postpone having children until later in life (Van Luijn, 1996). In Canada, the mean age at which women deliver their first child has risen from 23.8 years in the mid-1960s to 28.5 years in 2011 (Milan, 2013). At present, there is a growing trend for women to have their first child after the age of 30. The overall decrease in birth rates in many developed countries can be explained not primarily as a biological phenomenon, but rather as a personal/family decision. The increase in the proportion of older women considering motherhood is a reflection of several societal factors, including difficulty in combining further education or a profession with having children, the perception of a loss in personal freedom associated with becoming a mother and an unrealistic belief in recent advances in assisted reproduction technologies for ensuring conception (Balasch, 2010, Balen et al., 1995). An unintended consequence of this decision is that older women who choose to postpone the first birth are often faced with difficulties in conceiving due to decreased fecundity at that age. In fact, most women trying to have a child at around 35 years of age do not succeed because of low fertility (Balasch, 2010). As women reach the third decade of life, the number of follicles in the ovary, a measure of fertilizability, declines bi-exponentially rather than exponentially as in earlier ages (Faddy et al., 1992). When conception does happen in this late reproductive period, the rate of Down syndrome and trisomic miscariages are increased (Erickson, 1978; Hassold & Chiu, 1985). Alberman (1975) showed that the risk of abortions with chromosome abnormalities was significantly higher in women aged $\geq$ 30 years. Lazer et al., (1979) showed that the mean age of women who had a trisomic spontaneous abortion was 33.5 years from a study

of 1469 abortions. In general, the reported rate of chromosome abnormalities as a function of maternal age is very similar throughout the literature (summarized by Hassold & Chiu, 1985). Overall, trisomies account for less than 15% of abortions involving women 25 years or younger, but for about 33% in women aged 30 - 35 years and for more than 65% in women age 40 and over. In addition, data derived from the National Survey of Family Growth in 1995 showed that the proportion of American women who tried but did not succeed in conceiving their first child within 1 year, increases from 6% in the 15 - 24 years age group to over 30% in the 35 - 44 years age group (Abma, et al., 1997). Despite the important health and societal implications, it remains poorly understood why female fertility drops considerably as early as 10 years before the commencement of menopause. Traditionally, menopause has been regarded as the physiological age at which the stock of oocytes is exhausted, and sterility ensues (Velde & Pearson, 2002). In the 19th century, the mean age at last birth among Canadian women was 40.6 years while the onset of menopause occurred in average at 51 years of age (Velde et al., 2002). In the last decade before menopause sets in (between 40 and 50 years old), women still have sufficient follicles left to sustain normal follicle development and menstruation. However, the increased frequency of meiotic errors (chromosome abnormalities) in the remaining oocytes ultimately leads to a sharp decrease in successful pregnancies and an increase in pregnancy losses. This dramatic decline in female reproductive capacity, which starts after the mid-30s, poses important health challenges in the world today, as more women choose to have children later in life. Thus, to understand and prepare for the dramatic changes in the demographics of motherhood and its economic consequences in the future, we need to unravel the biology of reproductive aging.

From a physiological standpoint, the loss of fertilizability of gametes as a function of time is a hallmark of reproductive aging. Reproductive aging precedes the onset of classic signs of somatic aging in mammals and impacts fertility at a time when oocytes are still plentiful, but with compromised "quality". The maintenance of oocyte quality has been associated with several molecular factors regulating germ cell development, meiotic progression, oocyte maturation, fertilization and chromosome segregation (Luo, et al., 2010). During oogenesis, oocytes synthesize and accumulate significant quantities of

mRNA, lipids, proteins and carbohydrates which are required for the growth and maturation of oocytes as well as the embryonic development after fertilization (Hutt & Albertini, 2007; Marteil, et al., 2009; Reddy et al., 2008). Insufficient energy stores in oocytes may pose a particular risk to cellular functions that are highly demanding energetically such as spindle formation and chromosomal segregation, impacting the launch of the embryonic development program (Dumont & Desai, 2012).

Despite this direct correlation between oocyte quality and age, we still have only a cursory idea of the molecular factors that underlie reproductive aging. For instance, what are the molecular changes in cellular composition that accompany or launch these events and how are they triggered? Are there chemical markers that can be used to track and predict "how viable"an oocyte is at any given age? Addressing questions such as these *in vivo* requires the use of a tractable model organism with an abundant stock of oocytes suitable for cytological work, a comparable age-dependent loss of oocyte quality as humans, and a short lifespan. I outlined below a few reasons why the nematode *C. elegans* is an ideal choice for such studies.

1.2 *Caenorhabditis elegans*

1.2.1 *C. elegans* as an experimental model organism

Caenorhabditis elegans is a small, free living nematode (Figure 1.1). In the wild, these microscopic worms commonly feed on bacteria and microbes growing in decomposing material and rotting fruit. In the lab, the slow growing *E. coli* strain OP50 is typically used as food source for *C. elegans*. In 1948, *C. elegans* was first proposed as a multi-cellular organism with potential value in research (Dougherty & Calhoun, 1948). *C. elegans*'s recent history as a widely used model organism in genetics research started with its introduction by the molecular biologist Sydney Brenner who proposed its adoption to advance neurobiology studies in the mid 70's (Brenner, 1974).

C. elegans offers many intrinsic experimental advantages that make it a particularly attractive laboratory model system such as the low cost for culturing, easy observation and

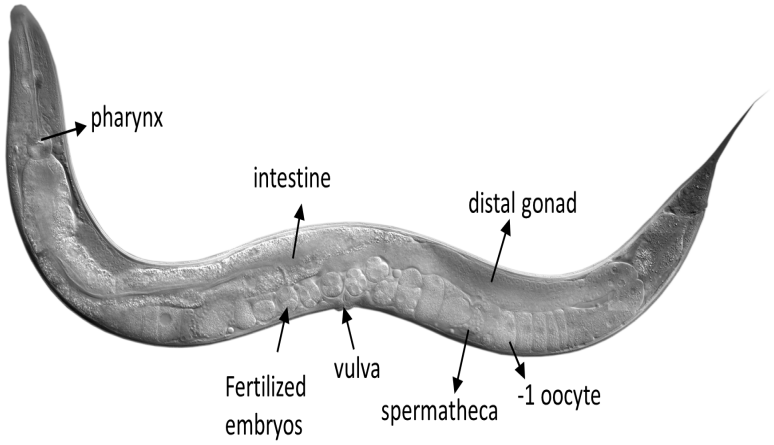

(a)

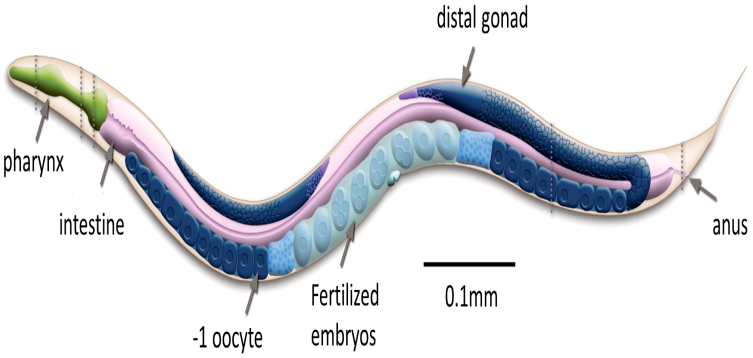

(b)

Figure 1.1: Differential Interference Contrast (DIC) (a) and (b) diagram of an adult *C. elegans* hermaphrodite. Adapted from worm Atlas.

manipulation. In addition, the hermaphroditic mode of reproduction, sporadic presence of males, rapid turn over from egg to reproductive mature adult (3 days) and high progeny numbers (∼300) significantly facilitate crosses. Owing to its small size (1 to 1.5 mm in length), large isogenic populations can be quickly grown on petri plates containing agar seeded with OP50. *C. elegans* is also transparent in all developmental stages making it ideal for *in vivo* tracking of fluorescently tagged proteins and the examination of age-related changes in live animals. Importantly, its short lifespan of approximately 2 to 3 weeks in wild-type animals (Gems & Riddle, 1996) allows for several experiments to be run in a relatively short timespan, increasing data significance while reducing sample errors. In addition, previous works have described an array of age-related phenotypes in worms. Finally, the availability of a substantial number of differently long and short-lived mutants and the conservation of aging pathways with vertebrates are also major advantages of using *C. elegans* as a relevant study object in aging research (Kenyon, 2010; Tissenbaum, 2015).

Typical of nematodes, *C. elegans* have a cylindrical body shape made up of an outer tube with a fluid filled body cavity, referred as the pseudocoelom, surrounded by an inner tube. The outer tube is made up of the cuticle, hypodermis, excretory system, neurons, and muscles. The inner tube is composed by the gonad and the alimentary canal made up of the pharynx and intestine. The pharynx is a muscle organ located in the anterior part in the head region that continuously pumps food into the animals. The pharynx connects to the intestine, which ends in the posterior part in the anus where defecation occurs. The reproductive system, consisting of germ cells and a somatic gonad, together with specialized tail structures and specific wiring of the nervous system constitute the main differences in the body plan of hermaphrodites and males.

C. elegans has two morphologically distinct sexes, XX hermaphrodites and XO males. Hermaphrodites are somatically females whose germ cells transitionally develop as sperm (stored in the spermatheca) during a short larval developmental window before switching to oogenesis for the rest of the adult life (Hubbard & Greenstein, 2000). Self fertilization using stored sperm and freshly produced oocytes is therefore the main mode of reproduction in these worms. Because sperm production is temporally restricted to a defined period in the L4 larval stage, the limited number of self-made sperm cells

pre-determines the reproductive lifespan of the animal. Contrary to humans, therefore, the limiting gamete in *C. elegans* fertilization is the sperm. Once self-sperm is exhausted, fertilization ends, and worms enter post-reproductive life unless they are mated with males and sperm repository reconstituted (Herman, 2005). Males, in contrast, produce only sperm throughout their lives, but never oocytes, and cannot self-fertilize. Males appear by the occasional non-disjunction of the X in the gametes and therefore their general frequency is significantly low in the population (around 0.2%) (Hodgkin et al., 1979). Upon mating, however, male sperm is used preferentially by hermaphrodites over self-sperm and progenies will consequently segregate 50% males to a 1:1 sex ratio (Ward & Carrel, 1979).

1.2.2 Development of the reproductive system in *C. elegans*

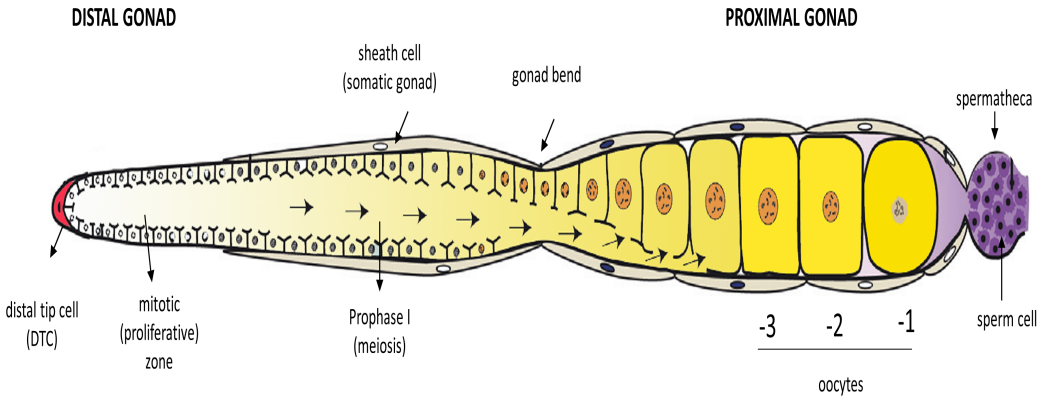

Figure 1.2: Schematic representation of a *C. elegans* hermaphrodite gonad stretched out. Oogenesis proceeds from left to right (distal to proximal). The gonad is a syncytium where macromolecules, RNAs and metabolites required for oocyte production are progressively stored in the developing oocytes (yellow gradient). As oocytes pass the bend, cellularization begins. The most mature (-1) oocyte arrests proximally next to the spermatheca. Sperm signals induce oocyte maturation and ovulation when these cells move through the spermatheca, are fertilized by sperm, and enter into the uterus to start embryonic development. Adapted from Huelgas-Morales and Greenstein (2018)

C. elegans presents considerable advantages relevant to reproductive aging research due to two main characteristics: its transparency which allows for real time

visualization of gametogenesis in live animals and, perhaps more crucially, the spatio-temporal layout of its reproductive system (Figure 1.2) (Hubbard & Greenstein, 2000; Kimble & Crittenden, 2007). In hermaphrodites, the germ line resides within two symmetrical U-shaped arms of the syncytial gonads, connected dorsally by a central uterus. Each arm contains approximately 1000 germ cell nuclei in different stages of differentiation and organized in a distal-proximal axis with immature cells housed in the distal end and fully matured gametes in the proximal end, adjacent to the uterus. To replenish germ cells, a stem cell population located in the distal end proliferates under the influence of the somatic Distal Tip Cell (DTC). The DTC signals germ cells in a gradient-dependent manner such that germ cells in proximity either continue to divide mitotically or, if distant enough, irreversibly enter the meiotic program in a domain specific manner inside the gonad (Kimble & Crittenden, 2007). As germ cells move farther down the syncytium, they enter prophase I of meiosis in the transition zone, a process regulated by levels of Notch signalling between the DTC and the germ cells. Midway through the gonad, germ cells undergo DNA recombination during pachytene and chromosome resolution and condensation in diplotene (Dernburg et al., 1998; Francis et al., 1995). Already at the end of pachytene stage, many germ cells begin to increase in size (Church et al., 1995), though more than half of the developing oocytes are at this stage eliminated by apoptosis (Gumienny et al., 1999; Jaramillo-Lambert et al., 2007). The surviving germ cells move into the proximal gonad where cellularization initiates. Finally, during diakinesis, large and compartmentalized oocytes are arrested in meiosis I until a signal from the sperm (MSP: Major Sperm Protein) in the adjacent spermatheca activates mature oocytes, triggering meiotic maturation (Miller et al., 2001). After maturation, oocytes are ovulated and fertilized as they squeeze through the spermatheca where sperm is stored. Before a hermaphrodite gonad switches to oocyte production in late L4 stage, it produces approximately 300 sperm cells (Hirsh et al., 1976; L'Hernault, 2006) which accumulate at the end of the proximal gonad arm until the first ovulation pushes them into the spermatheca (Ward & Carrel, 1979). Upon sperm entry, fertilized oocytes quickly complete meiosis, acquire an eggshell and begin embryogenesis. In the uterus, early embryos develop until around the 16-cell stage before being laid through the vulva (Figure 1.2).

The asymmetric disposition of cells at various meiotic stages inside the gonad is a critical advantage of *C. elegans* over other model organisms in studying germ cell senescence, as it allows for a relative temporal assessment of younger versus older oocytes originated from the same stem cell population (same gonad) or from different age matched animals. Germ cell differentiation occurs continuously throughout the life of the worm such that fresh oocytes are produced both in young as well as in old animals, hence from differently 'aged' stem cell precursors. Consequently, the effect of aging in the proliferative germ cell population as well as in the already differentiated oocytes can be dissected apart by comparing oocytes from the same gonad as well as oocytes matured in gonads from animals of different ages.

1.2.3 *C. elegans* and advances in aging research

Aging is not an adaptive trait nor is it dispensable to the survival of the individual, implying that aging is not programmed in the sense that development is. This led to the assumption that aging is not regulated by genetically controlled mechanisms and instead represents a series of stochastic events triggered by a progressive loss of homeostasis. It was not until the last few decades that the genetics of aging was properly studied with the isolation and cloning of genes whose mutations interfere with a normal lifespan. Michael Klass in 1983 first reported eight *C. elegans* mutants with extended lifespan by conducting a genetic screen using ethyl methanesulphonate (EMS) (Klass, 1983). Because several of these mutants also presented a feeding defect (decreased pharyngeal pumping) it was proposed that longevity was increased due to dietary restriction, a paradigm that prompted a whole field of research that connecting the genetic control of caloric intake and its influence on lifespan. Later studies showed that the feeding defect could be separated from the longevity (Age) phenotype (Johnson, 1986). One of these mutations mapped to a single genetic locus termed *age-1*. Mutations in *age-1* lead to 40% to 65% increases in lifespan. Subsequent cloning of *age-1* revealed it to be the *C. elegans* ortholog of the phosphoinositide 3-kinase (PI3K) catalytic subunit that mediates insulin signalling (IIS) in many systems. The involvement of IIS in lifespan regulation was further strengthen by the discovery that mutations in *daf-2*, the sole insulin receptor in *C. elegans*, also led to a

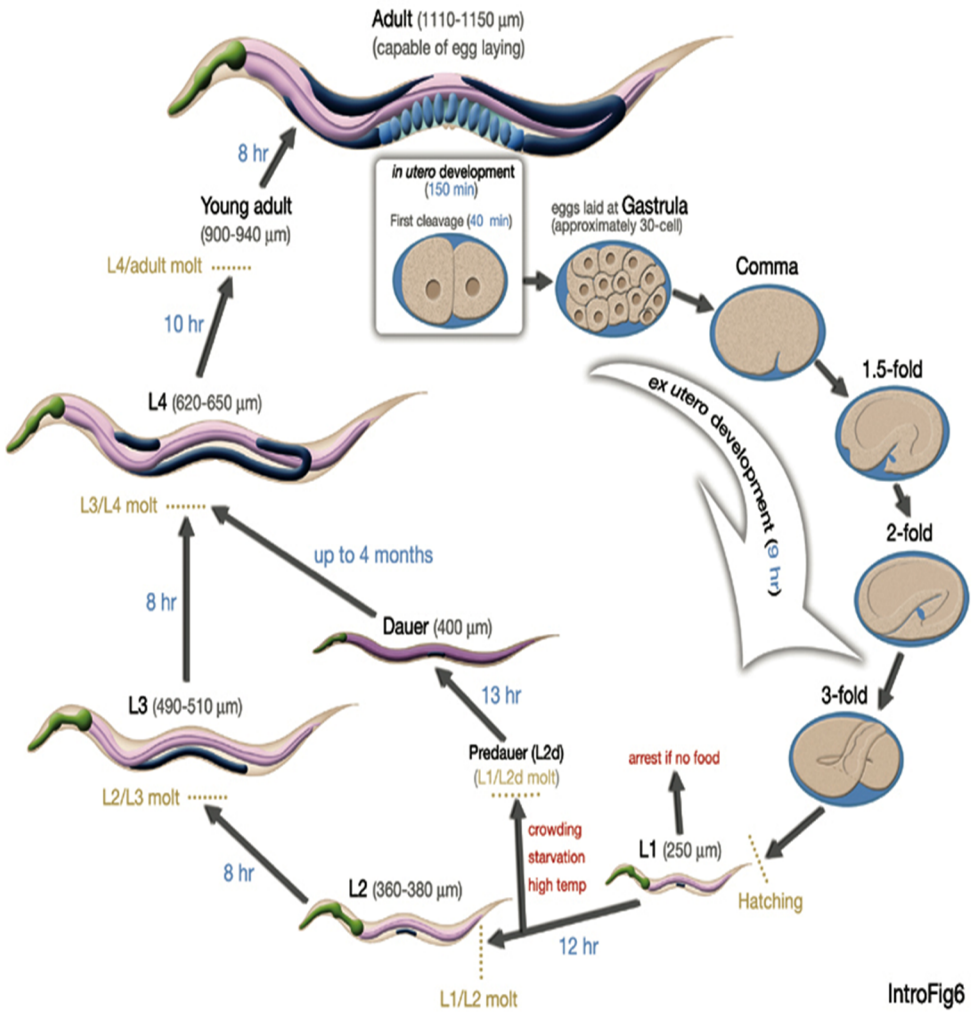

Figure 1.3: Life cycle of *C. elegans* grown at 20^{o}C on agar plates seeded with *E. coli*.

dramatic increase in lifespan (Kenyon et al., 1993). As with Age mutants, *Daf* mutants show other non-lifespan phenotypes. Daf stands for abnormal Dauer Formation in reference to defects that interfere with proper development of a life-stress form called *dauer*. Under favourable growth conditions, *C. elegans* proceeds through four larval stages (L1 to L4), each stage separated by a molt. After the fourth molt, worms reach adulthood and reproductive maturity within 3 days of L1 hatching (Figure 1.3). Worms typically live another two to three weeks but reproduce for only about 5 days after entering adulthood. In starved or high temperature conditions, however, larval development arrests in the L2 molt and animals take an alternative stress-resistant developmental mode called *dauer* that delays reproductive maturity. The dauer larvae has several morphological, metabolic and behavioural adaptations that allows it to survive up to 4 months without food and thus represents a natural long-lived form of the animal. Dauer worms are thin, with an altered cuticle that seals mouth and anus to preserve water content. When conditions improve, and food is again available, dauers will re-enter larval development, begin to feed and then molt to form an adult with a normal reproductive cycle and lifespan. The ability to take a dauer fate is limited by the developmental stage of the animals. Larvae that have progressed past the L2 molt cannot enter the dauer developmental program and die when environmental conditions deteriorate (Klass & Hirsh, 1976).

Several mutants affecting the ability to enter (*daf-d* - dauer defective) or exit (*daf-c* - dauer constitutive) the dauer program have been isolated, many of them with underlying changes in adult lifespan such as those conferred by mutations in *daf-2*. *daf-2(e1370)* is a temperature sensitive *daf-c* allele in which larvae will enter dauer stage when grown at the restrictive temperature (25^{o}C) even in non-limiting environment conditions. When grown at the permissive (16^{o}C) condition, *daf-2(e1370)* worms develop normally. If *daf-2(e1370)* animals are grown at 16^{o}C past the L2 molt, however, they can be transferred to 25^{o}C without affecting larval development, skipping the dauer-entry defect. In this context, overtly normal *daf-2* adult hermaphrodites that lack DAF-2 activity can be generated. These adult animals are slightly delayed in reaching reproductive maturity and display a 2-fold increase in lifespan (Kenyon et al., 1993). DAF-2, therefore, is also involved in other IIS-dependent processes in adult animals aside the regulation of larval development.

Further genetic analysis demonstrated that the extra longevity in *daf-2* mutants, as well as its control on dauer formation, is dependent on DAF-16/FOXO (Kenyon et al., 1993), the downstream transcriptional effector of the IIS pathway involved in the regulation of reproductive maturity, dauer formation and the responses to several types of stresses, including metabolic adaptation (Riddle et al., 1981). Taken together, these studies reveal that different components of the conserved IIS pathway (DAF-2, AGE-1 and DAF-16) dramatically influence aging in *C. elegans*.

1.2.4 Using *C. elegans* to study reproductive aging

Reproduction is not a vital process to the organism, but reproductive aging has obvious implications across generations in ensuring population viability. In societies in which modern economic and cultural demands postpone maternity, germ cell aging has become an increasingly relevant topic of research. When women reach their mid-30s, they experience a decline in fertility and more risk-prone pregnancies that result in higher rates of premature births, congenital malformations and interventions at birth. These reproductive challenges have been linked to age-related decline in oocyte quality (Velde et al., 2002). As in humans, *C. elegans* reproduces only for about one third of its lifespan. Progeny production in hermaphrodites is not limited by the number of oocytes available, which in contrast to women, are continuously generated throughout the life of the worm. Instead, and as described above, the pre-determined number of sperm cells defines reproductive span in hermaphrodites. As in women, however, oocyte quality and embryo viability in *C. elegans* dramatically decline before sperm is exhausted and reproduction ends. Thus, reproductive aging in worms and humans develop on *proportional time scales* and appears to be independent of gamete production and availability. Consistent with a conserved genetic toolkit regulating reproductive aging in humans and worms, oocytes in these organisms arrest in diakinesis in anticipation to fertilization and the molecular processes coordinating oocyte maturation have been shown to be highly conserved between them (Cant & Johnstone, 2008; Luo et al., 2009).

In the past decade, prompted by the promise of using an amenable model system to uncover conserved molecular processes underlying reproductive aging, different research

groups have characterized in detail the physiological changes associated with the loss of oocyte quality in *C. elegans* (Andux & Ellis, 2008; Hughes et al., 2007; Luo et al., 2010). Andux and Ellis (2008) concluded that *C. elegans* reproductive capacity is limited by oocyte quality which declines in mid-adulthood, as in humans. Hughes et al. (2007) demonstrated that *C. elegans* reproductive aging is a genetically regulated process. Finally, Luo et al (2010) established that reproductive decline in worms is independent of sperm contribution and determined that a reduced rate of ovulation does not extend reproductive span. Taken together, these findings indicated that loss of reproductive capacity in *C. elegans* is an event timed with the age of the organism and the product of an intrinsically regulated process triggered relatively early in adult life. I have used these studies as a research platform to further shed light on the molecular nature of these early cellular changes.

As most genes so far shown to impact lifespan, components of the IIS (insulin/IGF-1 signaling) pathway also signal to control the reproductive span in *C. elegans*. This pathway is extremely conserved in animal species ranging from worms to flies to humans (Kenyon, 2001). There are in total 40 genes encoding putative insulin-like molecules in the *C. elegans* genome identified so far (Gregoire et al., 1998; Hua et al., 2003; Kawano et al., 2006; Murphy et al., 2007; Pierce et al., 2001) and most of them can directly regulate DAF-2, the only insulin/IGF receptor tyrosine kinase in worms (Kimura et al., 1997; Rikke et al., 2000).

Under favorable conditions, environmental cues such as nutritional status, trigger the release of one or multiple insulin-like ligands from neurosecretory cells in the worm central nervous system that activate DAF-2-mediated signaling in target tissues (Porte et al., 2005). When an insulin-like ligand binds to DAF-2, it initiates a phosphorylation cascade via AGE-1, the phosphoinositide 3-kinase (PI3K), that involves AKT-1, AKT-2 and SGK-1 protein kinases leading to phosphorylation and cytoplasmic trapping of DAF-16. SGK-1 has an essential role in the regulation of stress responses, development and lifespan, while AKT appears to be more important in regulating dauer formation (Hertweck et al., 2004). When AKT-1 and SGK-1 are phosphorylated, they inactivate DAF-16 by inhibiting its translocation to the nucleus and consequently its transcriptional activity (Kimura et al., 1997; Lin et al., 1997; Paradis et al., 1999; Paradis & Ruvkun, 1998).

DAF-16 inactivation through DAF-2-mediated phosphorylation during development leads to the normal formation of reproductive organs and ultimately reproductive maturity. In the absence of insulin ligands, or in the case of an impairment in DAF-2 activity, the downstream phosphorylation events are shut off and hypo-phosphorylated DAF-16 is then free to translocate into the nucleus where it activates a transcription program that regulates, among other processes, dauer formation, fat metabolism, innate immunity, stress response and somatic maintenance.

In addition to its effect on lifespan, mutations on *daf-2* delay reproductive senescence, a phenotype also dependent on DAF-16 (Hsin & Kenyon, 1999; Hughes et al., 2007). The delay in reproductive aging in *daf-2* mutants is due in part to a slight delay in reaching reproductive maturity (Luo et al., 2010). When compared to age matched wild-type animals, old *daf-2 (e1370)* hermaphrodites have fewer unfertilized oocytes and non-viable embryos, consistent with continuous fertilization and improved oocyte quality (Luo et al., 2010). Though IIS controls somatic and reproductive aging in adult worms, it must do so through separate systemic mechanisms, since signaling through different tissues are required to ensure correct longevity and reproduction (Libina et al., 2003; Wolkow et al., 2000; Zhang et al., 2013, Luo et al., 2010). In addition, different temporal requirements for IIS exist in controlling longevity and reproduction. While IIS during adulthood impacts lifespan, IIS activity in late larval stages is required to regulate progeny production and reproductive span, indicating that the influence of IIS also responds to different life stages (Dillin et al., 2002; Luo et al., 2010). Despite the apparent independence of IIS's dual roles in regulating lifespan and reproduction, it is well established that reproduction is coupled with longevity in several organisms (Hsin & Kenyon, 1999), a fact highlighted in *C. elegans* with the discovery that the germline communicates with somatic tissues through lipid hormone signals (see below). More recently, genes that impact only organism or reproductive aging have also been characterized, indicating that these processes, although intertwined, also evolved exclusive regulatory networks (Luo et al., 2009). The TGF-β Sma/Mab was the first pathway identified to regulate reproductive aging independently of the major somatic aging regulator, *daf-16* (IIS pathway transcription factor) and *pha-4* (dietary restriction pathway transcription factor). Similar to reduced IIS mutants, mutants

with reduced TGF-β Sma/Mab such as *sma-2*, show significantly extended reproductive lifespan, at times doubling the progeny generation period without slowing aging (Luo et al., 2009). These findings provide further evidence that progeny production and longevity are not locked in an obligate trade-off and can be at times controlled independently.

What are the genes controlled by IIS in oocytes? Through comparative transcriptomics, Templeman et al (2018) identified cathepsin B proteases a target for DAF-2-mediated inhibition and implicated its activity in oocyte quality. In contrast to wild-type cells in which increased cathepsin B transcription correlates with post-reproductive life, old *daf-2* oocytes are essentially deprived of the activity of these enzymes. Furthermore, RNAi knockdown of cathepsin-B genes in adult wild-type gonads improved oocyte quality maintenance and extended fertility by about 10% (Templeman et al, 2018).

Aside from IIS and DAF-2, other regulatory networks have been shown to recruit DAF-16. One of these, the steroid hormonal signaling pathway, responds to reproductive inputs in the gonad to regulate DAF-16 localization in intestinal cells. The link between germline and lifespan has been well documented in *C. elegans*, where the removal of germline precursor cells by laser ablation causes constitutive nuclear localization of DAF-16 in somatic cells through the activity of the ankyrin-repeat protein, KRI-1 (Berman & Kenyon, 2006). Germ cell depletion in these animals leads to a significant increased in lifespan, consistent with the ability of the gonad to regulate homeostasis in the soma. Work in *Drosophila* and other model organisms subsequently reinforced the conservation of the gonad to soma communication, suggesting that in eukaryotes, aging may be in part a response to the physiological decline in reproduction (Hong et al., 2008).

The pathway behind the regulation of lifespan via gonadal signals was first characterized in worms. In *C. elegans*, mutations in genes required for germ cell proliferation such as *glp-1* results in empty gonads lacking germ cells. GLP-1, a Notch receptor, is expressed in germ cells along the pre-meiotic tip where it is activated by its ligand LAG-2. LAG-2 is produced by the DTC and its concentrations in the gonad syncytium decreases as germ cells travel away from the distal tip. GLP-1/LAG-2 signaling is required to promote mitotic proliferation and prevent meiotic entry. Disruption of *glp-1*

function results in premature entry into the meiotic program and consequent depletion of self-renewable germ stem cells. *glp-1* mutants are overtly wild-type, but sterile due to a gonad deprived of germ cells and consequently live significantly longer lives (Austin & Kimble, 1987). This enhancement of longevity upon to the ablation of the germline implicates a well describe signaling cascade involving steroid-like molecules and nuclear receptors that converges in DAF-16 activation. This signal depends on the nuclear hormone receptor DAF-12 and a cytochrome P450 homolog, DAF-9. DAF-9 activity mediates the production of a lipophilic ligand (dafachronic acid) that crosses the cell membrane to reach target somatic tissues where it activates DAF-12 in the cytoplasm. DAF-12 activation in intestinal cells, together with KRI-1, promotes DAF-16 nuclear localization cell autonomously (Berman & Kenyon, 2006). The DAF-12 pro-longevity signal is inhibited in normally reproducing animals, but elimination of germ cell proliferation upregulates the DAF-9/DAF-12 signaling axis leading constitutive nuclear DAF-16 and lifespan extension. Importantly, the removal of the entire gonads, with their germ as well as somatic cells, suppresses the longevity effect of germ cell depletion, indicating that the major source of DAF-9 activity resides in the somatic gonad (Yamawaki et al., 2010). Though well established in the context of germ cell depleted mutants, the role of this pathway in normally reproducing animals has been more controversial. Recently, Baxi et al (2017) reported that lysosomal pH in the intestine of wild-type worms is regulated by the dafachronic acid-dependent signaling pathway and DAF-16 in response to cessation of reproduction in the gonad, providing a potential explanation for how reproduction recruits the DAF-9/DAF-12/DAF-16 pathway to delay somatic decline until reproduction is complete in the gonads.

Taken together these studies point to a central and conserved role of DAF-16/FOXO in mediating aging-related phenotypes, including reproductive health. The similarities in the genetic regulation across these species suggest that research in *C. elegans* may reveal relevant insights about how these pathways regulate reproductive decline.

1.3 The major classes of biological macromolecules in the context of oocytes

In the last two decades, research in *C. elegans* has had a tremendous impact in our understanding of aging and reproductive mechanisms at the molecular level. Although the nematode germline is an established biological model widely used for cytological and molecular analysis, its use in synchrotron radiation imaging remains mostly unexplored at this time. This can be partially explained by difficulties in sample preparation and handling, since gonads represent small (< 1 mm) and delicate tissues, complicating their dissection. I took advantage of *C. elegans*'s suitability as a model for reproductive aging to investigate the possibility that major changes in the chemical composition of germ cells may underlie reproductive senescence and whether these potential age-related alterations in macromolecule signatures can be used as predictive markers to evaluate the intrinsic and extrinsic factors that contribute to the loss of reproductive health and their relationship with germ cell differentiation, metabolism and aging by using FTIR microspectroscopy.

This section described a brief introduction of the main types of biological molecules that can be studied using FTIR techniques in the context of oogenesis.

1.3.1 Proteins

Proteins are the most abundant and functionally versatile of the cellular macromolecules and serve crucial functions in essentially all biological processes including biological catalysis, structural support, signaling, recognition and immunity. In *C. elegans*, vitellogenins are among the most predominant proteins required in eggs to fuel the high energetic demands of the developing embryo (Dunning et al, 2014). Together with their associated lipids, vitellogenins are integral part of yolk. Yolk particles are spherical lipoprotein macromolecules with a diameter of 5 - 1200 nm and composed of 86% vitellogenin, 8% phospholipids, 3% triglycerides and 3% other lipids (Sharrock et al., 1990). Vitellogenins are divided into distinct subclasses named according to their molecular weight: the large yolk proteins YP170A and YP170B encoded by the *vit-1, vit-2, vit-3,*

vit-4 and *vit -5* genes, and the smaller proteins YP115, and YP88 encoded by the *vit-6* genes (Sharrock et al. 1990; Spieth & Blumenthal 1985). Worm vitellogenins are lipid transporter proteins with domains shared with vertebrate vitellogenins and with human apolipoprotein B-100 (apoB-100), a serum component of the mammalian low-density lipoprotein family (LDL) (Smolenaars et al., 2007; Spieth & Blumenthal, 1985). In *C. elegans*, which does not have a circulatory system, yolk functions to bind and deliver lipids such as phospholipids, triglycerides and cholesterol, from the intestine, the source tissue, to peripheric tissues, particularly the gonad, where they are taken up via receptor mediated import (Blasiole et al., 2007).

In different animals, *vitellogenin* genes are expressed in various tissues of adult females specialized in yolk production (vitellogenesis) and storage, such as the fat body in insects, liver in vertebrates and intestine in nematodes. Vitellogenesis has been well characterized in a few oviparous species (such as *Xenopus laevis*, and chicken) as well as in invertebrates (such as *Drosophila, Aedes sp*, and *C. elegans*). In all these species, vitellogenesis is hormonally regulated. In insects, this role relies on Juvenile hormone (JH), which is promoted by IIS in these animals. In *Drosophila*, mutants for the insulin receptor InR fail to produce vitellogenic eggs, a defect that can be rescued in these flies by exposure to methorpene, an artificial JH analog (Flatt et al., 2005; Tatar et al., 2001). Thus, the impact of IIS in reproduction is to a large extent achieved by an evolutionary conserved pathway that controls vitellogenesis in yolk producing animals (Carnevali et al., 1998; Corona et al., 2007; Gulia-Nuss et al., 2011; Richard et al., 2005; Wuertz et al., 2007). In *C. elegans* with low DAF-2 activity, DAF-16 inhibits vitellogenin gene transcription in the intestine to reduce yolk protein loads. The premature loss of vitellogenin production, with its detrimental effects for oocyte development and progeny production, has been shown to increase lifespan in mutants with impaired IIS (Dong et al., 2007; Murphy et al., 2003). In this context, vitellogenesis, an IIS-regulated process that is critical for reproduction, antagonizes longevity.

At the chemical level, vitellogenins share characteristics common to all proteins. In simple terms, proteins are large biological polymers composed of one or more long chains of amino acid residues. Each of these amino acids consists of a central carbon (alpha carbon)

linked to a hydrogen atom (H), an amino group (-NH_2), a carboxyl group (-COOH), along with a specific sidechain that determines the chemical identity of amino acids (Figure 1.4). The side chain, represented by the "R" group, is classified according to its composition, structure and proprieties into four groups: hydrophobic, polar, positive or negative charge. A set of twenty different amino acids, which are bonded to each other to form peptide chains via peptides bonds, (-CO-NH-) are used to make up proteins.

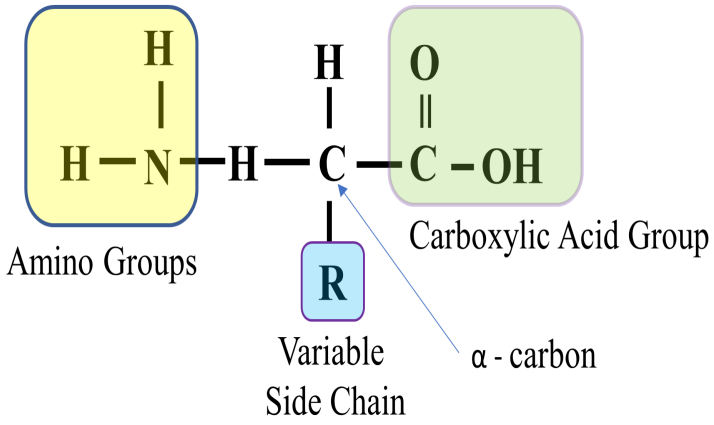

Figure 1.4: Amino acid structure.

Understanding the identity of all proteins in a complex living cell is not currently feasible. However, IR (Infrared) spectroscopy is an analytic technique that can provide hints of the dynamic changes in proteome composition by quantitatively revealing certain general signature characteristic of protein structures. FTIR spectroscopy deals with vibrational motions of molecules resulted from radiation that is absorbed by chemical bonds at different frequencies and intensities. This collection of absorbance information is then graphed in the form of a spectrum where different peaks represent the different absorptions of radiation by one or more chemical bonds. This association between a specific vibration mode and a chemical bond feed information about structure, ligands, cofactors, and aminoacidic side chains that have particular spectral parameters like band position and absorption coefficient of peaks (Hellwig et al., 1998; 1999). In the specific case or proteins, the Amide A, B,

I through VII are the nine characteristic bands found in the IR spectra that inform on proteins and polypeptides (Fabian et al., 1995; Susi, 1972). Among these bands, Amide I and Amide II bands are the most extensively investigated, since they can be traced to protein backbone structures useful for conformation studies (Blout et al., 1961; Kong & Yu, 2007; Susi, 1972). The Amide I band found between 1700 - 1600 cm^{-1} represents the most intense absorption band in proteins and is primarily caused by C=O stretching vibrations of the amide group coupled to the C-N stretch and N-H bending modes (Krimm & Bandekar, 1986). The exact wavenumber of this band is determined by the geometry of the polypeptide backbone and the strength of hydrogen bonds involving the C=O and N-H groups (Haris & Severcan, 1999). The Amide II band occurs between approximately 1500 and 1600 cm^{-1} and is mainly derived from N-H bending with a contribution from C-N stretching. Although it is conformationally sensitive, the Amide II band is not usually used to quantify the secondary structure of proteins since the relationship between structure and band positions is more complex than for the Amide I band.

Proteins have four different structural levels as illustrated in Figure 1.5. The first level, or the primary structure, refers to the linear sequence of amino acids in a polypeptide chain. The next level, the secondary structure, refers to the folding of the polypeptide chains into local sub-structures formed by hydrogen bonding between the N-H and C=O groups. The two most common types of secondary structures are α-helices and β-sheets. An α-helix is a right-handed coiled strand where the hydrogen bonding occurs between successive turns of the helix. In β-sheets, the polypeptide strands are stretched out and aligned up next to each other in the same direction or in the opposite direction. There are also β-turns which are sharp turns that connect the adjacent strands in an antiparallel β-sheet and unordered structures which do not fall into any of the previous defined categories. FTIR spectroscopy using the Amide I region has been shown to provide information about the secondary structure of proteins. This stretching carbonyl band is generated in part by specific frequencies associated with α-helices, β-sheet, turns and random coils and can be used to extrapolate the proportional distribution of these structures in the proteome. The approximate wavenumbers that correspond to the 3 common structures found in proteins are located at 1650 cm^{-1} for α-helices, 1632 cm^{-1} and at 1685 cm^{-1} for β-sheet and 1658 cm^{-1} for random coil structures. When the various

elements of a protein's secondary structure are considered, a well defined 3-D conformation referred as the tertiary structure is formed. Unlike FTIR spectroscopy, X-ray crystallography and NMR spectroscopy provide information about the tertiary structure of proteins. At a higher level, the quaternary structure describes the arrangement of multiple folded protein molecules into a single structure.

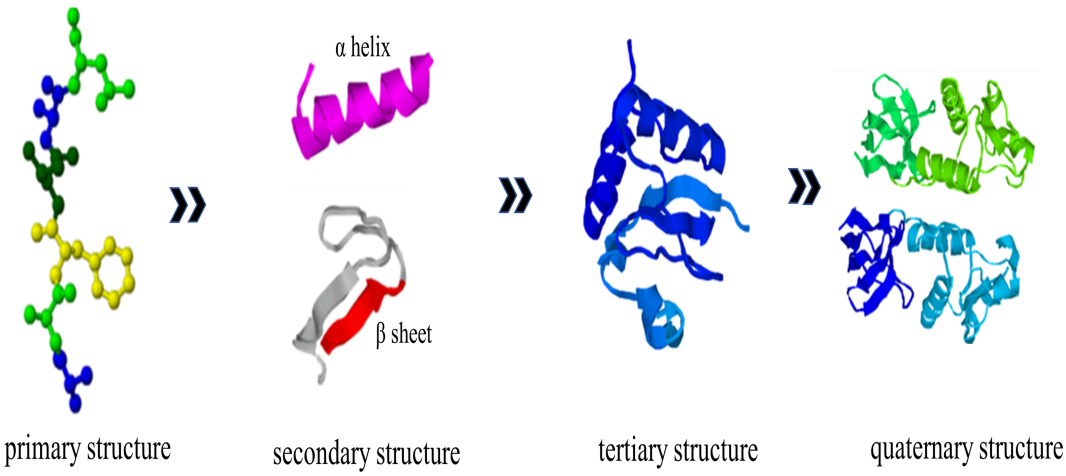

Figure 1.5: The four levels of protein structure.

To be considered as a protein, a polypeptide must be able to fold into a well defined 3-D structure (native state) that plays an essential role in protein function. Defects in folding affecting the native protein structure and its normal function are the cause of a number of genetic disorders such as cystic fibrosis and sickle cell anemia, which are the result of a single residue deletion and a point mutation, respectively (Baker et al., 2000; Caughey & Lansbury, 2003; Carugo et al., 2007). Misfolded proteins are also behind a growing number of age-related disease such as Alzheimer's Disease (AD) which is associated with the accumulation of abnormally folded amyloid-β peptides in the brains of AD patients (Dobson, 1999; 2002). Although amyloid-β monomers are soluble and contain short regions of secondary structure made of β-sheet and polyproline II helices in solution,

they undergo a dramatic conformational change at sufficiently high concentrations to form β-sheet rich tertiary structures that facilitate the aggregation into amyloid fibrils (Jens et al., 2006; Ohnishi & Takano, 2004).

FTIR spectroscopy is an established and powerful analytical technique to investigate the secondary structure of proteins, making it a valuable approach to study protein aggregation. Aberrant protein aggregation is known to be a hallmark of a variety of age-related diseases including neurodegenerative diseases such as Alzheimer', Huntington' and Parkinson's disease as well as systemic amyloidosis which are triggered by the formation of stable and ordered aggregated proteins, referred as amyloid fibrils (Kelly, 1998). Recently, David et al (2010) revealed that protein aggregation also occurs without the development of disease in *C. elegans*, as the result of normal aging. Since then, several *C. elegans* proteins prone to misfolding and aggregation in aging cells have been identified using spectrometry - based proteomics (Reis - Rodrigues et al., 2012). Corresponding aggregation prone proteins in humans have been shown to be overrepresented in Alzheimer's disease and exhibit distinct features, in particular a significantly enrichment in β-sheets in their secondary structure (David et al., 2010). These studies contributed to the establishment of protein aggregation biomarkers of aging.

In age related diseases, a wide variety of proteins escape or overwhelm the cell's quality control systems and have the capability to change their soluble and native forms to insoluble amyloid fibrils which oligomerize and aggregate with age in a variety of tissues (Uversky & Fink, 2004). For example, natively unfolded proteins such as Tau and β-amyloid are known to aggregate in Alzheimer's disease. Partial unfolding of globular proteins rich in β-sheets, α-helix or both can also lead to protein aggregation in different types of systemic amyloidosis (Uversky & Fink, 2004). Despite these differences, X-ray diffraction studies indicate that all these proteins adopt a specific β-amyloid conformation in aggregates that have a characteristic cross-β-sheet structure formed by β-strands oriented perpendicular to the long axis of fibrils, resulting in β-sheets propagating in the direction of the fibril (Sunde & Blake, 1997). This observation was confirmed by attenuated total reflectance (ATR)-FTIR studies in various aggregated protein forms which have common secondary structural compositions dominated by β-sheet structures (Fink, 1998;

Oberg et al., 1994). Consistent with these findings, structural studies of protein misfolding and aggregation *in vivo* using FTIR spectroscopy revealed that certain regions in the diseased tissue have high β-sheet content, as demonstrated by a strong Amide I absorbance between 1634 and 1620 cm^{-1} (Bonda et al., 2011; Choo et al., 1996; Miller et al., 2006; Szczerbowska-Boruchowska et al., 2007).

1.3.2 Lipids

FTIR spectroscopy can also reveal valuable structural information about lipids which are the most heterogeneous class of naturally occurring molecules. Lipids are water insoluble biomolecules that play a myriad of functions in biological systems such as serving as energy storage, fuel for metabolic reactions, reservoir of second messengers for cellular signaling and building blocks for the construction of biological membranes (Vance & Vance, 2002). Lipids are classified into eight categories: fatty acids, glycerolipids, glycerophospholipids, sphingolipids, sterol lipids, prenol lipids, saccharolipids and polyketides (Fahy et al. , 2011).

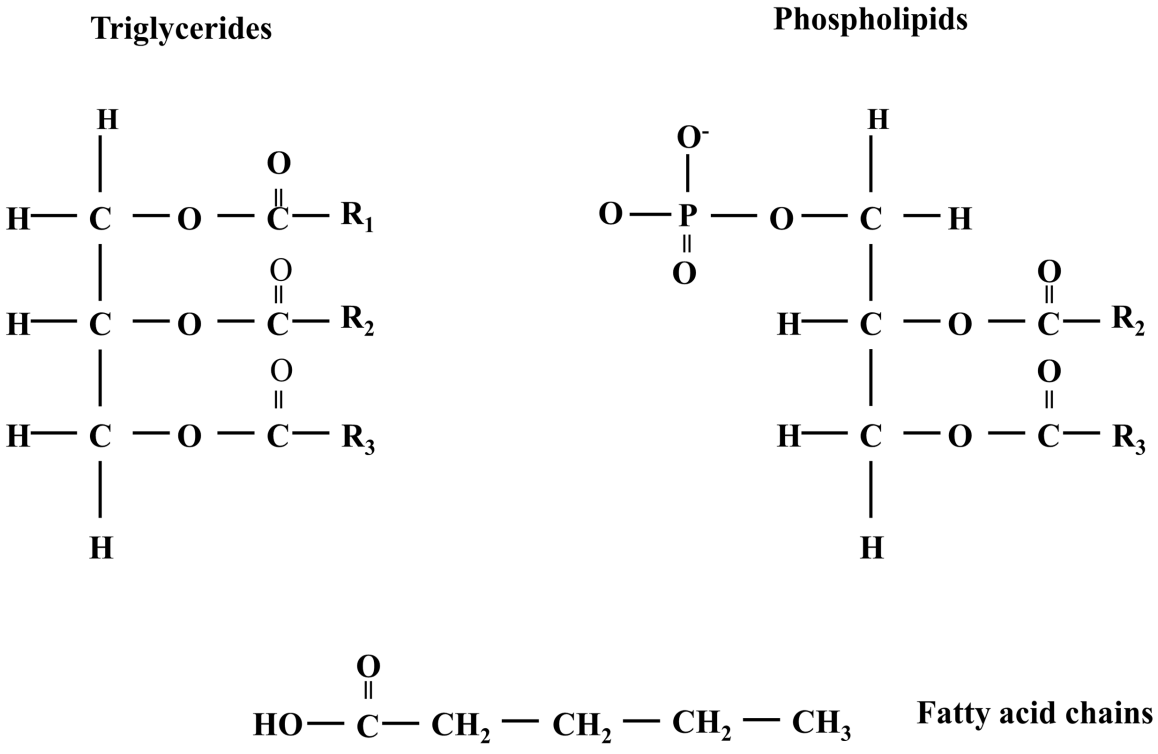

Figure 1.6: Schematic representations of three major types of lipids.

Among the different lipid groups, phospholipids (Figure 1.6) are the major component of yolk (Kubagawa et al. 2006; Sharrock et al. 1990). These molecules associate with vitellogenins, synthesized in the intestine of adult hermaphrodites and secreted into pseudoceolomic space that surrounds all internal organs in worms (Matyash et al., 2001; Sharrock et al., 1990). From the pseudocoelom, yolk crosses the oocyte membrane via the RME-2 receptor, a member of the low-density lipoprotein receptor (LDL) receptor superfamily (Grant & Hirsh, 1999). Inside oocytes, yolk is then partially processed in an endosomal compartment and stored in yolk platelets (YPs), membrane surrounded-granules in the cytoplasm (Kimble & Sharrock, 1983). YPs seem to be modified lysosomes with a low proteolytic activity initially. During embryogenesis, a gradual degradation of YPs can be observed, a process that is thought to involve the activity of hydrolases (Grant, 2006) (Figure 1.7).

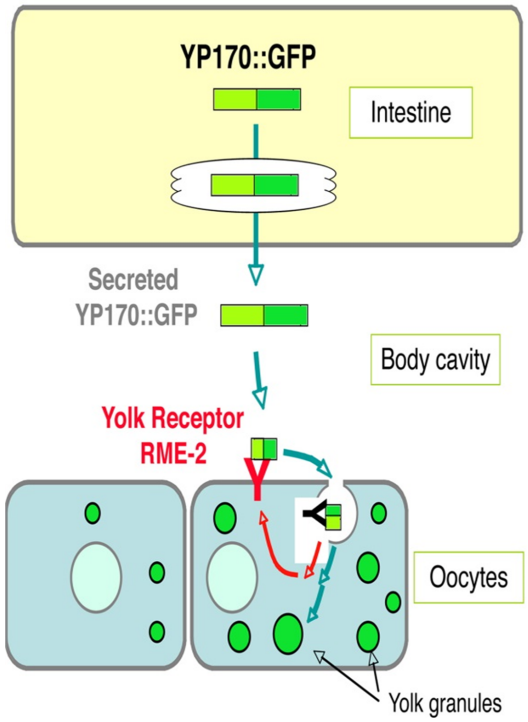

Figure 1.7: YP170::GFP endocytosis by oocytes: a transgene expressing a GFP-labelled vitellogenin (YP170::GFP) is secreted in the intestine and secreted into the body cavity from which it is endocytosed by oocytes. RME-2 is the yolk receptor expressed in oocytes.

Impairment of the endocytic pathway, for example by depleting RME-2 function, causes a substantial decrease in lipid (in the form of yolk) import into oocytes and a consequent accumulation of yolk in the pseudocoelomic space. *rme-2* loss - of - function mutants are characterized by morphologically normal oocytes that appear devoid of yolk and extra-gonad yolk accumulation. Though *rme-2* oocytes can be fertilized, the resulted embryos fail to develop, presumably because an early energetic deficit during embryogenesis (Bembenek et al., 2007; Paupard et al., 2001; Sönnichsen et al., 2005). Until recently, RME-2 was considered to represent the only pathway for lipid transport into oocytes. There is, however, growing evidence of RME-2-independent yolk import, suggesting the presence of alternative import systems. Consistent with this possibility, Matyash et al (2001) described cholesterol accumulation in oocytes of *rme-2* mutants. Recently, the concept that bulk yolk import is essential for embryogenesis has been challenged by the characterization of three new yolk uptake mutants; *vrp-1, ceh-60* and *lrp-2*. In contrast to *rme-2* mutants, *vrp-1, ceh-60* and *lrp-2* animals do not show significant embryonic lethality, even though intracellular yolk content is low in these oocytes. These findings suggest that perhaps only a low threshold of oocyte yolk is sufficient to properly launch and complete embryonic development (Rompay et al., 2015).

Phospholipids are made by a hydrophobic fatty acid chain and a hydrophilic phosphate group connected by a glycerol molecule or a more complex alcohol. The IR spectra of phospholipids can be divided into spectral regions that originate from molecular vibrations of the functional groups in the head-group, the characteristic carbon-hydrogen vibrations of the acyl or alkyl chain, and the interface region (Lewis & McElhaney, 2006). The CH_2 asymmetric and symmetric stretching vibrations are the strongest bands in the IR spectra of lipid systems observed in the region between 3100 and 2800 cm^{-1}. The structure of the interfacial region of lipid assemblies can be examined via the ester group vibrations, in particularly the C=O stretching bands in the region between 1750 and 1700 cm^{-1} (Mushayakarara & Levin, 1982). In diacyl lipids, this region consists of two absorption bands originating from the stretching of two ester carbonyl groups: one around at 1742 cm^{-1} with a trans-conformation in the C-C bond adjacent to the ester grouping and the other one around 1728 cm^{-1} with gauche

conformation (Lewis et al., 1994). The head contains the negatively charged phosphate groups which give rise to several strong vibrations in the IR, but the most intense ones are due to asymmetric and symmetric PO_2^{-1} stretching mode at around 1228 and 1086 cm^{-1}, respectively (Arrondo et al., 1984; Casal & Mantsch, 1984).

Quantitative IR spectroscopic analysis can be applied to quantify the relative amounts of lipid that are present in blood serum. Triglycerides, phospholipids and cholesterol esters are the classes of lipid that occur in blood serum which can be characterised using FTIR spectroscopy by their carbonyl bands between 1750 and 1700 cm^{-1} (Stuart, 2006). Among these classes of lipids, triglycerides are known to be the main reservoirs of energy for biological systems and contain more energy density (9 kcal/g) than carbohydrate and proteins (4 kcal/g) (Berg et al., 2002). In *C. elegans*, triglycerides are deposited and accumulate as lipid droplets in the intestine, epidermis, and germline. Lipid droplets are typically in the size range of 0.5 - 2 μm and consist of a core of triglyceride surrounded by a monolayer of phospholipids and proteins as revealed by the electron microscopy and lipodomic analysis of lipid droplets (Li et al., 2016; Vrablik et al., 2015; Zhang et al., 2010). Triglycerides are made of a glycerol backbone with three fatty acids groups, forming a non-polar lipid molecule. Fatty acids consist of a long chain of hydrocarbons (CH_2) with an even number of carbon atoms in the ranges from 14 to 20 carbons to which a carboxyl group is attached at one end and a methyl group at the other end (Tanaka et al., 1996; Watts & Browse, 2002).

1.3.3 Carbohydrates

Carbohydrates are hydrated organic molecules consisting of carbon (C), hydrogen (H), and oxygen (O) characterised by the formula $C_x(H_2O)_y$. They are the immediate source of energy for most living organisms and can be stored in the form of glycogen, a polymer of thousands of monosaccharide units in animals which is analogous to starch, long polymers of amylose and amylopectin, in plants. Carbohydrates give rise to a complex sequence of bands in IR spectral range between 1200 and 950 cm^{-1} due to C-O and C-C stretching vibrations coupled to C-O-H bending of polysaccharides.

When polymerised, carbohydrates are able to serve different functions as long-term energy storage molecules, structural supports and forming protective coatings. Glucose is

the central ingredient for metabolic activity and can be converted into glycogen when glucose molecules are not required for immediate energy production. Glycogen is degraded through glycogenolysis that converts glycogen polymers back into more readily used glucose monomers. Glycogen is catabolised via the activity of the enzyme glycogen phosphorylase that removes glucose monomers to generate glucose-1-phosphate glucose (Bhatt et al., 2003). This derivative of glucose is then converted to glucose-6-phosphate (G6P) by action of the enzyme phosphoglucomutase to enter the metabolic mainstream. G6P can be in turn hydrolysed by the enzyme glucose-6-phosphatase to cleave the phosphate groups on G6P for the formation of free glucose to enable the start of glycolysis (Bhatt et al., 2003). During glycolysis, glucose is converted into pyruvate, which is further degraded to form Acetyl CoA in the absence of oxygen to generate ATP. Likewise, fatty acids and certain amino acids can also be oxidized to Acetyl CoA to generates ATP. In turn, the excess of Acetyl CoA can also be converted into fatty acids, triglycerides, cholesterol.

As in other animals, glycogen is the main storage carbohydrate in *C. elegans*. Evidence for glycogen storage as well as glucose mobilization from glycogen comes from studies in dauer larva, where glycogen is detected in neurons, body wall muscle and pharynx, presumably to provide a lasting source of energy to full basic metabolic reactions until food becomes again available (Lant & Storey, 2010; Popham & Webster, 1979). In the bivalve *Sinonovacula constricta*, where yolk precursor for vitellogenesis derive from vesicular connective tissue cells, a large quantity of glycogen particles accumulate in oocytes to support oogenesis (Chung et al., 2008). Consistent with a role of glycogen consumption during oocyte maturation, an increase in carbohydrate metabolism enzymes has been reported in fish oocytes (Boulekbache, 1981). Finally, active glycogen synthesis in worms is required to fuel glycolysis during hypo-osmotic stress and anoxic states (Depuydt et al., 2014; Frazier & Roth, 2009; LaRue & Padilla, 2011), again highlighting the importance of glycogen stores in coping with physiologically stressful situations.

Carbohydrate groups can be covalently attached to many different proteins in post-translational modifications via the process called glycosylation. Glycosylation has important functions in mediating proper protein folding, stability and active biological conformation (Spiro, 2002). Consequently, the removal of carbohydrate moieties from

proteins can lead to protein unfolding or aggregation (Ermonval et al., 2000). Carbohydrate moieties can also be attached to lipids in cell membranes where they act as recognition signals in modulating self-immune response, for example (Naik, 2011).

1.4 Fourier Transform Infrared microspectroscopy

In the last decade, FTIR microspectroscopy has been increasingly used in biochemical sciences to collect information on the composition and structure of cellular biomolecules such as proteins, lipids and carbohydrates. This technique has been widely applied in medical diagnostic research for many years to distinguish malignant from normal cells in tumors and understand their unique molecular composition. For instance, the spectra of benign and malignant forms of prostate, breast, colon, and brain cancer cells have been characterized using FTIR microspectroscopy to better understand the process of metastasis (Bellisola & Sorio, 2012; Hands et al., 2016; Kumar et al., 2017; Li et al., 2017; Siqueira & Lima, 2016). Spectroscopy is also a powerful tool for monitoring the developmental changes in bone and other mineralized tissues and the therapeutic effects of drugs on certain tissues (Cakmak et al., 2011; 2012). Particularly relevant to aging research, FTIR microspectroscopy has been used to monitor changes in the secondary structure of proteins associated with neurogenerative conditions such as Parkinson's, Huntington's and Alzheimer's diseases. In *C. elegans*, FTIR microspectroscopy was first employed to distinguish the biochemical features associated with different anatomic regions (pharynx, intestine, and tail) of intact nematode specimen using single point spectra (Ami et al., 2004). Remarkable differences between the spectra of these different body parts were noted. This was particularly so in the Amide I band. The sub-band Amide I at 1690 cm^{-1} assigned to β-sheets/turn structures was almost negligible in the tail region compared to the pharynx and intestine where vitellogenesis takes place, potentially indicating an overrepresentation of vitellogenin-derived signatures in these bands (Garigan et al., 2002). However, this study did not investigate the FTIR profile of the gonad nor did it focus on changes that occur with aging. On the other hand, FTIR microspectroscopy has been previously applied to investigate molecular changes on murine oocytes at different

maturation stages (Wood et al., 2008). This study revealed a marked increase in lipid bands in later developmental stages. Additionally, Gioacchini et al (2014), using this vibrational technique on human eggs collected from older women, noted an increase in acyl chain peroxidation signatures, an altered protein pattern previously characterized by a higher amount of unordered structures and with increases in carbohydrate consumption. Though these studies contributed a great deal in revealing the composition of aged cells *in vitro*, dynamically investigating the process of aging in live animals is not feasible in mammalian systems due to the relatively small number of oocytes ovulated, access to reproductive organs and the relatively long time between reproductive maturity and reproductive decline. In this study, I explored the advantages of *C. elegans* biology, anatomy and research tools and the benefits of FTIR imaging to identify biomarkers of aging in live oocytes from intact gonads.

In the sections below, I give a brief introduction to the fundamental principles of FTIR spectroscopy.

1.4.1 Principles of molecular spectroscopy

All spectroscopy methods are mainly based in the study of the interaction of the electromagnetic radiation with matter or the measurement of radiation emitted from the medium. Electromagnetic radiation is characterised by its energy E which is linked to wavelength λ and frequency by the Planck relationship:

$$E = h\nu = h\frac{c}{\lambda} \tag{1.1}$$

where c is the speed of light in a vacuum (2.998 x 108 m/s) and h is Plank's constant (6.626 x 10^{-34} J.s).

However, instead of these quantities, vibrational spectroscopy, in particular, uses the wavenumber which is the reciprocal of the wavelength. The units of wavenumbers is cm^{-1}.

Infrared radiation is a part of the electromagnetic radiation which lies between the microwave and visible region with a wavenumber roughly between 13300 cm^{-1} and 3.3 cm^{-1}.

This region can subdivided into three main regions: near-IR (in the wavenumber range 13300 - 4000 cm^{-1}), mid-IR (in the wavenumber range 4000 - 400 cm^{-1}) and far-IR (in the wavenumber range 400 - 100 cm^{-1}) (Tipler, 2016). The mid infrared region is used in this thesis because most of vibrational frequencies of biological molecules fall within this region (Coleman, 1993).

When IR radiation passes through the sample, only selected frequencies of IR radiation that correlate to the vibration of specific sets of chemical bonds are absorbed by the sample while the remaining frequencies pass through without interacting with the molecules. In addition, not all bonds are capable of absorbing IR energy, even when there is a matching frequency between the radiation and the bond motion. Only the bonds that have a change in dipole moment during vibration are capable of absorbing infrared radiation. Thus, symmetric bonds which have identical or nearly identical groups on each end are inactive to IR since there is no change in the dipole moment caused by the vibration.

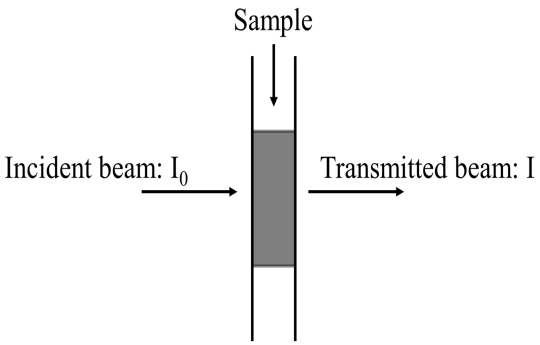

Figure 1.8: Definition of transmission light.

The detector measures usually the remainder of the energy of the electromagnetic radiation that was not absorbed by the sample. The transmittance is defined by the ratio of the intensity of the transmitted beam to that of incident beam as shown in Figure 1.8 and the equation below (Pavia et al., 2001):

$$T(\lambda) = \frac{I(\lambda)}{I_o(\lambda)} \tag{1.2}$$

Absorbance is the negative logarithm of the transmittance (T):

$$A(\lambda) = log(1/T_\lambda) = -log(T_\lambda) = -log(I(\lambda)/I_o(\lambda) \tag{1.3}$$

Beer- Lambert's law, the fundamental law of quantitative absorption spectroscopy, states that the absorbance of any component is proportional to its concentration and the pathlength of the light within the sample as described by the following equation (Li-Chan et al., 2010):

$$A(\lambda) = -log(I(\lambda)/I_o(\lambda) = \epsilon_\lambda lC \tag{1.4}$$

ϵ_λ is the molar absorption coefficient of the substance, l is the thickness of the sample, and C is the molar concentration.

According to latest equation, the concentration of the molecules in the sample can be determined by the area under the peak in the IR spectrum which is originated from the vibration of specific molecules.

1.4.2 Vibrational modes

The absorption of IR radiation corresponds to energy changes on the order of 8-40 KJ/mol, which corresponds to the range encompassing the stretching and bending vibrational frequencies of the bonds in most covalent molecules (Pavia et al., 2001). When those frequencies of IR radiation match the natural vibrational frequencies of the molecules, energy is absorbed, increasing the amplitude of the vibrational motions of the bonds in the molecule (Pavia et al., 2001). The vibration modes are subdivided into 2 classes and classified according to the type of movement of the atoms which depends on changes in the bond length and angle. A stretching vibration occurs along the line of the chemical bond with increasing and decreasing of the interatomic distance. This mode comes in two variations: symmetric and asymmetric where the asymmetric vibration occurs at a slightly higher frequency than symmetric vibration. For example, with the C-H stretch of a CH_2

functional group, CH_2 symmetric stretching vibration appears at about 2853 cm^{-1} and an antisymmetric stretch vibration at 2926 cm^{-1} (Pavia et al., 2001). Bending vibrations, on the other hand, result in a change of the bond angle of the group and these motions can be classified as scissoring, wagging, rocking or twisting motion. Stretching vibrations typically occur at higher frequencies than bending vibrations of the same groups since the bonding force directly opposes the change in the case of stretching vibrations (Pavia et al., 2001). The vibrational modes associated with a non-linear tri-atomic molecule are presented in Figure 1.9.

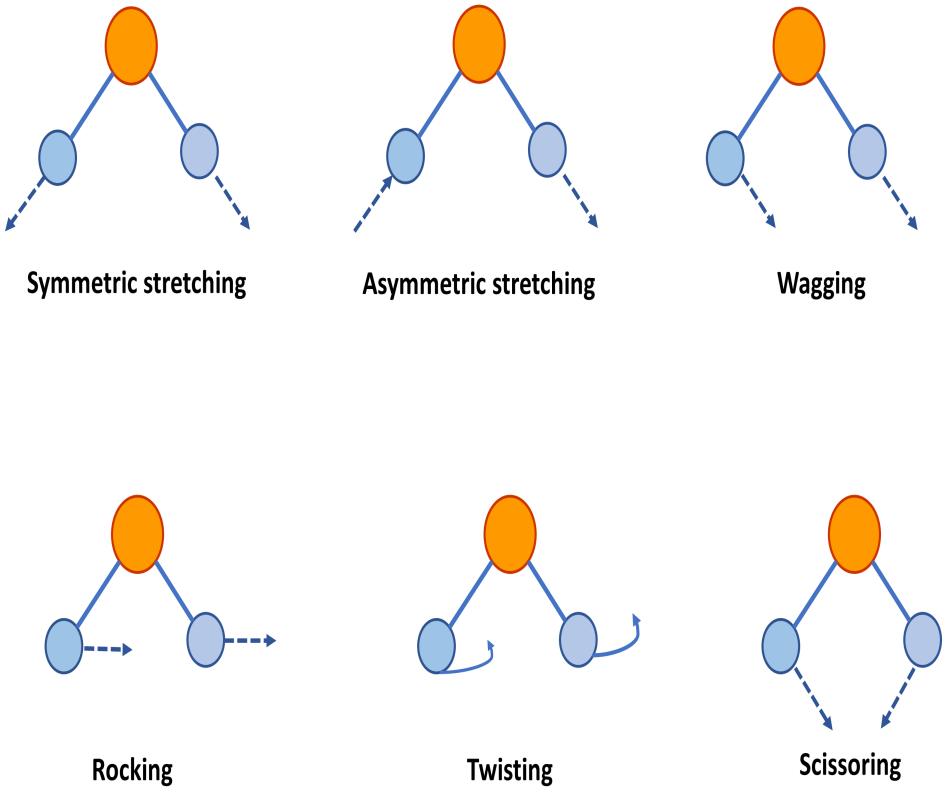

Figure 1.9: Simple layouts of the vibrational modes associated with a molecular dipole moment change detectable in an IR absorption spectrum.

The number of normal modes for vibration for a given molecule can be calculated by considering the atom's degree of freedom. A molecule composed of N atoms possesses 3N degrees of freedom of motion, six of which correspond to the rotational and transitional

motion of the entire molecule. Therefore, the number of ways in which atoms in a nonlinear molecule can vibrate is 3N-6, whereas linear molecules have 3N-5 degrees of vibrational modes because the rotation around its molecular axis cannot be observed (Griffiths & Griffiths, 2006). In each normal mode of vibration, all atoms in a molecule oscillate with the same frequency and simultaneously pass through their equilibrium positions without changing the position of the center of mass. If two or more modes have the same frequency, they are called degenerate. Degeneracy is more severe in lager molecules such as proteins which have a vast amount of normal modes (Colthup et al., 1990).

The presence or absence of functional groups is the second important type of information that can be extracted from vibrational spectra and compared to normal vibrations. Absorption bands of functional groups are independent of the structure of the rest of the molecule that the functional group is in. This is the case if the bond strength in the functional groups is either much stronger or weaker than others nearby or the atoms constituting the functional group are much lighter or heavier than their neighbors. The absorption band of functional groups is called group frequencies and developed by functional groups containing H atoms or isolated double and triple bonds. The corresponding wavenumber region of functional groups range from 4000 to 1400 cm^{-1} and can be used to identify the molecular composition of the sample. The region below 1400 cm^{-1} is called the fingerprint region, as these vibrations are used to distinguish one molecule from another (Kellner & Mermet, 2004).

1.4.3 Advantages and limitations of FTIR spectroscopy for biological research

One of primary advantages of FTIR spectroscopy is that it provides detailed qualitative and quantitative chemical information in a short time and without causing overt damage to the sample. FTIR spectroscopy can be applied to any kind of material such as solids, liquids, powders, films, fibers and gases with a judicious choice of sampling techniques and a requirement of very small amounts of samples for measurements (Dogan et al., 2007; Haris & Severcan, 1999; Liu et al., 1996; Mantsch, 1984; Mendelsohn et al.,

1984). For instance, near-IR requires 0.1 - 0.2 ml of sample whereas samples with 10 μl or less can be examined with mid-IR spectroscopy (Shaw et al., 2000). FTIR spectroscopy is also inexpensive when compared to other high resolution techniques such as X-ray crystallography and nuclear magnetic resonance (NMR) (Müller U., 2010). Besides high accuracy in determining the three-dimensional structure of proteins with X-ray crystallography and NMR (Barton, 1995), these two techniques have their own limitations. Protein crystallography is time consuming and not all proteins can form the well-ordered crystals required for diffraction of X-rays at high resolution (Arrondo & Goñi, 1999; Brahms & Brahms, 1980). Protein size limitation (less than 200 residues) and analysis time and complexity are the main drawbacks of NMR (Raman et al., 2010). Therefore, an additional advantage of FTIR is its relative simplicity in collecting precise measurements without the need of external calibration (Haris & Severcan, 1999). This technique can detect, in a single measurement and at the same time, changes in different biomolecules at the level of functional groups.

The most distinguishing feature of FTIR spectroscopy is that it provides direct biochemical information without any requirement of hazardous reagents or any sort of special preparation for the examined samples such as bathing samples in radiation or adding radioactive dye. In this condition, samples are kept free from chemical modifications and artifacts.

One paradoxical downside of using IR spectroscopy is the high sensitivity of this technique. Small amounts of impurities may significantly disturb certain signals. The application of IR spectroscopy in aqueous samples or samples containing water also causes some difficulties (Baker et al., 2014; Tobin et al., 2010). This is a particular problem for biological samples which often need hydration to maintain structure. The presence of water molecules in the sample masks certain important regions of the spectra because water has a strong broad absorption of IR in the Amide I (1700 - 1600 cm^{-1}) and Amide A (3750 - 3000 cm^{-1}) region of proteins due to O-H bending mode, complicating the analysis (Jackson et al., 1997; Stuart , 2006). Vacuum drying is generally adopted to remove the presence of water in the sample but removing water can also incur in other important chemical and structural alterations of the sample that may hinder interpretation of the results.

1.5 Main hypothesis

As in humans, old *C. elegans* display a progressive loss of reproductive capacity that is explained by a reduction in the quality of oocytes. In principle, this phenomenon could be mirrored by changes at the molecular composition of aging oocytes that are detectable globally by spectroscopic techniques. This thesis investigates whether oocytes in young and old *C. elegans* indeed differ in their corresponding FTIR profiles to identify potential changes that correlate with aging. These changes, in turn, may be represent the consequences of cell senescence and metabolic distress or may provide insights on the causes underlying aging and loss of oocyte quality.

1.6 Research goals

This thesis is focused in drawing a biochemical map of reproductive cessation in *C. elegans* in an attempt to understand how its molecular composition relates to changes in oocytes quality, fertility and reproductive span by using FTIR microspectroscopy. The first step in this direction required the characterization of changes in the profile of macromolecules in oocytes from animals at reproductive and post-reproductive age to establish basic (causal or consequential) correlations between aging cells and specific biomolecular signatures. The analysis centered in the most proximal oocyte (-1) in the gonad representing the mature, pre-fertilization cell. By standardizing on imaging -1 oocytes from age-matched animals the analysis eliminated important variables as differences in developmental stage and maturation. As a proof of concept, FTIR profiles from young and old yolk-deprived *rme-2* oocytes were taken to validate the usefulness of FTIR imaging in detecting known variations in yolk-derived lipids and protein content in these cells. This was particularly important in order to validate the relative contributions of yolk derivatives to protein and lipid bands from spectra of young and old oocytes. Finally, standard staining and transgenic techniques commonly used to assess increases in yolk contents in *C. elegans* were used to cross-check the FTIR results (Paupard et al., 2001)

Chapter 2

MATERIALS AND METHODS

2.1 Growth and maintenance of *C. elegans* strains

C. elegans strains were maintained on nematode growth medium (NGM) plates with OP50 bacteria at 20^{o}C , unless specified. Temperature sensitive (*ts*) mutants were switched between permissive (propagation) and restrictive (testing) temperatures (15^{o}C and 25^{o}C, respectively) in specific developmental times to elicit phenotypes as specified below. A list of strains used in this study is provided in Table 2.1.

STRAIN	GENOTYPE	SOURCE
N2	*C. elegans* Bristol isolate (wild-type)	CGC*
RT130	*pwls23(vit-2::GFP)*	CGC
DH1390	*rme-2(b1008)IV*	CGC
CEC 173	*rme-2(b1008);pwls23(vit-2::GFP)*	Carvalho lab

*CGC - *Caenorhabditis elegans* Genetics Center

Table 2.1: List of strains used in this study

2.2 Age synchronization protocol

All experiments were carried out with age-matched animals. Synchronized populations of L1 larvae were prepared by treating mix populations with sodium hypochlorite solution, which penetrates the cuticle, killing larvae and adult *C. elegans* but not the hardier egg-shell of embryos. After washing three times with M9 buffer, recovered eggs were placed on NGM agar plates without food and allowed to hatch for 12 hours at 20^oC. Diapause arrested L1 larvae were collected in M9 buffer and transferred to NGM-OP50 plates to allow for re-entry and completion of larval development. Day 1 of adulthood was standardized as 24 hours post-L4 molt at 20^oC, when worms start to lay progeny. Two time points were used to evaluate oocytes produced in reproductive (young) and post-reproductive (old) life stages: day 3 and day 8 of adulthood, respectively. In wild-type worms, reproduction is generally completed by day 5. However, in mutants with delayed larval development and extended reproductive span, such as *daf-2*, reproductive maturity is achieved relatively later, and progeny generation extends past day 5.

2.3 Development of protocols for FTIR imaging of *C. elegans* oocytes

Sample preparation is the most critical step in acquiring high quality spectra (Miller & Dumas, 2006). To arrive at a protocol for sample preparation that gave out consistent high-quality spectral data, several different preliminary trials to troubleshoot early difficulties and to optimize the conditions were made.

Essentially, three sample treatments were tested for their ability to provide good quality spectra of whole oocytes while incurring in as little water interference and chemical alternation as possible; a) freeze dried dissected samples, b) microtome sections of whole animals fixed and resin embedded and c) dissected gonads in heavy water. These experiments represented the first attempts to establish useful protocols for FTIR imaging of *C. elegans* oocytes, and as such will likely be of interest for future researches in the field.

After a quick description of each protocol, and to facilitate consultation, this section lays out the individual steps in recipe formats.

2.3.1 Freeze-drying protocol

- **Rationale**

  The freeze-drying of dissected nematodes on slides was the first method to remove sample water, thus avoiding interference caused by water molecules in FTIR spectra. The process involves low temperature drying when most of the water is lost via sublimation from a thin front on the surface of a frozen core which gradually recedes into the sample. The freeze-drying process is classically split in 3 parts: freezing, primary and secondary drying.

- **Procedure**

  Live worms were dissected in M9 buffer and transferred to a BaF_2 (Barium Fluoride) window. To preserve the fine structure of cells, 10 μl of 10% DMSO was added to the sample followed by incubation at 37^{o}C for 5 min. Subsequently, the sample was immersed in liquid nitrogen. The BaF_2 window containing the frozen dissected nematodes was put inside a petri dish and placed in -80^{o}C for 2 hours and -20^{o}C for another 2 hours. To remove the water, the sample was put in a flask attached to the freezer port for overnight drying with a stepwise increase in temperature (-40^{o}C to 25^{o}C). Freeze-dried samples were placed in a desiccator until imaging.

- **Reagents**

  M9 buffer (1 l in H_2O):

  3g Na_2PO_4

  3g KH_2PO_4

  5g NaCl

1ml 1M $MgSO_4$

Add H_2O and autoclave.

- **Protocol**

1. Dissect nematodes in M9 buffer.
2. Transfer sample onto the centre of a BaF_2 window.
3. Add 10 μml of 10% of DMSO cryoprotectant into the sample to preserve the fine structure of cells.
4. After incubating it at 37^{o}C for 5 min, first exposed the sample to liquid nitrogen (LN) vapours for 5 minutes before plunging into LN.
5. Put the BaF_2 window containing the frozen dissected sample inside a petri dish and place it in a -80^{o}C freezer for 2 hours. Transfer the dish to a -20^{o}C for another 2 hours.
6. Freeze-dry using a LABCONCO freeze dryer for about 20 h.
   The dryer needs to be turned on about 10 min prior to the start of the experiment to allow for correct temperature adjustment. The compressor automatically turns on when the temperature reaches – 40^{o}C, after which the vacuum pump needs to be manually started. Place the sample in the flask attached to the freezer port for overnight drying with a stepwise increase in temperature (-40^{o}C to 25^{o}C). This process can be initiated once pressure is below to 133 x 10^{-3} mBar.
7. In the morning, the frozen sample was taken out from the chamber placing it inside a desiccator until imaging.

2.3.2 PFA fixation and embedding of whole animal protocol

- **Rationale**

As an alternative to freeze-drying, whole worms were fixed and embedded in a two-step process, first in agarose then in plastic resin. Samples were prepared by

sectioning and processed to remove the resin.

- **Procedure**

Worms were anaesthetized in 2 mM levamisole, fixed in 4% paraformaldehyde and immobilized in agarose blocks (approximately 3 x 3 x 3 mm). After a series of dehydration steps with ethanol, the agarose blocks were infiltrated and embedded in resin. Embedded samples were incubated at 4^oC overnight for curing, removed from the mold and sectioned with the microtome at 10 μm thickness at room temperature.

- **Reagents**

PBS buffer:

80g NaCl

2g KCl

14.4g Na2HPO4

2.4g KH2PO4

Dissolve in 800 ml of H_2O

Adjust pH to 7.4 with HCl

Bring volume to 1 litre and autoclave

Infiltrating solution:

Add 1.25 g of Benzoyl Peroxide (catalyst) into 100 ml of JB-4 Solution A resin. Mix in a 100 ml conical tube using a stir plate at room temperature for 20 minutes or until dissolved. Store at 4^o C in the dark.

Embedding Mixture:

To embed, make a fresh infiltration solution by mixing 1 ml of JB-4 Solution B with 25 ml of infiltration solution in a 50 ml conical tube by using a plastic pipette. This mixture will begin to solidify quickly and maintain on ice until needed.

- **Protocol**

Embedding in agar:

1. Wash live worms off the culture plate.
2. Anaesthetize live worms with 2mM levamisole and fix with 4% paraformaldehyde (PFA).
3. Embed worms in 2% agar, positioning them close together.
4. Cut out agar containing worms into small cubes of approximately 3 x 3 x 3 mm with a razor blade.

Dehydratation:

1. Before beginning the embedding procedure, dehydrate the agarose blocks containing the worms in ascending concentrations of ethanol using a step-wise series at room temperature as follows: 95% PBS/5% ethanol for 10 min, 75% PBS/25% ethanol for 5 min, 50% PBS/50% ethanol for 5 min – 25% PBS/75% ethanol for 5 min and 100% ethanol for 1 min.
2. After the last wash of 100% ethanol, quickly rinse the blocks twice in EtOH and proceed directly to the infiltration step.

Infiltration and embedding:

1. Drop the dehydrated blocks in a tube with 1 ml of infiltration solution and incubate at 4^oC for around 24 hours with one solution change in the middle.
2. Transfer the agarose blocks into embedding molds and add embedding solution.
3. Put the mold tray on top of ice in a sealed foam box and incubate foam box at 4^oC overnight for curing.
4. Remove samples from the mold for sectioning at 10 μm thickness with the microtome at a later date at room temperature.
5. Place the section sample in the desiccator until the measurement.

2.3.3 Hydrate samples on D_2O (heavy water) protocol

- **Rationale**

  Completely removing water in the two protocols above come with adverse consequences to tissue integrity and chemistry. A hydrated protocol that minimizes water contribution to FTIR spectra was therefore also considered. In this protocol, heavy water was used to quickly prepare dissected oocytes for immediate imaging. As indicated below, this protocol resulted in the best quality spectra of the attempts made.

- **Procedure**

  Worms were dissected in heavy water. Extruded gonads were separated from the carcasses and moved onto a 13 mm x 1 mm BaF_2 polished window. A second window was placed on top of the sample with the appropriate 6 - 15 μm Mylar spacer and the assembly was sealed in a microscope sample holder that was developed in CLS to avoid desiccation.

- **Protocol**

  1. Transfer live nematodes into heavy water droplets on glass slides.
  2. Quickly sever heads using a blade under the stereomicroscope.
  3. Transfer extruded gonads onto a 13 mm x 1 mm BaF_2 polished windows.
  4. Add second window on top of the sample with appropriate 6 - 15 μm Mylar spacer
  5. Assemble in a microscope sample holder that was developed in CLS to avoid desiccation.
  6. Image immediately after.

In FTIR measurements with transmission mode, sample thickness is a critical parameter in determining the quality of spectra. Typically, a thin sample, between 5 and 30 μm thick, is used (Miller & Dumas, 2006). Thick samples can lead to, excessive absorption

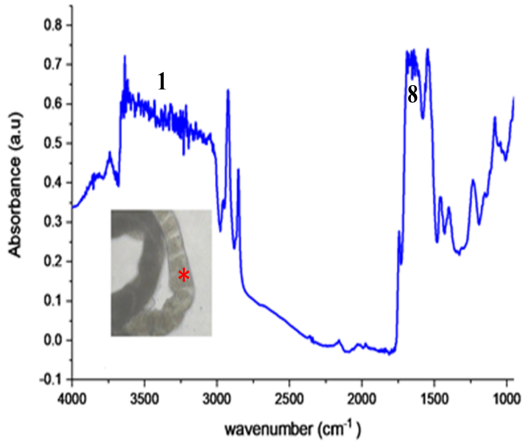

(a) living in water with 15 μm spacer

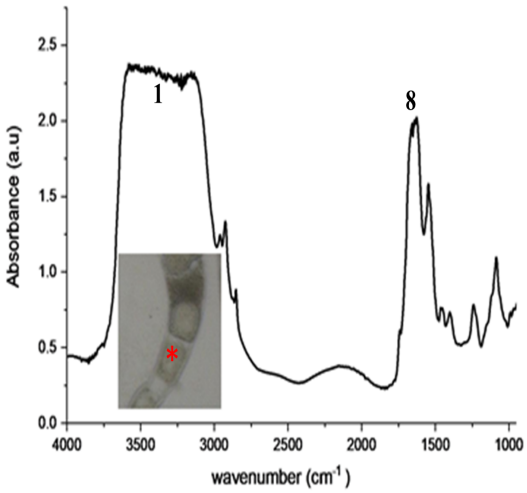

(b) living in water with 10 μm spacer

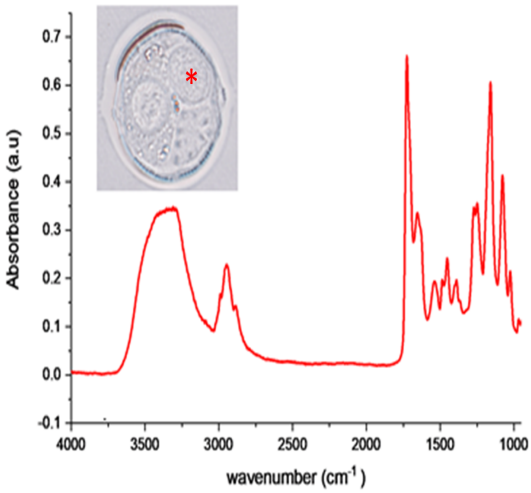

(c) chemical fixation

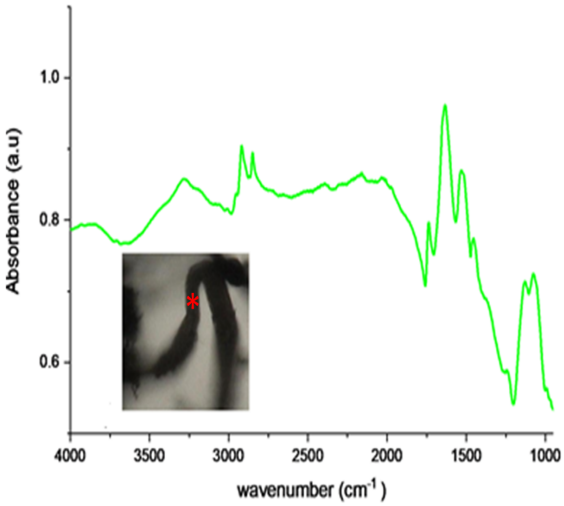

(d) freeze dryed

Figure 2.1: Extracted IR absorption spectrum of cytoplasm of oocytes from a) dissected nematodes in water with 15 μm spacer b) dissected nematodes in water with 10 μm spacer c) representative section of fixed, dehydrated, embedded whole nematode samples d) representative image of freeze dried dissected samples. (asterick indicates the selected region from which the spectrum was taken with single point measurement).

in the IR beam or intensity of resultant absorbance bands in some spectral regions, specifically in Amide I regions (Jackson & Mantsch, 2006).

As mentioned above, an important drawback of using live cells in FTIR analysis concerns the amount of water generally present in biological samples. The thicker the sample, generally the more water it will carry, further complicating the analysis. Nevertheless, Moss et al (2005) reported good quality spectra from single cells in a demountable sample cell with a 15 μm thick Teflon spacer between two CaF_2 (Calcium Fluoride) windows. As an initial test to image live *C. elegans* oocytes, a similar protocol was used. *C. elegans* gonads were dissected in liquid media (M9 buffer), and oocytes transferred into demountable liquid cells with 15 μm Mylar spacer and mounted between two CaF_2 windows. As illustrated in Figure 2.1.a, the sample spectra using M9 buffer as vehicle resulted in strong water interference in the the Amide I (see # 8 in Figure 2.1.a) and Amide A (see # 1 in Figure 2.1.a). To mitigate this problem, thinner spacers were used to further reduce water in the samples in accordance to published (Jackson & Mantsch, 2006). Tobin et al (2010) revealed that the use of the 9 μm spacer reduced the level of water absorption in the Amide I region to a level that the Amide I and II and ester carbonyl absorption bands could routinely be observed in rapidly acquired spectra. However, the use of the 9 μm spacer did not completely remove water interference in the spectra from dissected *C. elegans* oocytes (see # 1 and # 8 in Figure 2.1.b).

To investigate possible water-free alternative methods for sample preparation, whole *C. elegans* were embedded in resin for sectioning. Worms were first anaesthetized and fixed in 4% PFA before embedding in melted agarose to preserve the physical integrity of the sample during sectioning. Samples were cooled on ice for 20 minutes to allow for agarose to solidify. After solidification, the agarose blocks containing the worms were dehydrated in ascending concentration (5%, 25%, 50%, 75%, and 100%) of ethanol at room temperature and later infiltrated with an infiltration solution for replacing the dehydrating fluid with plastic resin. Though this improved water absorption issues, the embedding process considerably altered the cellular chemistry as determined in IR spectra collected. These spectra show strong IR absorptions bands in the region between 1500 and 950 cm^{-1} that probably reflect the embedding matrix composition rather than the biological sample itself

(Figure 2.1.c). In addition, dehydration using ethanol removes lipids and denatures proteins, likely altering the ability to properly quantify these macromolecules in cells (Gazi et al., 2005; Jackson & Mantsch, 2006; Kiernan, 1981). Overall, though fixation and embedding of worms resulted in clear spectra, the biological significance of the absorbance information extracted from these experiments is arguable.

A method to physically remove water molecules from samples is to freeze dissected gonads using liquid nitrogen followed by vacuum drying overnight. Prior to freeze-drying, cryopreservation using cryoprotectant and liquid nitrogen are used to minimize subsequent cell damage due to water sublimation. However, this protocol caused severe structural damage to oocytes (Figure 2.1.d). These changes included tissue shrinkage, cracking and other morphological alterations. This is likely the result of water loss disrupting cell and tissue integrity. Considering the drawbacks associate with chemically or physically removing water from samples, the suitability of overcoming the issues related to the overlap of the water bending mode with the protein Amide I region using heavy water (D_2O) was assessed. Essentially, D_2O replaces the hydrogen atoms in the water molecule with deuterium. The use of D_2O in place of H_2O has been shown to shift down the water-related bands at 3360 and 1643 cm^{-1} to around 2740 cm^{-1} (see # I in Figure 2.2.a) and 1210 cm^{-1} (see # II in Figure 2.2.a) respectively (Fabian & Schultz, 2006). Indeed, when D_2O was used instead of M9 buffer in dissected samples, IR bands at lower wavenumbers than those of regular water were observed (see results below, Figure 2.2). The use of D_2O to prepare untreated dissected gonads using the mounted set up developed by the CLS was ultimately adopted as the standard protocol to collect all spectra presented hereon, as it allowed for the use of fresh, untreated cells and implicated in little water interference, facilitating the analysis of spectra information.

2.4 Spectrum manipulation

Following spectra acquisition and prior to spectral analysis, data was pre-processed to correct for noise, sloping baseline effects, difference in sample thickness and to select the regions of interest. This data pre-processing as described in the following sections is carried

out to improve the spectral features in order to facilitate spectral interpretation and analysis.

2.4.1 Normalization

In order to compare spectra from different samples, the spectra must be normalized using relatively unchanging and stable bands between different samples. In the OPUS software, there are three different spectral normalization methods:

Min-Max normalization: This method was set up to shift the spectrum in such a way that the minimum absorbance y-value becomes zero and the maximum absorbance y-value is expanded in the y-direction to 2 absorbance units.

Vector normalization: The vector normalization is carried out in the following way:

1- Calculate the average y-value of the absorbance of the spectrum: y_m

2- Subtract the average value from the spectrum so that the middle of the spectrum is pulled down to around y=0: $\tilde{y}_k$

3- Calculate the sum of the squares of all $\tilde{y}_k$ - values.

4- Divide the spectrum by the square root of this sum and therefore, the vector norm of the resulting spectrum is always 1.

Offset correction: This method was used to shift the spectrum in such way that the minimum occurring y-value is set to an extinction zero.

Normalization is applied to scale the spectra and to remove changes accountable by the sample thickness or concentration so that different sample spectra can be directly compared. In this study, the Min-Max normalisation was used to normalize the spectra in which the intensity is positive in the whole range. As a comparison, the intensity is negative in the vector normalization. In addition, the vector normalisation is not useful in calculating metabolites such as integration and ratios of intensity. Therefore, in this study, the spectra were normalised to the Min-Max intensity or area of a peak expected to be constant between samples.

A number of bands such as Amide I, Amide II and the CH_2 asymmetric stretching

band in biological samples are often used as internal standards for normalization. This method is feasible if any of these bands are stable and consistent across the specimens. In aqueous sample, the Amide I band is not recommended to be used for normalizing the spectra since it overlaps with the absorption band of water and the water content can vary between samples. In addition, preliminary work indicated that lipid and protein contents vary significantly in aging *C. elegans* oocytes. Therefore, Amide I or Amide II or CH_2 asymmetric bands were not used for normalization. Signals that do not change significantly appear usually at low frequencies in the region between 1500 - 1200 cm^{-1}. The band in this region is mainly due to symmetric stretching vibrations of the COO^- functional groups with a little wagging vibration of CH_2 and CH_3. This band shows weak IR absorption. In this study, the band between 1421 and 1357 cm^{-1} was therefore chosen to be used to normalize the spectra.

2.4.2 First or Second Derivatives

The first and second derivative spectra are taken to minimize the baseline effects due to scattering and background effects in the spectra, resolve overlapping peaks and amplify spectral curvature. The first derivative eliminates the baseline effects (offset), resolving the broad overlapping band of raw spectra but in the process adding a straight line with a constant slope to the original spectra. Therefore, the calculation of the first derivative is not appropriate for determining quantitative assignments. The slope can be removed by the second derivative which is more useful for spectral interpretation as it gives a negative peak for each band with the same wavelength as in the original spectra and shoulder in the absorption spectrum (Rinnan et al., 2009). In addition, the calculation of the second derivative enhances the sharp lines in complex spectra since the band intensity of the second derivative is inversely proportional to the square of the original band half-width.

The first and second derivative spectra are calculated from the raw absorbance spectrum using the Savitzky-Golay algorithm with a 17-point window involved in the OPUS software. The Figure 2.2 shows a typical raw spectrum (panel a) and its corresponding first (panel b) and second derivative spectra (panel c) in the cytoplasm of mature oocytes in

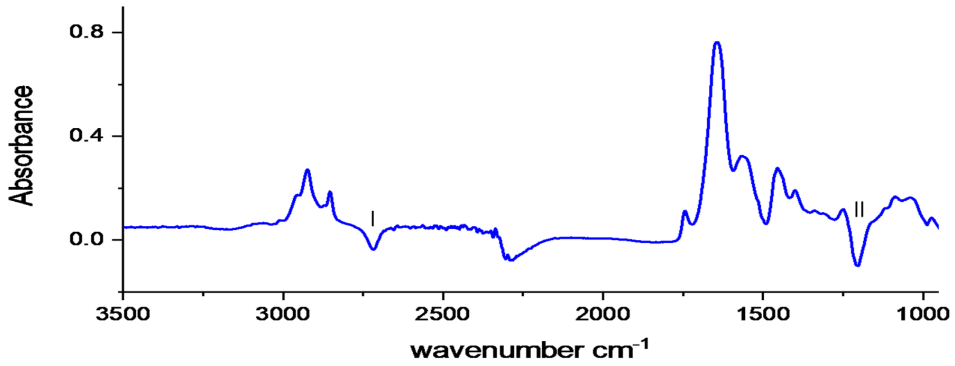

(a)

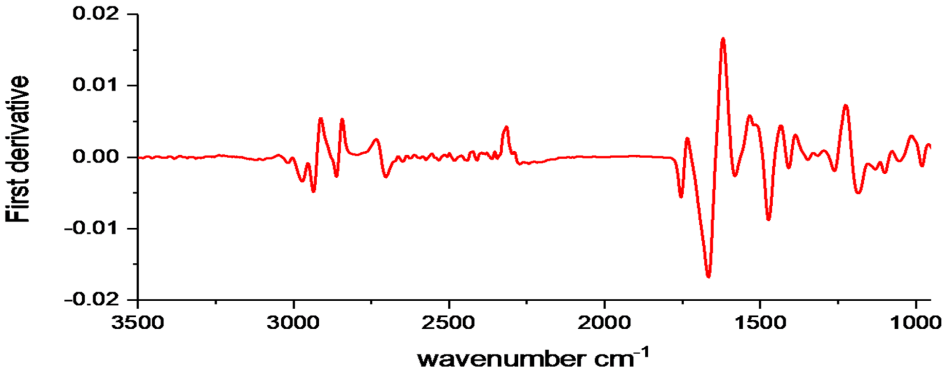

(b)

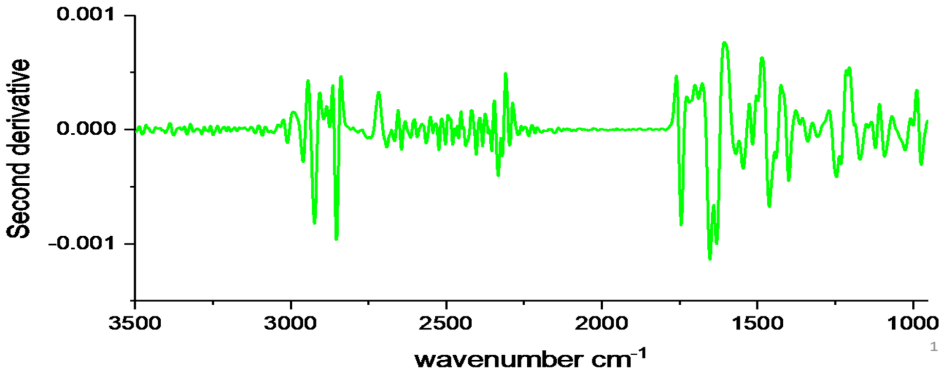

(c)

Figure 2.2: Average extracted IR absorption spectrum of cytoplasm of -1 oocytes from an adult wild type nematode (a) and its first (b) and second (c) derivative transformations. The developed protocol with D_2O hydratation was used.

young wild-type nematodes in the mid-IR region between 4000 to 900 cm^{-1}. The region 4000 to 3100 cm^{-1} represents O-H stretching vibration of hydroxyl groups (Smith, 1999). The regions between 3050 to 2800 cm^{-1} shows the asymmetric and symmetric stretching vibration of C-H groups in methylene groups of long chains fatty acids (Andrus & Strickland, 1998; Fabian et al., 1995; Wu et al., 2001; Yoshida et al., 1997), while the region between 1770 to 1720 cm^{-1} is associated with C=O stretching of carbonyl group esters (Fabian et al., 1995; Wolkers et al., 1998; Wu et al., 2001). As mentioned above, the region between 1700 and 1500 cm^{-1} carries contribution from proteins, and has two primary features, the Amide I (1700 - 1600 cm^{-1}) and Amide II (1600 - 1500 cm-1) bands (Kong & Yu, 2007; Subramanian et al., 2009). Moreover, absorption in the region between 1500 and 1250 cm^{-1} is due to O-C-H, C-C-H and C-O-H bending vibrations associated with amino acids, aliphatic chain of fatty acids and amide III. The region between 1250 and 950 cm^{-1} is associated with contributions from phosphodiester groups of phospholipids and C=O absorption of glycogen and other carbohydrates (Fabian et al., 1995; Fung et al., 1996; Huleihel et al., 2002; Mordechai et al., 2004). Table 2.2 presents a summary of the band positions in the secondary derivative spectra and their biological origins.

2.5 Sample preparation for FTIR microspectroscopy

For all FTIR experiments, approximately 30 animals from synchronized populations were transferred onto M9/D_2O droplets and placed on glass slide. M9/D2O was freshly prepared by adding 900 μl of D_2O to 100 μl of M9 buffer. D_2O was used to minimize spectral absorbance of some specific H_2O vibrational modes at $\sim$ 3285 cm^{-1} and $\sim$ 1640 cm^{-1}, as discussed above (Bertie et al., 1989; Bertie & Lan, 1996). The heads were then quickly cut under the stereomicroscope using two syringe needles (gauge 30) which forces gonads and the intestine out of the carcass. Dissected gonad suspension of 50 μl (containing extruded gonads, embryos and carcasses) were carefully transferred into the centre of a BaF_2 window and a second window (Crystran, Poole, UK) was placed on the top of the sample using a 6 μm Mylar spacer. The assembly was sealed in a sample holder developed at the Canadian Light Source (CLS) to avoid desiccation (Figure 2.3). All

Band number	Peak position on FTIR spectra per cm	Assignment of bonds
1	3200	N-H stretching of Amide A in proteins
2	3010	olefinic = C-H stretching vibration: unsaturated lipids, cholesterol esters
3	2970	CH_3 asymmetric stretching: equal contribution from lipids, protein side chains with some contribution from carbohydrates
4	2930	CH_2 asymmetric stretching: mainly lipids with little contribution of proteins and carbohydrates
5	2875	CH_3 asymmetric stretching: mainly protein side chains with a little contribution from lipids and carbohydrates
6	2850	CH_2 asymmetric stretching: mainly lipids with little contribution of proteins and carbohydrates
7	1745	carbonyl groups (C = O): C = O ester stretch from phospholipids, triglycerides,and cholesterol esters

Table 2.2: General band assignments of absorbance IR spectrum of *C. elegans* oocytes

Band number	Peak position on FTIR spectra per cm	Assignment of bonds
8	1700 -1600	Amide I band (protein C = O stretching)
9	1690	Amide I of random coils and β-turn structure of proteins
10	1655	Amide I of α-helical structure of proteins
11	1630	Amide I of β-sheet structure of proteins
12	1600 - 1500	Amide II band (protein N-H bend, C-N stretch)
13	1500 - 1300	COO - symmetric stretching from fatty acids and amino acids CH_3 symmetric bending from lipids CH_2 wagging from phospholipids, fatty acids, triglycerides and amino acids side chain
14	1300 -1240	Amide III band components of proteins
15	1150 - 950	C - O -C , C-O dominated by ring vibrations in various polysaccharides (asymmetric stretching from glycogen)
16	1090	PO_2^- symmetric stretching in phospholipids
17	1023	glycogen

Table 2.2 (following): General band assignements of absorbance IR spectrum of *C. elegans* oocytes

reagents were purchased from Sigma-Aldrich.

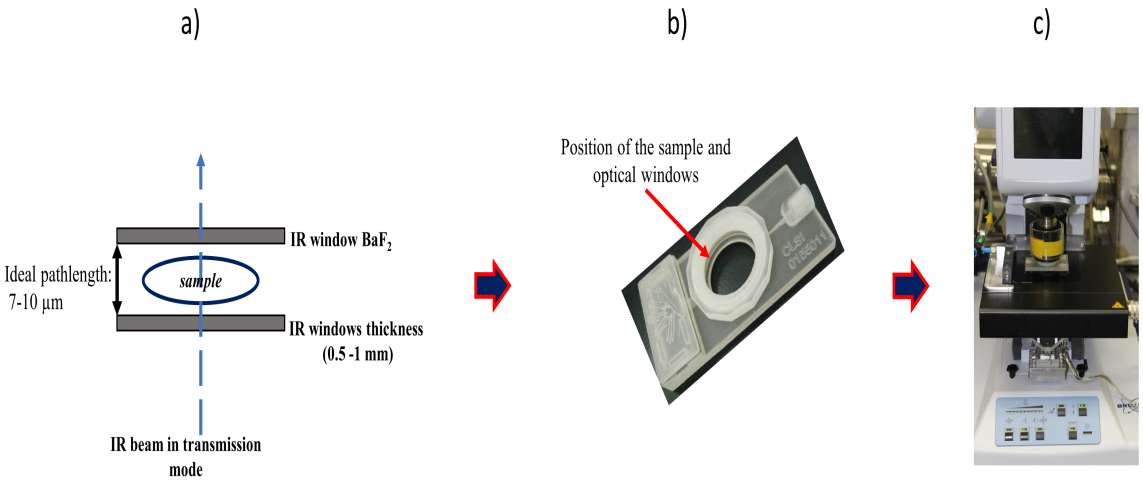

Figure 2.3: (a) Schematic representation of the BaF_2 cell used for dissected *C. elegans* imaging, (b) sample holder developed at CLS for IR measurement of living cells in aqueous media, (c) assembled cell in place on a Bruker microscope.

2.6 FTIR microspectroscopy imaging

FTIR microspectroscopy measurements of dissected *C. elegans* were taken in a Bruker Hyperion 3000 imaging microscope, coupled to a Bruker vertex 70v/s spectrometer (Bruker Optics, USA) equipped with a liquid nitrogen cooled MCT (Mercury - Cadmium-Telluride) 64 x 64 Focal Plane Array (FPA) detector. Spectral images of samples were collected at a spectral resolution of 4 cm^{-1} in the spectral range between 4000 and 800 cm^{-1} using a 15x objective at room temperature. This setup acquires simultaneous spectral data from a 170 x 170 μm^2 sample area for unit image with a pixel size of 2.65 x 2.65 (170/64) μm^2 (Figure 2.4). As such, total 4096 spectra were obtained from each selected area taken in approximately 2 min and the average spectrum from the interest area was then used for each sample to calculate the spectral parameters. All image spectra were collected in transmission mode with 128 scans. Prior to recording the sample images, background spectra were collected at a nearby empty spot containing only liquid medium and subtracted

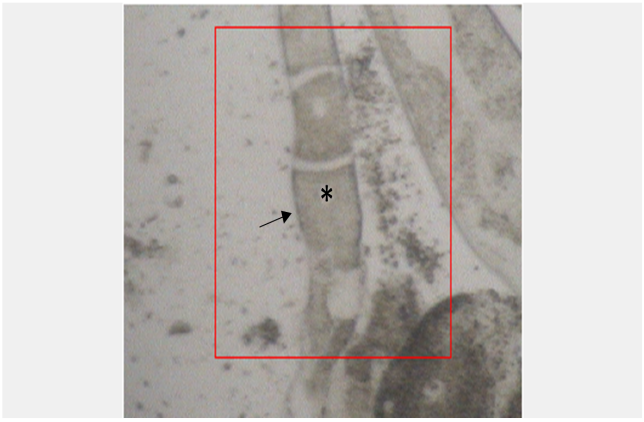

(a)

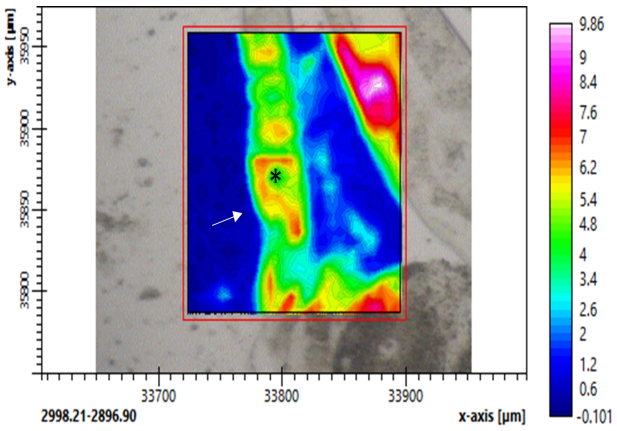

(b)

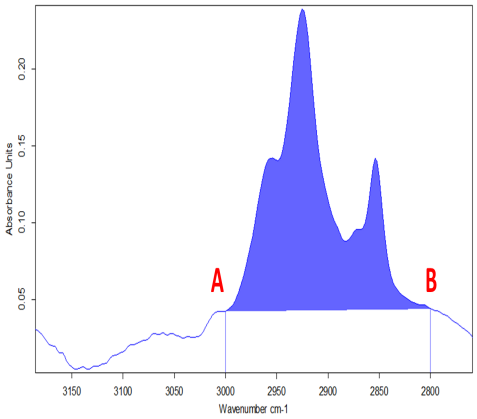

(c)

Figure 2.4: (a) Optical image and (b) its corresponding FPA-FTIR image of a gonad dissected from a young (reproductive age) wild-type nematodes, (c) this FTIR image was obtained by integrating the area under the lipid bands (3000 - 2800 cm^{-1}). Arrows indicate the cytoplasm and asterick the nucleus of the mature, -1 oocyte, from which spectra were taken throughout this work

automatically from the spectra of nematode sample by auto-image software (OPUS version 7.0). FTIR measurements were performed at the CLS 01B1-01 (Mid-IR) facility using a conventional globar source.

2.7 FTIR data analysis

All data processing and image generation were carried out using the Bruker software (OPUS version 7.0). At least 3 images were taken per genotype and the measurement was repeated twice in two separate occasions. About 20 spectra were extracted and averaged from the cytoplasm of each cell imaged to obtain a representative spectrum of that cell.

All raw spectra were first normalized in the region between 1421 and 1357 cm^{-1} and after normalization, the raw spectra were transformed to their second derivatives using Savitzky-Golay function with 13 smoothing points.

Spectral analysis was conducted in the rage between 4000 and 950 cm^{-1}, with particular focus on the lipid region (2800 - 3000 cm^{-1} and 1770 - 1720 cm^{-1}), Amide I region (1700 - 1600 cm^{-1}) and carbohydrate region (1150 - 950 cm^{-1}).

The C-H region is informative for lipid analysis because it includes significant vibrations from acyl chains. The C-H region is characterised by CH_2, CH_3 asymmetric and symmetric stretching bands. The area under these bands was calculated to give information about the concentration of the corresponding functional groups. To determine the change in lipid contents in the system, the area associates specifically with lipid bands (CH_2 asymmetric and CH_2 symmetric) were calculated. The ratio of these lipid-specific bands (CH_2 asymmetric and symmetric stretching) to the CH_3 asymmetric band were evaluated, since CH_3 asymmetric band at the end of long chain fatty acids is originated from proteins also. The use of these bands to evaluate lipid content has been reported in a number of studies (Bozkurt et al., 2010; Elibol-Can et al., 2011; Forfang et al., 2017; Kumar et al., 2017). In FTIR spectroscopy, this ratio of the area between the methylene and methyl bands can be used as an index of the lipid chain lengths present in the system (Ami et al., 2011; Gasper et al., 2009). This ratio also has been used to investigate the oxidative stress

effects on cells and to quantify the lipid content in malignant tissues (Gazi et al., 2004; Lipiec et al., 2014; Petibois & Déléris, 2005, 2006). Finally, the ratio of band area between CH_2 symmetric to CH_3 asymmetric provides information about the variation in lipid synthesis (Bozkurt et al., 2010).

The other important peak relevant for the lipid analysis at 1740 cm^{-1} is assigned to C=O stretches of ester functional groups originated from triglycerides, phospholipids and cholesterol esters. This band was used to quantify lipid uptake into oocytes.

The analysis of the second derivative spectra of the Amide I band was performed to determine the changes in concentrations of different protein secondary structures. The second derivative spectra were normalized in the range of 1670 to 1644 cm^{-1} assigned to α-helix band for the visual demonstration of the spectral variation. For obtaining more accurate values, the band area ratio between the β-sheet and β-turn structure to α-helices were calculated as a means to investigate changes in protein aggregation and yolk protein levels respectively. Yolk in *C. elegans* is hypothesized to be structurally similar to the mammalian LDL protein human apoB-100 (Grant & Hirsh, 1999), which has a pentapartite structure with a high β-sheet/turn content (Segrest et al., 1994). Apo-B has also been shown to have a high β-sheet and turn content by analyzing the Amide I band in FTIR studies (Krilov et al. 2009).

Finally, the band between 1150 and 950 cm^{-1} was investigated to examine the variations in glycogen (1023 cm^{-1}) and phosphate level (1080 cm^{-1}).

Statistics: All the integration was carried out in the B type integration method of OPUS for each peak. This method allowed to choose 2 points which were considered left and right of the interested band and the spectral regions for the calculation of band areas are presented in Table 2.3 (Figure 2.4.c). The band area and ratios are expressed as mean ± standard error of mean (SE).

2.8 *In vivo* yolk protein tracking

Quantification of GFP in strains *vit-2*::GFP reporter was accomplished by taking images with Delta vision Elite (GE) microscope which were captured with Softworks® (G.E./

IR bands	Integrated region (cm^{-1})
CH_3 asymmetric stretching	2970 – 2953
CH_2 asymmetric stretching	2936 – 2912
CH_2 symmetric stretching	2860 – 2844
Carbonyl (C=O) stretching	1765-1730
β sheet structures	1641-1622
α helix structures	1666-1640
β turn structures	1700 – 1680
Glycogen	1035-1014
PO_2^- symmetric	1100 – 1080

Table 2.3: Spectral regions used in calculations of band area ratios from the secondary structure spectra.

Applied Precision). Images were taken at the following condition: 40 x lens, 876 x 876 pixels resolution, and 1.5 ms exposure time with brightfield and fluorescence using the FITC filter set (Excitation bandpass 470/40 nm; Emission bandpass 525/5 nm). At least 15 worms per genotype / per age were imaged on two separate occasions to quantify the yolk protein level from -1 oocytes and results were consistent between these two different periods. For this imaging, the worms were anesthetised with the 20 μl of 2mM levamisole and mounted on slides with 2% agarose pads.

After image acquisition, the quantification of *vit-2*::GFP intensity was performed using ImageJ. Briefly, 2 to 3 different areas in the cytoplasm of -1 oocytes were selected for measurement in each image. Fluorescence intensity for each cell was calculated by measuring the average integrated intensity of these selected regions and subtracting this value to its corresponding background signal values. Background signals were collected from regions outside the gonads, in the pseudocoelom of the same samples. At least 15 oocytes per genotype / per age were used for each analysis.

2.9 Yolk lipid staining

Research from the model organism *C. elegans* pointed to a connection between lipid metabolism and aging. These studies have applied several staining techniques to probe lipid content in whole organisms. Dye specificity, reproducibility and delivery to tissues have presented some problems and generated controversial results. The lipophilic dye Nile Red has been extensively used in mammalian cells to visualized lipid droplets (Genicot et al., 2005; Greenspan et al., 1985). In agreement with results in other biological samples, Nile Red signals in the intestine of live *C. elegans* were previously interpreted as indicative of fat stores (Asharafi et al, 2003). Subsequent work in *C. elegans*, however, clarified that Nile Red marks instead the content of lysosome-related organelles (LROs) and not lipid granules in unfixed samples worms (O'Rourke et al, 2009; Schroeder et al, 2007). In fixed samples, as indicated by co-localization with Oil Red, another lipophilic dye, Nile Red does produce the expected staining patterns consistent with lipid stores (Brooks et al. 2009; O'Rourke et al., 2009; Pino et al. 2013; Wahlby et al. 2014). The reasons why this dye shows different chemical affinities

in live and fixed *C. elegans* tissues are not fully understood. Furthermore, Nile Red only weakly stains other lipid-rich tissue of live *C. elegans* such as the gonads, suggesting it is not an ideal dye for germ line studies (Jones et al., 2009). Sudan Black, another alternative lipid-staining dye, can be used in fixed tissues to reveal intestine lipid droplets as well as germline and epidermal lipid content, but staining with this dye is inconsistent, partially because of the need to ethanol wash residual dye from the sample after staining (O'Rourke et al, 2009). BODIPY is a different family of vital dyes that have also been used as lipid tracers. Specifically, BODIPY 493/503 is a green fluorescence neutral lipid stain which has been used as a dye to investigate lipid droplets in bovine and mouse oocytes (Aardema et al., 2011; Yang et al., 2010). BODIPY 493/503, was recently reported to stain live *C. elegans* cells where it associates with lipid droplets after a short incubation time. The BODIPY 493/503 staining profile corresponds with lipid stores visualized by Coherent Anti-Stokes Raman Scattering (CARS) microscopy, particularly in the gonad and embryos (Klapper et al., 2011). CARS has been used to monitor *C. elegans* lipid stores in label-free animals (Folick et al., 2011; Hellerer et al., 2007; Yen et al., 2010). Because of its correspondence in signal detection with lipids peaks in spectroscopic analysis, BODIPY 493/503 was used as a complementary method to FTIR microspectroscopy to detect and quantify lipid stores in *C. elegans* oocytes.

2.9.1 BODIPY Staining protocol

BODIPY 493/503 (Sigma-Aldrich) staining was used to detect neutral lipid stores in live *C. elegans* oocytes as previously described (Klapper et al., 2011). 25 to 30 worms from synchronized populations were placed in 80 μl of a 6.7 μg/ml BODIPY 493/503 M9 solution on a slide and incubated in a humid chamber for 20 min in the dark at room temperature. After the incubation, worms were carefully collected and washed three times in M9 buffer. For imaging, worms were immediately mounted on slides with 2% agarose pads, immobilized in 20 μl of 2 mM levamisole and mounted. A Delta vision Elite (GE) microscope was used for imaging the mounted samples. Images of GFP expressing worms were captured with Softworks® (G.E./ Applied Precision). Standard conditions were: 40x lens, 876 x 876 pixels resolution, 1.5 ms exposure time. Brightfield and fluorescence images

were taken using the FITC filter set (Excitation bandpass 470/40; Emission bandpass 525/50). At least 15 worms per genotype / per age were imaged on two separate occasions to quantify the BODIPY 493/503 staining intensities from -1 oocytes and results were consistent between these two different periods. Quantification of BODIPY 493/503 fluorescence intensity was performed using ImageJ. Briefly, 2 to 3 different areas in the cytoplasm of -1 oocytes were selected for measurement in each image. Fluorescence intensity for each cell was calculated by measuring the average integrated intensity of these selected regions and subtracting this value to its corresponding background signal values. Background signals were collected from regions outside the gonads, in the pseudocoelom of the same samples. At least 15 oocytes per genotype / per age were used for each analysis.

Chapter 3
RESULTS

3.1 Biochemical profiling of aging wild-type oocytes using FTIR microspectroscopy

Mid-IR microspectroscopy was used to compare FTIR spectra of oocytes from reproductive animals with those from post-reproductive nematodes. First, the molecular landscape of aging wild-type oocytes was characterized and probed to narrow down possible informative regions in the FTIR spectra of these cells (qualitative analysis). This analysis was then followed by dissecting in more detail the band regions that showed possible age-dependent changes to arrive at a clearer map of the modifications in molecular composition of aging oocytes (quantitative analysis).

3.1.1 Qualitative analysis of age-dependent changes in the chemical profile of oocytes

As a first step to understand the general similarities and differences in the FTIR spectra of oocytes of different ages, this study concentrated in imaging wild-type cells. Spectra from young (day 3) and old (day 8) -1 oocytes dissected from adult wild-type animals were acquired and evaluated for lipids, proteins and carbohydrate signatures in order to probe whether the transition between reproductive and post-reproductive stages was accompanied by detectable differences in the amount and/or distribution of these biomolecules. Day 3 represents the peak in progeny generation when the germline shows no overt signs of aging. On day 8, wild-type animals have ceased to reproduce and their oocytes have visibly degraded, some becoming much smaller and some losing contact with

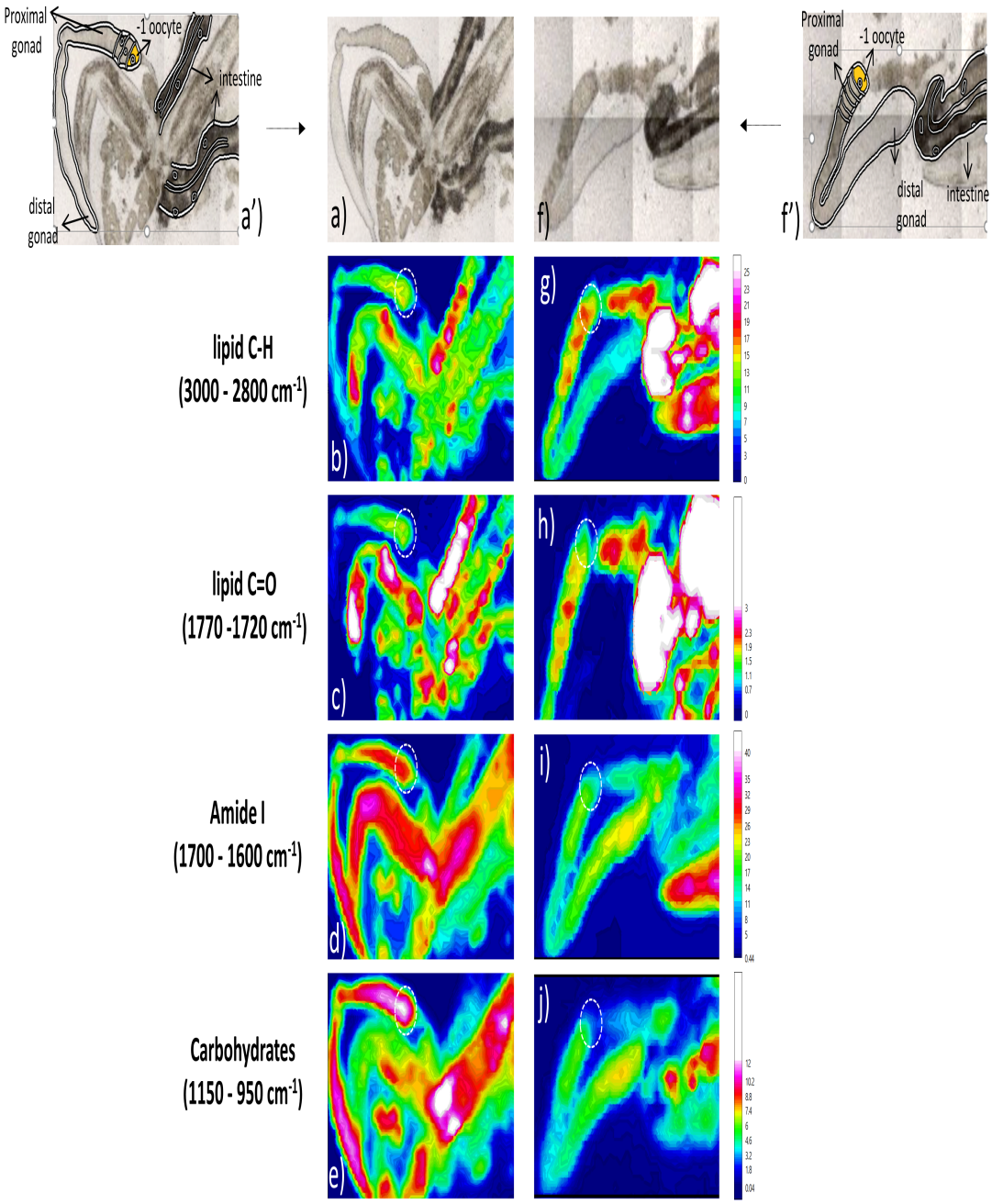

Figure 3.1: FPA-FTIR images of dissected *C.elegans* samples: (a, a') and (f, f') - visible light images of a dissected nematode identifying gonad regions and the intestine. (b) and (g) chemical maps of the integrated area of the CH stretching region (3000 - 2800 cm^{-1}); (c) and(h) chemical maps of the integrated area of the ester carbonyl band (1770 - 1720 cm^{-1}); (d) and (i) chemical maps of the integrated area of the Amide I band (1700 - 1600 cm^{-1}); (e) and (j) chemical map of the integrated area of the carbohydrate area (1150 - 950 cm^{-1}) from reproductive in the left and in the right post-reproductive wild-type nematodes. Corresponding heatmap scale bars for each image pair is depicted on the right. The -1-oocyte region is the FPA-FTIR images is encircled. The -1 oocyte is painted in yellow in (a') and (f') panels to facilitate its identification in the other panels.

their neighbors (Luo et al., 2009).

Figure 3.1 shows a series of images from single representative dissected gonads of a reproductively active wild-type nematode on the left (panels a to e) and a gonad from a post-reproductive worm on the right (panels f to j). For clarification purposes, the gonads, -1 oocyte position (colored in yellow) and intestines are indicated in the bright field images on the top left (a' and f' panels). The -1 oocyte is encircled in the FTIR heat (chemical) maps to facilitate the identification of the region of interest for this work. The remaining tissue in these samples correspond to the carcass, notably the cuticle of the head and tail regions that resulted from the dissection process. Notice that intestines appear darker in bright field images (panels a and f), due to the high lipid content in the cytoplasm of these cells, as attested by the FTIR heatmaps (compare panels b-g and c-h, as indicated below). Corresponding FTIR-generated images representing the distribution of biomolecules using false colors are shown where the areas coloured in white/pink indicate high concentrations whereas areas with reduced concentrations are visualized in darker hues (see color coded scale bar on the right). Overall, the FTIR-FPA images show remarkable differences between young and aged gonads. Particularly, lipid content appears higher in distal gonad regions and intestines of post-reproductive nematodes compared to samples from reproductive nematodes, as suggested by the lipid C-H stretching band of the FTIR absorbance spectra between 3000 and 2800 cm^{-1} (Figure 3.1.b and g). This lipid accumulation in the FTIR image from reproductive to post-reproductive nematodes correlate with the darker areas observed in the visible image. The chemical maps of the integrated area under the C=O stretching band of FTIR absorbance spectra between 1770 and 1720 cm^{-1}, associated with presence of ester carbonyl band, are also consistent with an increase in lipid contents in aged gonads and intestine (panels c and h). Conversely, FTIR signatures associated with proteins show the opposite pattern. As seen in panels (d) and (i), which represent the chemical maps of the integrated area of the Amide I band of FTIR absorbance spectra between 1700 and 1600 cm^{-1}, there appears to be a considerable reduction in signal intensity from reproductive to post-reproductive gonads as well as intestines. This is similar to what is observed for carbohydrates, as suggested by the integrated area between 1150 and 950 cm^{-1} (panels e and j). In view of these observations,

it was hypothesized that discrete changes in relative contents of lipids, proteins and carbohydrates could underlie the process of oocytes aging in *C. elegans*.

3.1.2 Quantitative analysis of age-dependent changes in the chemical profile of oocytes

The FTIR-FPA images in Figure 3.1 confirmed the possibility that *C. elegans* tissues considerably change their biochemical make up in the span of only 5 days, a time early in the *C. elegans* adult life that coincides with the entirety of its reproductive span. It is possible, therefore, that these changes reflect the cellular and molecular that characterize reproductive aging in the gonad. To validate these observations and arrive at a quantitative measurement of the changes in molecular composition of oocytes, the following set of FTIR imaging experiments concentrated in the cytoplasm of the most developed oocyte in the -1 position (Figure 3.1) in the gonad, next to the spermatheca (n=6 for each genotype in each age group). The information from oocytes of reproductive and post-reproductive nematodes were then compared to determine the changes that could potentially be associated with a decline in oocyte quality overtime.

Figure 3.2 shows typical average spectra in the range of 3050 to 950 cm^{-1} extracted from the cytoplasm of young (blue line) and old (red line) wild-type oocytes without (left) and with (right) normalization with respect to the band between 1421 and 1357 cm^{-1}, in order to minimize the variability in cell density and to correct for differences in path length of the IR beam. Overall, these spectra show a similar shape but under a more thorough examination they reveal important differences in terms of specific band intensities that are consistent with the findings identified in FTIR-FPA images described in Figure 3.1. To address these differences in more detail, the analysis concentrated on four different spectral ranges: C-H region (3050 to 2800 cm^{-1}), C=O region (1770 - 1720 cm^{-1}), related to lipid band also), Amide I region (1700 to 1600 cm^{-1}, corresponding to protein bands) and the carbohydrate region (1150 to 950 cm^{-1}). The analysis of these spectral regions is reported below.

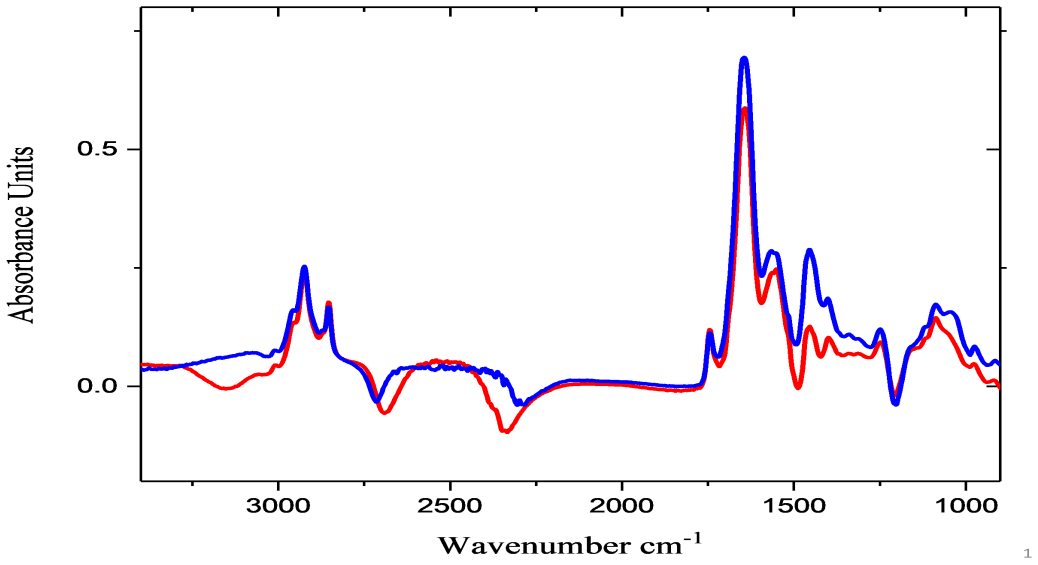

(a)

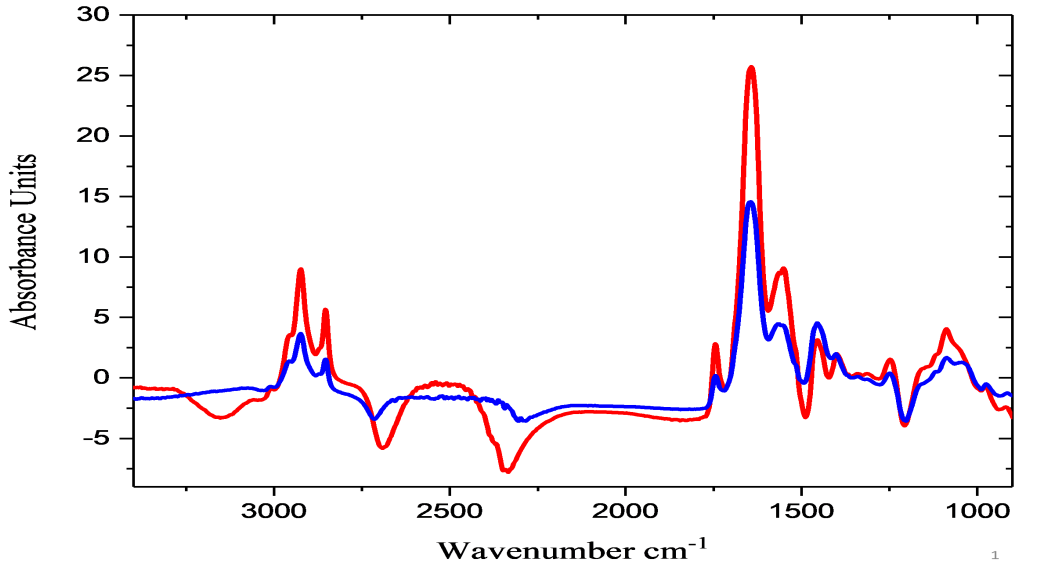

(b)

Wild type (N2)
young (reproductive)
old (post-reproductive)

Figure 3.2: Comparison of an extracted IR absorption spectra from the cytoplasm of oocytes from reproductive (young, day 3 of adulthood, shown in blue) and post-reproductive (old, day 8 of adulthood, shown in red) wild-type nematodes (a) without and (b) with normalized in the region 1421 to 1357 cm^{-1}

3.1.2.1 Variations in C-H and C=O regions

Oocytes are large cells that contain significant lipid stores. Lipids play important roles in oocyte differentiation and maturation, influencing reproductive efficiency through metabolic as well as signalling functions. At the same time, lipotoxicity can result from exacerbated lipid metabolism in some situations. The C-H stretch region between 3050 to 2800 cm^{-1} gives information on acyl chain vibrations (Casal & Mantsch, 1984), and as such can be used to assess major shifts in lipid stores in cells. It is important to note that while this region is primarily impacted by lipids, there are also minor contributions from protein and carbohydrates signatures.

The FTIR spectra in Figure 3.3.a show the C-H region taken from young and old wild-type oocytes. The spectrum in this region is characterized by the asymmetric and symmetric methyl (CH_3) and methylene (CH_2) stretching vibrations from lipid acyl chains. The shapes of the C-H band between these two samples are similar, but there are differences in terms of band intensities. These changes are more clearly observed in the second derivative IR spectra shown in panels (b) and (c), in particular peaks at 2930 cm^{-1} (see peak # 4 in Figure 3.3) and 2856 cm^{-1} (see peak # 6 in Figure 3.3). To investigate the corresponding changes in concentrations that these apparent differences imply, the relevant band areas were calculated (Figure 3.4). This analysis revealed an increase in the area of the bands at 2930 cm^{-1} (see peak # 4 in Figure 3.3, CH_2 asymmetric stretching) and as in the area ratio of CH_2 asymmetric stretching to CH_3 asymmetric stretchingas wild-type oocytes transitioned from reproductive (0.42 and 3.42 respectively) to post-reproductive (0.25 and 4.85 respectively) stages (Figure 3.4.a and b) (Bozkurt et al., 2010; Elibol-Can et al., 2011; Kumar et al., 2017; Petibois & Déléris, 2006). Similarly, an increase in the area of the bands at 2856 cm^{-1} (see # 6 in Figure 3.3, CH_2 symmetric stretching) and the band area ratio of CH_2 symmetric to CH_3 asymmetric stretching was noted in old (0.64 and 3.53 respectively) as compared to young (0.25 and 2.02 respectively) oocytes (Figure 3.4. c and d) (Bozkurt et al., 2010; Elibol-Can et al., 2011).

Another important region that informs on lipid content can be observed at 1745 cm^{-1} (see # 7 in Figure 3.3.d) and represents the contribution of C=O stretching vibrations

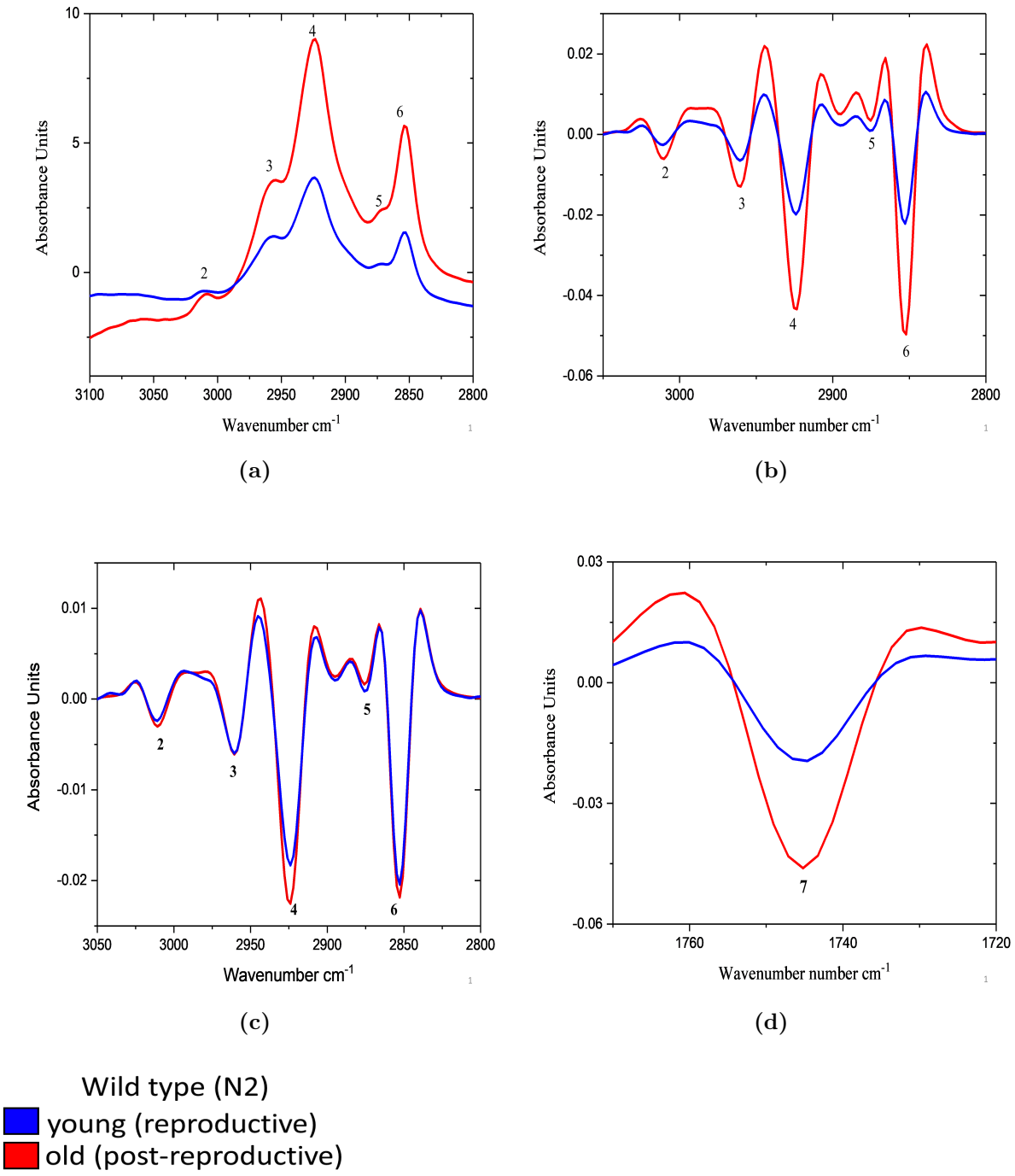

Figure 3.3: Representative IR spectra from the cytoplasm of wild-type -1 oocytes: (a) shows the spectra collected from reproductive (young, shown in blue) and post-reproductive (old, shown in red) nematodes in the region 3100 - 2800 cm^{-1}, after normalizing with the respect to the region between 1421 to 1357 cm^{-1}, (b) its corresponding second derivative FTIR spectra, (c) corresponding second derivative FTIR spectra after normalization to the CH_3 asymmetric stretching mode at 2970 cm^{-1}, and (d) in the carbonyl region 1770 - 1720 cm^{-1} after normalizing with the respect to the region between 1421 to 1357 cm^{-1}.

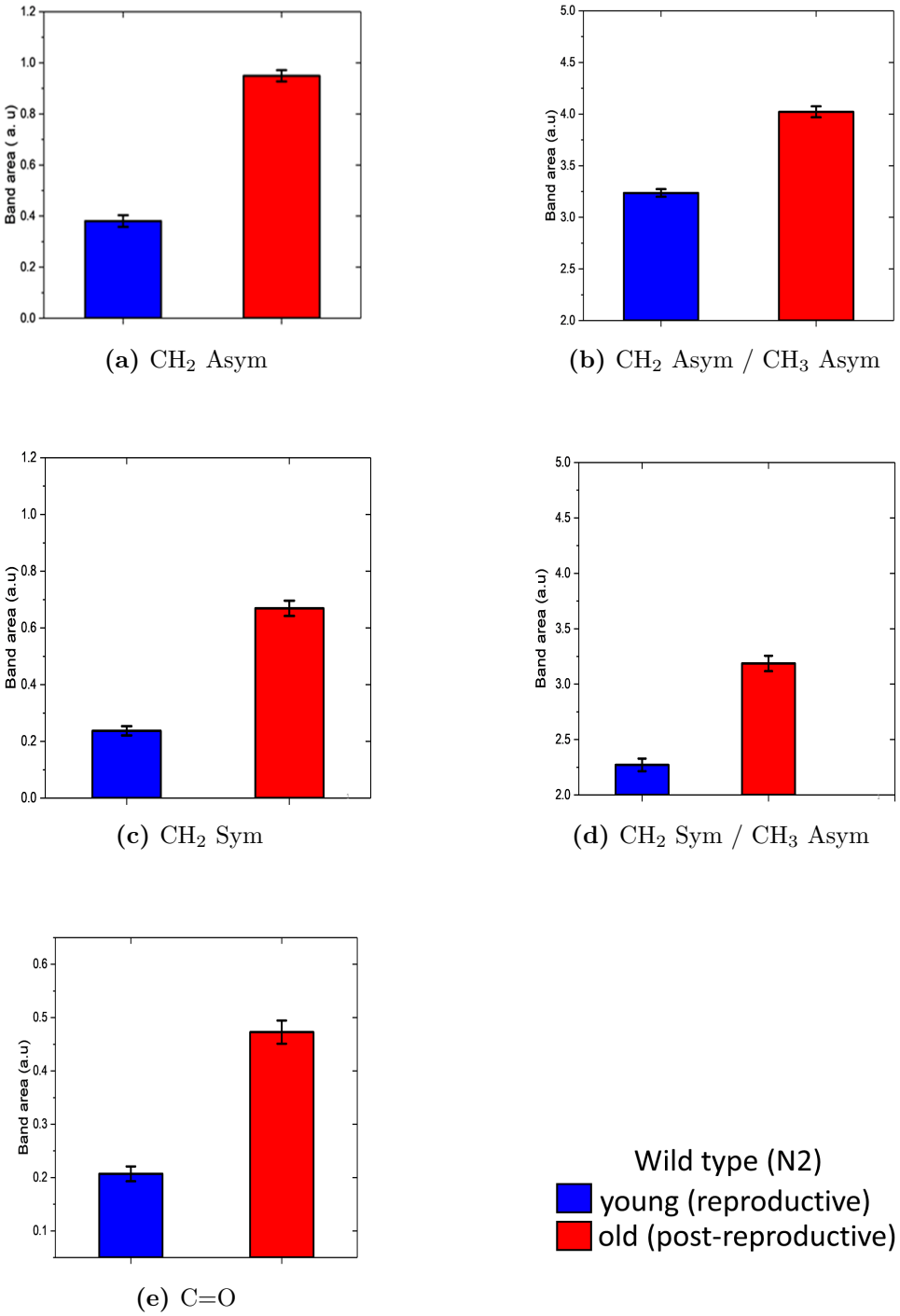

(a) CH_2 Asym

(b) CH_2 Asym / CH_3 Asym

(c) CH_2 Sym

(d) CH_2 Sym / CH_3 Asym

(e) C=O

Figure 3.4: Quantification of the band areas from the spectra in Figure 3.3: (a) CH_2 asym, (b) sym stretching, (c) CH_2 asym to CH_3 asym ratio, (d) CH_2 sym to CH_3 asym ratio and (e) C=O ester stretching of -1 oocytes from young (blue) and old (red) wild-type nematodes. Data are presented as mean ± SE.

from ester functional groups present in triglycerides, phospholipids and cholesterol ester. As shown in Figure 3.4.e, and consistent with the C-H analysis, the area of ester carbonyl band increased in oocytes from (0.42) old worms when compared to oocytes from (0.25) reproductively active (young) animals. Because a substantial fraction of triglycerides and phospholipids in oocytes are stored as yolk, these results could be explained by an increase in yolk uptake or delayed yolk mobilization which is the process in breaking down lipids stored in lipid droplets into free fatty acids (FFA) in response to changes in cells growth and energy demand, in oocytes from post-reproductive animals. In concert, theses finding suggests an increase in the lipid content present in older oocytes, consistent with previous reports (Garigan et al., 2002; Herndon et al., 2002; Mari et al., 2015).

3.1.2.2 Variations in the Amide regions

Analysis of the spectral region between 1700 and 1500 cm^{-1} is used as an indication of the total protein content in cells. It also allows for a more detailed examination of protein secondary structures (Dousseau & Pezolet, 1990; Gorbenko & Trusova; 2011). This region has two prominent features, the Amide I band (1700 - 1600 cm^{-1}) that arises mainly due to a C=O vibration and the Amide II band (1600 - 1500 cm^{-1}) that represents a combination of NH2 bending and C-N stretching vibration. Both Amide I and Amide II bands derive from the peptide backbone. With a smaller contribution of amino acid side chains and as Amide I vibration is affected by protein backbone structure, the Amide I band is particularly informative on protein secondary structures (Barth & Zscherp, 2002; Barth, 2007). Since β-sheets, in particular, are recognized structural elements associated with protein aggregation and cellular aging, the Amide I band in the spectra of young and old oocytes was explored in more detail below.

The second derivative infrared spectra in the Amide I region is characterized by three main absorption bands located at 1630 cm^{-1} (intermolecular β-sheet structures. See # 11 in Figure 3.5a and b), 1652 cm^{-1} (α-helix structure, see # 10 in Figure 3.5a and b) and 1690 cm^{-1} (β-turn structures, see # 9 in Figure 3.5a and b) (Eckel et al., 2001; Krafft et al., 2004). When the spectra of young and old oocytes are compared (Figure 3.5a and b), the bands at 1630 (see # 11 in Figure 3.5a and b) and 1690 cm^{-1} (see # 9 in Figure 3.5a and b) appear

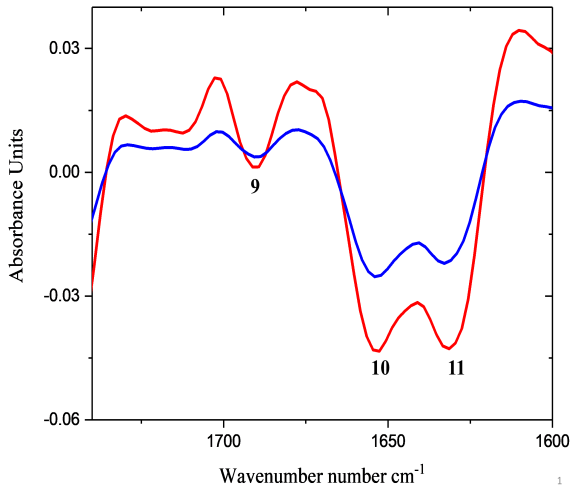

(a)

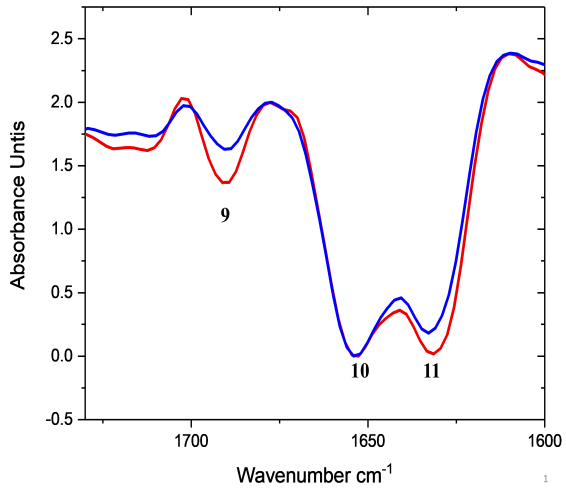

(b)

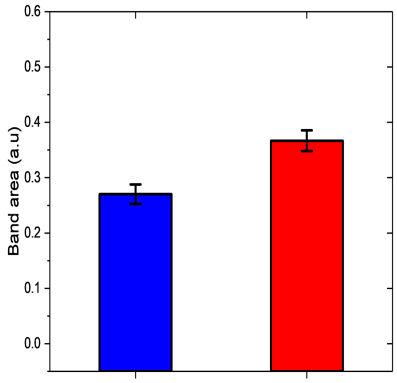

(c) β-turn structure

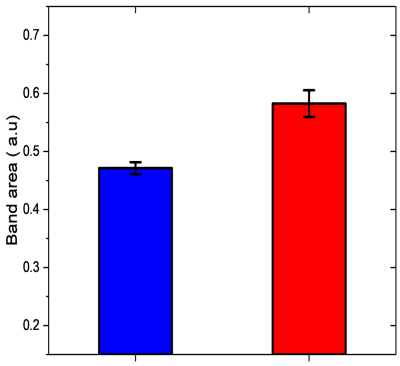

(d) β-sheet structure

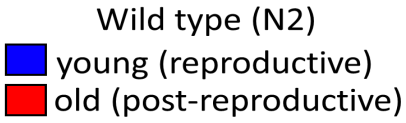

Figure 3.5: Changes in the Amide I (1600 - 1500 cm^{-1}) region in the spectra of young and old wild-type oocytes. (a) second derivative of representative IR spectra taken from the cytoplasm of -1 oocytes and normalized with the respect to the region between 1421 to 1357 cm^{-1}. (b) The same spectra after normalization to the α helix structure region at 1645 cm^{-1}. Blue - young oocytes from day 3 adults. Red - old oocytes from day 8 adult worms. Quantification of relative secondary protein structures in the IR spectra of wild-type -1 oocytes. Values are presented as (c) β-turn to α-helix ratio and (d) β-sheet to α-helix ratios. Values from young oocytes (day 3) are shown in blue, oocytes from post-reproductive nematodes (day 8) are depicted in red. Data are presented as mean $\pm$ SE

to vary in intensity while the band at the 1652 cm^{-1} (see # 10 in Figure 3.5a and b) region seems mostly unchanged, suggesting a higher prevalence of β-sheet and β-turn structure in the protein load in older cells. To investigate this possibility further, the sub-band area in the Amide I region was divided to the area of the stable band at 1658 cm^{-1}. This calculation revealed an increase in the band area at 1690 and 1632 cm^{-1} in oocytes from (0.37 and 0.58 respectively) post-reproductive (old) animal cells compared to (0.27 and 0.47 respectively) reproductive cells, consistent with an overrepresentation of β-sheet structures associated with age-related deterioration in these cells (Figure 3.5c and d respectively). However, this later result is contradicted to the FPA-FTIR imaging results showing of a reduction in signal intensity associated with protein (Amide I region) from reproductive to post-reproductive gonads as well as in the intestines of wild-type *C. elegans* .

3.1.2.3 Variations in the carbohydrate region

To investigate changes in the carbohydrate region in oocytes produced during reproductive and post-reproductive life stages, the IR spectral absorption in the region between 1150 and 950 cm^{-1} were analysed. Signal in this region is mainly attributable to contributions from phosphodiester groups and to the C=O absorption of glycogen and other carbohydrates in tissues and cells. As shown in Figure 3.6a, the peaks at 1090 cm^{-1} (see # 16 in Figure 3.6a) and 1025 cm^{-1} (see # 17 in Figure 3.6a) are the two most conspicuous bands observed in this region, asigned respectively to symmetric stretching vibrations of phosphodiester groups and of C=O stretch vibration of glycogen (Wang et al., 1997; Wood et al.,1996; 1998). The comparison of the second derivative spectra of young and old oocytes in these regions revealed two noticeable features. First, an apparent attenuated peak at 1025 cm^{-1} in older oocytes (Figure 3.6a) was observed, corroborated by the calculation of the area of the corresponding band that showed a marked reduction from reproductive (0.034) to (0.020) post-reproductive oocytes (Figure 3.6b). This result could be explained by an increase in glycogen consumption or a decrease in glyconeogenesis as oocytes transition from reproductive to post-reproductive stages. In contrast, the peak at 1090 cm^{-1} is more prominent in spectra of oocytes from (0.093) reproductive animals and appears to raise in the spectra of (0.152) older cells (Figure 3.6a). This finding was

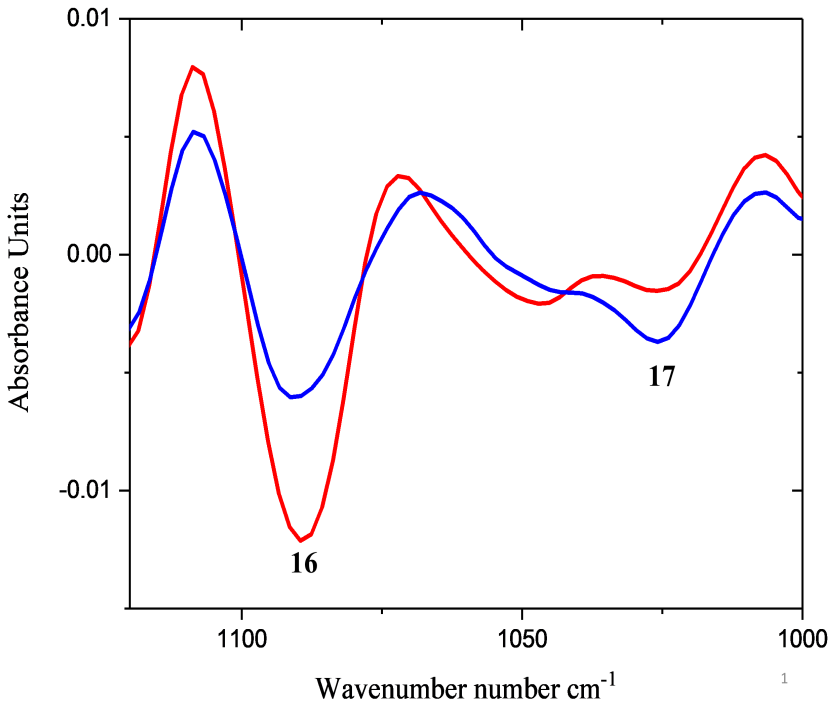

(a)

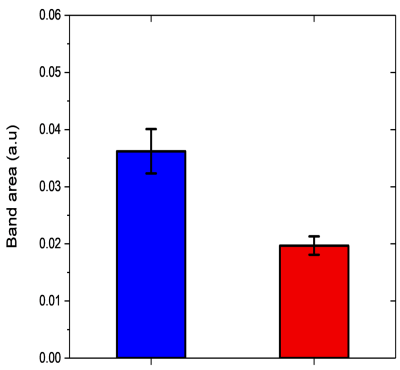

(b) glycogen

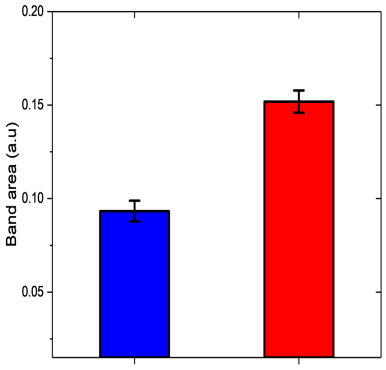

(c) phosphate

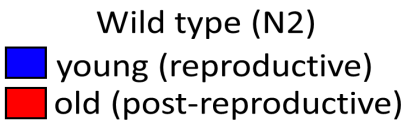

Figure 3.6: Second derivative spectra from young (blue) and old (red) wild-type oocytes in the carbohydrate (1100 - 950 cm^{-1}) region normalized to the region between 1421 to 1357 cm^{-1} (a). Quantification of the band areas corresponding to glycogen (b) and phosphate (c) levels extracted from the normalized spectra in the panel (a). Blue and red indicate young and old wild-type oocytes, respectively. Data are presented as mean ± SE.

confirmed by the calculation of the band area at 1090 cm^{-1} (Figure 3.6c). Therefore, this elevated rate of a phosphorylated process observed in post-reproductive oocytes associated with an increase in the carbohydrate consumption may be due to the dysregulation of carbohydrate metabolism and of cellular activity (Conti et al., 2009).

3.1.3 Changes in yolk content in oocytes

The FTIR results presented above strongly suggest that normal oocyte aging is underlined by a significant increase in lipid content. Oogenesis depends on a continuous cycle of extra-gonad yolk production, export from the intestine and subsequent import into oocytes. The rate of yolk synthesis to yolk consumption is therefore regulated by fertilization rates, as fresh oocytes are generated and continuously ovulated. Upon sperm depletion, that characterizes the start of post-reproductive life, newly produced oocytes stack up proximally and are not ovulated. In the meantime, yolk production and intake remain unabated. Thus, alterations in yolk uptake or usage in this stage could explain the increase in lipid content in older oocytes detected in the FTIR analysis. In fact, yolk deposition in somatic tissues of older animals have been previously reported and associated with accelerated aging phenotypes (Blagosklonny, 2008; Garigan et al., 2002). These studies used more traditional biochemical ways to assess yolk content in live *C. elegans* such as lipophilic dyes and *vit*::GFP transgenic lines. In this section, these tools were used to validate the age-dependent accumulation of lipids observed in the FTIR spectra of wild-type oocytes.

3.1.3.1 Yolk visualization via a *vit-2*::GFP reporter

A *vit-2*::GFP translational reporter (*pwIs23*) was used to examine the changes in yolk levels in aging oocytes (Grant & Hirsh, 1999). The *pwIs23* transgene contains the *vit-2* promoter and coding sequence fused in frame with a genomic GFP cassette downstream. As with other native *vit* genes, the *vit-2* promoter drives expression specifically in the intestine. GFP signals in *pwIs23* expressing animals recapitulate the endogenous transition of yolk from the intestine where it is synthesized, to distal oocytes where it accumulates. For this reason, the *vit-2::*GFP transgene has been widely used in the field as a transgenic alternative to assessing yolk lipids through staining, allowing for the in vivo study of the endocytic

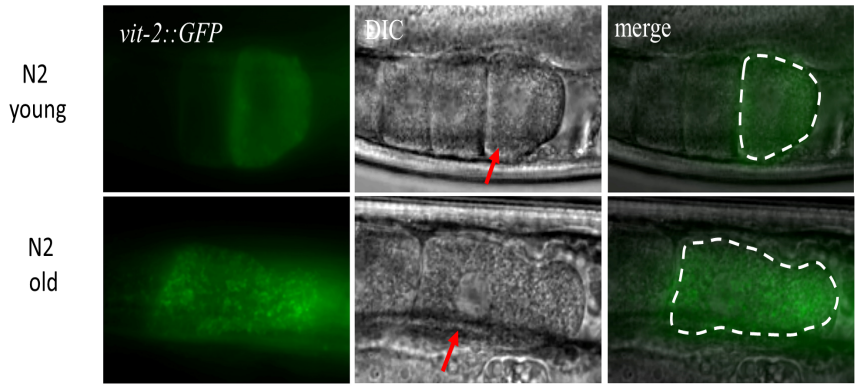

(a)

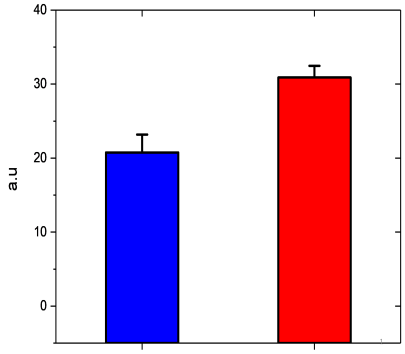

(b)

vit-2::GFP (RT130)
young (reproductive)
old (post-reproductive)

Figure 3.7: Vitellogenin (VIT-2) accumulation in oocytes from reproductive (young) and post-reproductive (old) RT130 worms. (a) DIC and corresponding fluorescence images of proximal oocytes in live animals expressing $vit-2::GFP(pwIs23)$. The -1 oocytes are marked by red arrow in the DIC image and outlined in the corresponding fluorescent panels. (b) relative fluorescence intensity values extracted from -1 oocytes. Values from young and old oocytes are shown in blue and red, respectively. Data are presented as mean ± SE.

machinery involved in yolk transport (Grant & Hirsh, 1999; Rompay et al., 2015).

Consistent with FTIR results, an increase in fluorescent signals was observed in *vit-2*::GFP expressing oocytes from (30.91) post-reproductive animals when compared to cells from (17.14) reproductive wild-type animals type, indicating an elevated yolk content in old oocytes (Figure 3.7).

3.1.3.2 Yolk visualization via BODIPY staining

Lipid stores in aging oocytes were also analysed by staining living nematodes with the vital dye BODIPY 493/503. This dye detects neutral lipids that also occur in oocytes unassociated to yolk droplets. As shown in the panels in Figure 3.8a and quantified in Figure 3.8b, oocytes from (89.64) post-reproductive wild-type nematodes showed substantially higher BODIPY fluorescent signals than cells from (56.03) younger animals in reproductive stages. These results are in agreement with both FTIR spectra and *vit-2*::GFP analysis that pointed to a consistent increment in lipid stores, likely of an yolk-origin, in oocytes generated in post-reproductive animals.

3.2 Impaired yolk import in *rme-2* mutants impacts lipid accumulation and protein signatures associated with aging oocytes

If yolk is indeed behind the changes in lipid and protein content observed in aging oocytes using FTIR, *vit-2*::GFP and BODIPY approaches, interrupting access of oocytes to yolk should substantially impact not only the total amount of lipids detected in oocytes, but also the progressive lipid accumulation that occurs after reproduction is completed. Conversely, if lipid changes in these cells are not directly or indirectly dependent on yolk, the pattern of lipid deposition as age progresses should not be proportionally affected.

As a proof of method to test the applicability of FTIR microspectroscopy for measuring these changes as well as testing whether yolk depletion, per se, could reverse the age-dependent accumulation of lipids in oocytes, lipid content in *rme-2* oocytes were

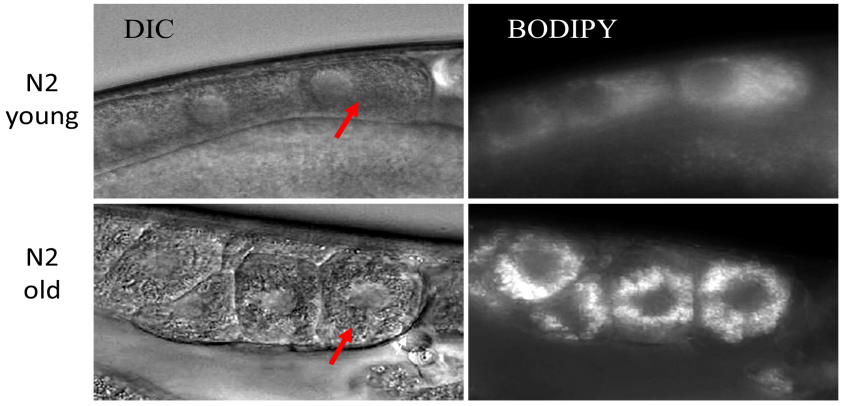

(a)

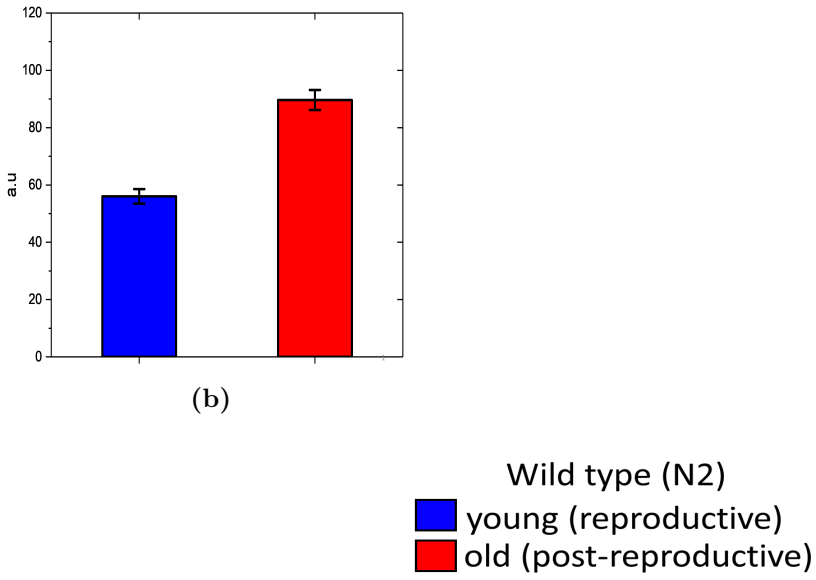

(b)

Figure 3.8: Neutral lipid stores in wild-type oocytes revealed by BODIPY 493/503 staining. (a) DIC and fluorescence images of the proximal gonad regions from intact animals fed BODIPY 493/503. The -1 oocyte position is indicated by a red arrow. (b) Relative fluorescence intensity values extracted from -1 oocytes of young (blue) and old (red) oocytes. Data are presented as mean ± SE.

assessed using the same panel of techniques described above for wild-type (N2) cells. As mentioned, RME-2 is the main yolk transporter in the membrane of oocytes. Yolk production in *rme-2* mutants is unaffected, though oocytes are generally deprived of yolk due to their inability to import these molecules. As a consequence, yolk is deposited in somatic tissue (extra-gonad). Aside from a reduction in oocyte viability, depletion of *rme-2* also leads to defects in ovulation, suggesting multiple requirements for yolk-derived lipids and proteins (Bembenek et al., 2007; Sönnichsen et al., 2005). Given the crucial role of *rme-2* and its specific disruption of yolk-dependent processes, its use provides a convenient platform to test the suitability of these technical approaches involved in evaluating the age-dependent fluctuations of lipid and protein stores in aging oocytes.

3.2.1 Yolk visualization in *rme-2* oocytes by FTIR microspectroscopy

Oocytes in *rme-2* mutants were examined by FTIR microspectroscopy to investigate:

a) the decrease in yolk-dependent lipid and protein reservoir in oocytes and as a proof of method for the suitability of using FTIR capturing yolk-dependent changes in the molecular composition of oocytes.

b) the age-dependent dynamics in lipid and protein content in aging oocytes depleted of yolk.

3.2.1.1 Change in yolk loads in oocytes are detectable by FTIR microspectroscopy

Since yolk disproportionally accounts for the bulk of the oocyte lipidome, it is reasonable to assume that its depletion should impact the FTIR spectra of these cells. To test that, the spectra of young oocytes from wild-type animals were compared to those of young *rme-2* mutants. A reduced intensity in the lipid bands at 2930 cm^{-1} (CH_2 asymmetric, see # 4 in Figure 3. 9b) and at 1745 cm^{-1} (ester carbonyl, see # 7 in Figure 3.9b), but not at 2856 cm^{-1} CH_2 symmetric, see # 6 in Figure 3.9b) was observed in oocytes from reproductive *rme-2* mutants relative to reproductive wild-type animals, suggesting that there is evidence for

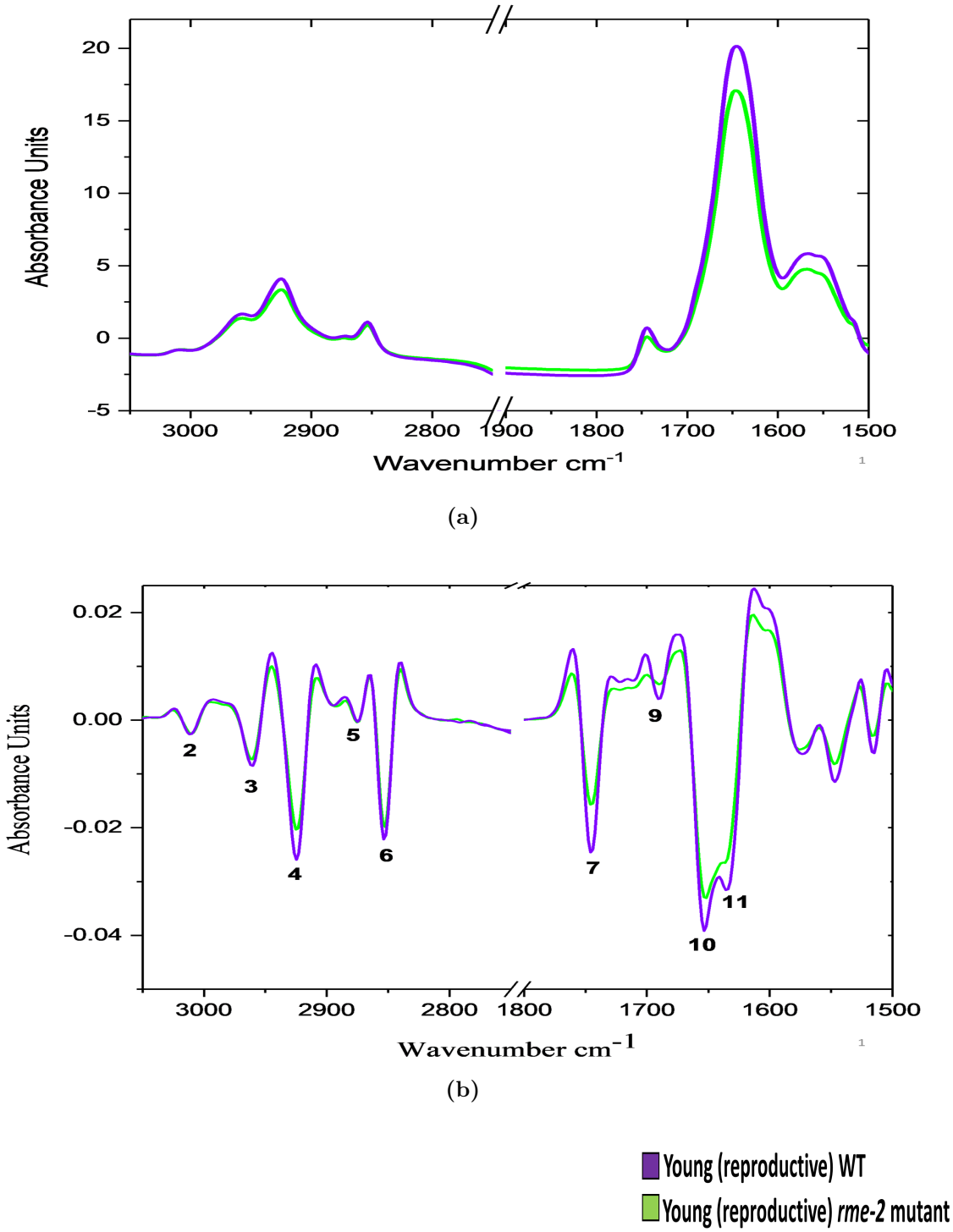

Figure 3.9: Comparison of an extracted IR absorption spectra on the cytoplasm of -1 oocytes from reproductive (young, day 3 of adulthood) *rme-2* mutant (shown in green) and wild-type (shown in purple) after normalizing in the region between 1421 and 1357 cm^{-1} and its corresponding secondary derivative FTIR spectra in the region between 3050 and 1500 cm^{-1}

less lipids in *rme-2* oocytes relative to wild-type nematodes at reproductive stage. Similarly, vitellogenin produced in the intestine represents the most abundant proteins in oocytes. It follows that impairment in yolk import may significantly reduce protein abundance in these cells. As observed in the band at 1690 cm^{-1} (β-turn structure, see # 9 in Figure 3.9b) and at 1630 cm^{-1} (β-sheet structure, see # 11 in Figure 3.9b) which were less intense in oocytes from reproductive *rme-2* mutants compared to reproductive wild-type animals, there is an evidence on a reduced protein loading in *rme-2* oocytes as compared to age matched wild-type cells. The spectra differences between *rme-2* and wild-type cells support the use of FTIR microspectroscopy for detecting physiological variation in lipid and protein contents in oocytes. Furthermore, this analysis confirms the major role that yolk derived lipids and proteins play an important role in the oocyte lipidome and proteome, respectively.

3.2.1.2 Lipid content changes in aging *rme-2* oocytes

To address the possibility that yolk import is essential to drive some level of lipid accumulation as oocytes progress past reproductive stages (see 3.2.1), FTIR spectra from young and old *rme-2* oocytes were compared. Figure 3.10 shows the representative spectra from these samples either without (panel a) and with (panel b) normalization with respect to the region between 1421 and 1357 cm^{-1}. As with the analysis of wild-type oocytes, the FTIR spectra from young and old *rme-2* oocytes have a similar overall shape but differences in band intensities that could indicate changes in molecular composition are apparent in the corresponding regions of the spectra of wild-type cells. The analyses of these regions are presented below.

The C-H (3050 to 2800 cm^{-1}) and ester carbonyl C=O (1770 - 1720 cm^{-1}) regions in the spectra of *rme-2*, representing mostly the contribution from lipid molecules, were exploited in more detail in Figure 3.11. The normalized second derivative spectra shown in panels (b) and (c) point to a relative increase in two regions in samples from old *rme-2* oocytes relative to young cells. A better visualization of these differences can be determined by calculating the area of lipid bands at 2930 cm^{-1} (CH_2 asymmetric - see # 4 in Figure 3.11, Figure 3.12 panel a), 2856 cm^{-1} (CH_2 symmetric - see # 6 in Figure 3.11, Figure 3.12 panel c) and the area ratios of CH_2 asymmetric and CH_2 symmetric stretching to CH_3 asymmetric

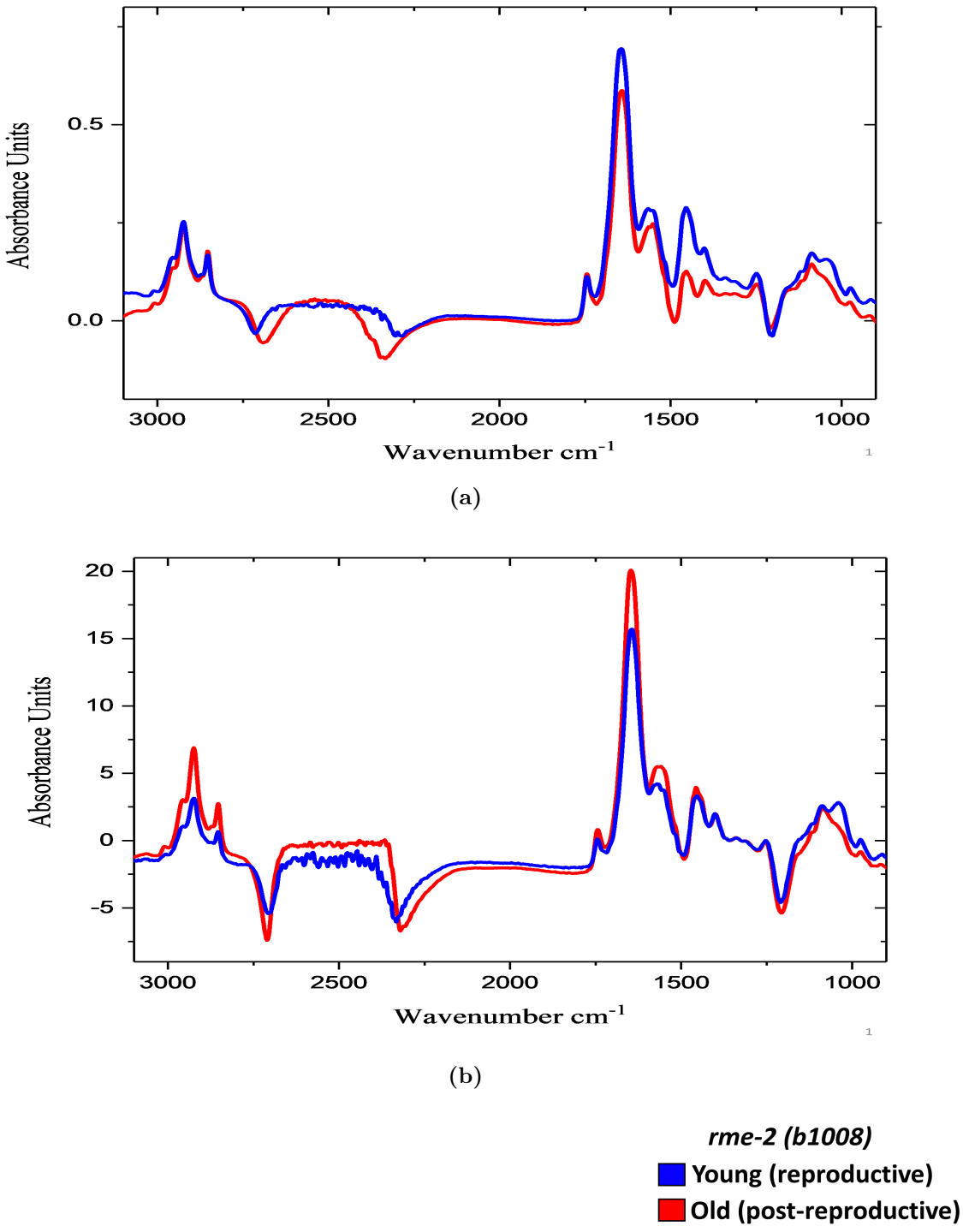

Figure 3.10: IR absorption spectra extracted from the cytoplasm of *rme-2(b1008)* -1 oocytes (a) without normalization spectra and (b) with normalization using the region 1421 to 1357 cm^{-1}. Spectra from day 3 (young, reproductive) cells is depicted in blue and day 8 (old, post-reproductive) in red.

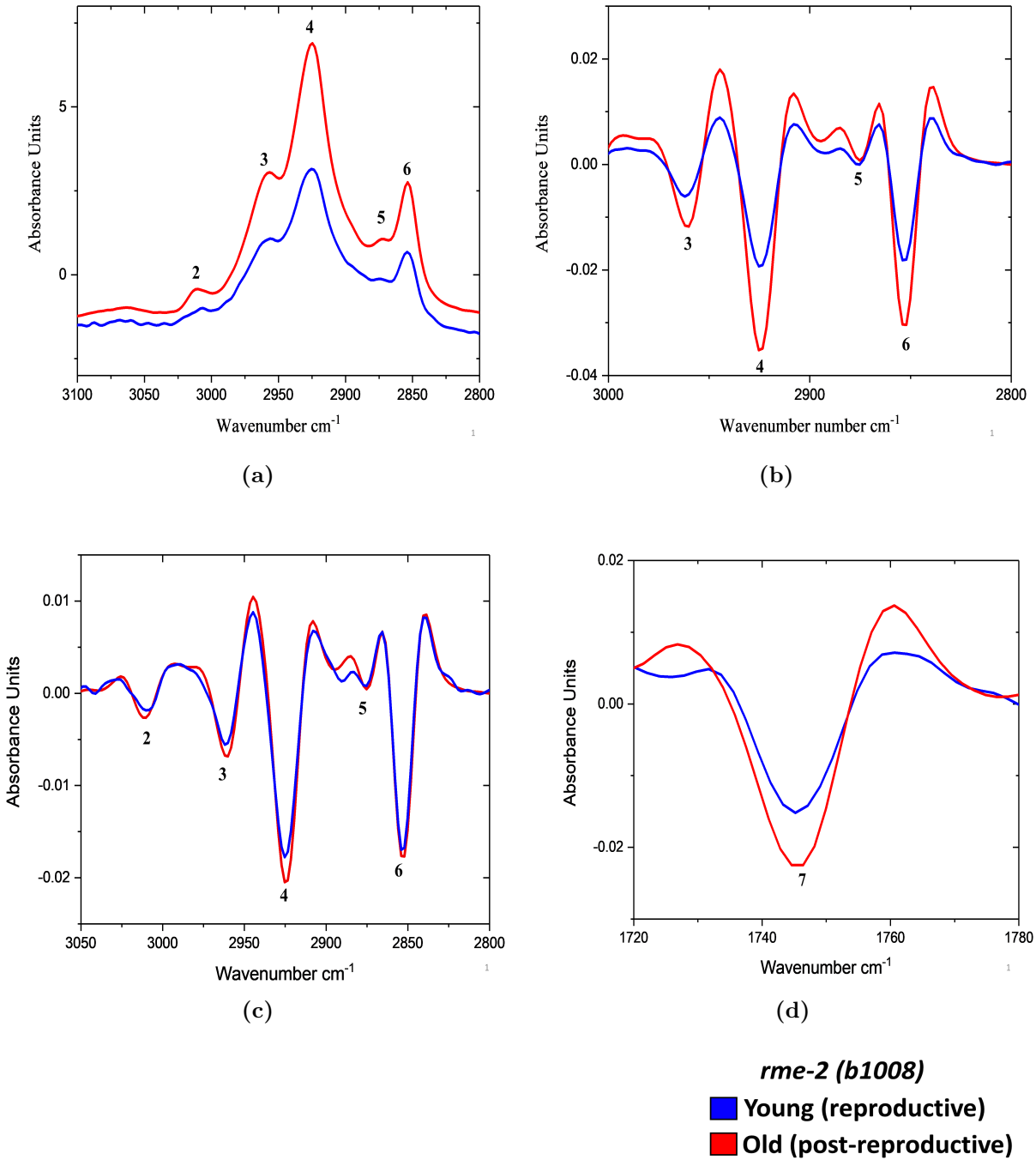

Figure 3.11: Representative IR spectra from the cytoplasm of *rme-2(b1008)* -1 oocytes. (a) shows the spectra collected from cells dissected from reproductive (young, shown in blue) and post-reproductive (old, shown in red) *rme-2* worms in the region 3050 - 2800 cm^{-1} after normalizing with the respect to the region between 1421 to 1357 cm^{-1} (b) and its corresponding second derivative IR spectra (c) and its corresponding second derivative IR spectra after normalization to the CH_3 asymmetric stretching mode at 2970 cm^{-1}. (d) in the carbonyl region 1770 - 1720 cm^{-1} after normalizing with the respect to the region between 1421 to 1357 cm^{-1}.

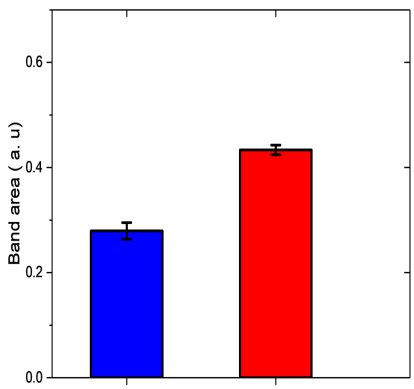

(a) CH_2 Asym

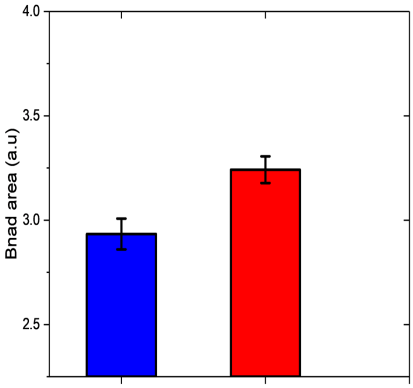

(b) CH_2 Asym / CH_3 Asym

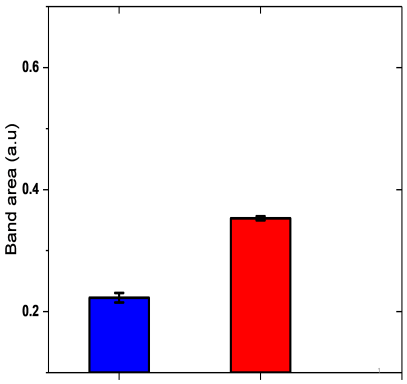

(c) CH_2 Sym

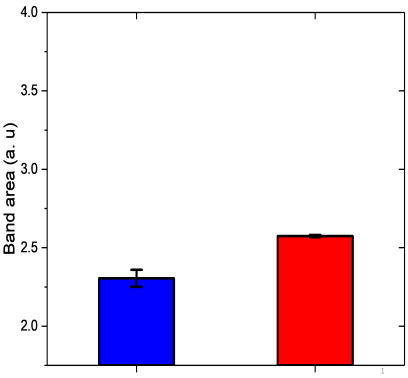

(d) CH_2 Sym / CH_3 Asym

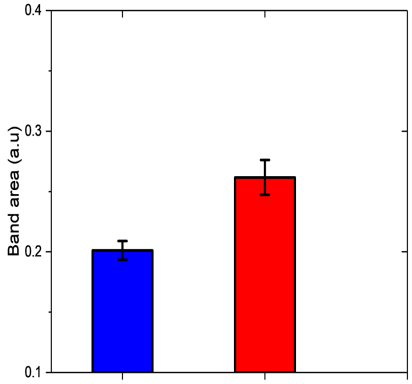

(e) C=O

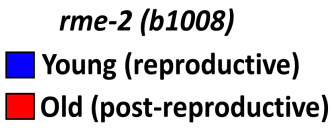

Figure 3.12: Quantification of the band areas from the spectra in Figure 3.11: (a) CH_2 asym, (b) sym stretching, (c) CH_2 asym to CH_3 asym ratio, (d) CH_2 sym to CH_3 asym ratio and (e) C=O ester stretching of -1 oocytes from young (blue) and old (red) wild-type nematodes. Data are presented as mean ± SE.

band individually (Figure 3.12 panels b and d, respectively). Finally, the area of carbonyl band also increased from reproductive to post-reproductive oocytes in *rme-2* mutants (Figure 3.12 panel e), suggesting that some lipid accumulation does take place in aging *rme-2* oocytes, though the total lipid contents in these mutant cells are significantly lower as compared to age matched wild-type oocytes (Figure 3.12 and Figure 3.4). Together these findings indicate that while depletion of yolk dramatically reduce yolk content in oocytes across different ages (Figure 3.12), it does not prevent some accumulation of lipids as oocytes age. This accumulation, however, appears to occur on a much slower rate with 1.4 times as aging in *rme-2* oocytes compared to wild-type animals with 2.1-fold. It seems likely, therefore, that both yolk-related and unrelated lipids contribute to the age-dependent accumulation of these molecules in oocytes.

3.2.1.3 Protein content changes in aging *rme-2* oocytes

In view of the overall reduction in total lipid and protein content observed in the FTIR spectra of *rme-2* oocytes relative to wild-type cells (Figure 3.9) and the reduced lipid accumulation noticed as these cells age (Figure 3.13), it was important to check whether the corresponding exclusion of vitellogenin import also impacted the spectra. For this analysis, the Amide I region related to protein signatures, was investigated in *rme-2* oocytes. To monitor structural changes in the total protein content, the secondary structure spectral response to Amide I region was used. The spectra in this region is shown in Figure 3.13a and b. Of particular interest are bands at 1690 cm^{-1} (see # 9 in Figure 3.13a and b) and at 1630 cm^{-1} (see # 11 in Figure 3.13a and b), which inform mostly on β-turn and β-sheet structures, respectively. When normalized to the region between 1421 to 1357 cm^{-1} (Figure 3.13a and b) or to the region representing α-helix contribution (band at 1650 cm^{-1}, see # 10 in Figure 3.13a and b), it became apparent that a decrease in the band area at 1690 cm^{-1} (see # 9 in Figure 3.13a and b) was evident in post-reproductive *rme-2* oocytes (Figure 3.13c). This finding suggests that in contrast to wild-type cells (Figure 3.5), aging *rme-2* oocytes do not show a significant accumulation of a recognized marker of protein aggregation. Under this interpretation, and paradoxically, considering the overall negative impact of yolk depletion to reproduction, old *rme-2* oocytes appear to display a younger molecular profile than age

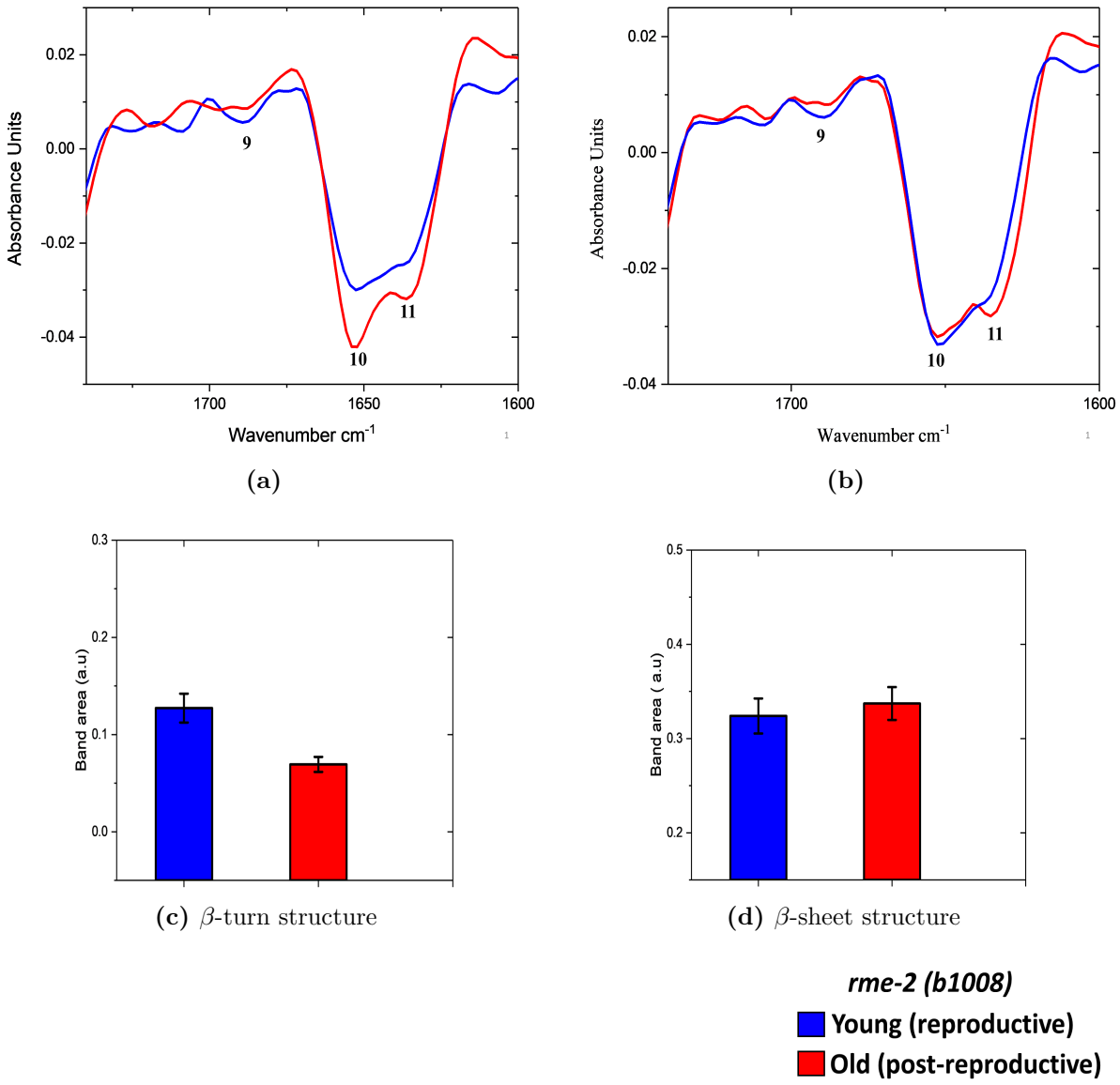

Figure 3.13: Changes in the Amide I (1600 - 1500 cm^{-1}) region in the spectra of young and old *rme-2* oocytes: (a) second derivative of representative IR spectra taken from *rme-2* -1 oocytes and normalized with the respect to the region between 1421 to 1357 cm^{-1}, (b) The same spectra after normalization to the α-helix structure region at 1645 cm^{-1}. Blue - young oocytes from day 3 adults. Red - old oocytes from day 8 adult worms. (c) Quantification of relative secondary protein structures in the IR spectra of *rme-2* -1 oocytes. Values are presented as (a) β-turn to α-helix ratio and (b) β-sheet to α-helix ratios. Values from young oocytes (day 3) are shown in blue, oocytes from post-reproductive nematodes (day 8) are depicted in red. Data are presented as mean $\pm$ SE.

matched wild-type cells. However, the analysis of the area band at 1630 cm^{-1} (see # 11 in Figure 3.13 and b), which informs on β-sheet structures, does not support this conclusion. As shown in Figure 3.13d, a slight increase in the area band at 1630 cm^{-1} can be seen in old relative to young *rme-2* oocytes. Therefore, the role of vitellogenin depletion, insofar as influencing aging signatures in this spectral range, needs further clarification.

3.2.2 Yolk visualization in *rme-2* oocytes by *vit-2*::GFP reporter

The comparison of FTIR spectra from young and old *rme-2* oocytes suggested that reproductive aging could proceed more slowly in these mutants. This analysis assumed a diminished yolk, and therefore vitellogenin, import by *rme-2* oocyte. However, *rme-2* spectra also showed that signatures associated with lipids in these oocytes did indeed increase in old cells, suggesting that some lipid deposition, though at a much lower abundance than observed in wild-type, occurs yolk-independently (Figure 3.14). To further investigate this apparent contradiction, the relative abundance of vitellogenins in young and old *rme-2* oocytes was investigated using the *vit-2*::GFP reporter.

In oocytes from wild-type nematodes, an increase in VIT-2::GFP signals was observed during the transition from reproductive to post-reproductive life stages. In these animals, VIT-2::GFP is essentially only observed in the gonad, aside from the intestine where it is synthesized (Figure 3.7). As expected, *rme-2* mutants that are unable to transport yolk into oocytes show strong accumulation of VIT-2::GFP in the pseudocoelom while fluorescence in oocytes is weak (Figure 3.14a). With age, extra-gonadal accumulation of VIT-2::GFP in *rme-2* mutants increases further, as the intestine pumps ever more yolk into the pseudocoelom. Surprisingly, however, in *rme-2* oocytes appear to lose VIT-2::GFP signals as they age (Figure 3.14b). A significant decrease in VIT-2::GFP fluorescence signals in post-reproductive in *rme-2* oocytes cannot be simply explained by a reduced level of yolk import but likely reflects a reconfiguration of the oocyte's proteome upon the end of reproduction. If, as suggested by FTIR analysis, vitellogenin accumulation in oocytes upon increased yolk import is responsible for the expansion of molecular signatures associated with protein aggregation in older cells (compare Figure 3.5 and 3.13), then depletion of VIT proteins in young oocytes may curtail the progressive deposition of these aggregates as

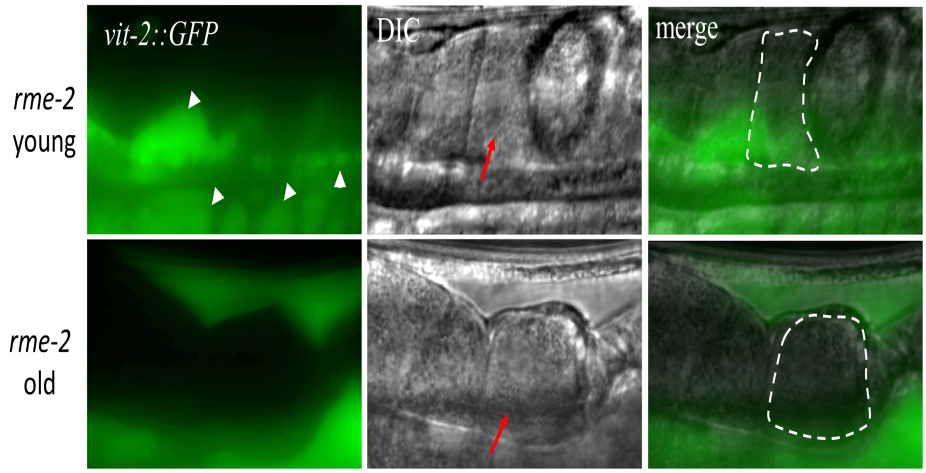

(a)

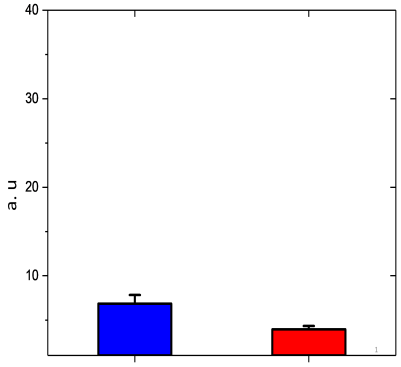

(b)

rme-2 (b1008); vit-2::GFP
young (reproductive)
old (post-reproductive)

Figure 3.14: Vitellogenin (VIT-2) accumulation in oocytes from reproductive (young) and post-reproductive (old) *rme-2(b1008);pwIs23* animals. (a) DIC and corresponding fluorescence images of proximal oocytes in live *rme-2* mutant animals expressing *vit-2::GFP (pwIs23)*. The -1 oocytes are marked by red arrow in the DIC image and outlined in the corresponding fluorescent panels. (b) relative fluorescence intensity values extracted from -1 oocytes. Values from young and old oocytes are shown in blue and red, respectively. Data are presented as mean ± SE.

reproduction wanes down, slowing the aging process and resulting in a 'younger' oocyte profile in post-reproductive *rme-2* mutants, relative to wild-type animals.

Overall, the *vit-2*::GFP analysis of *rme-2* mutants is consistent with the major trend found in FTIR spectra that suggests that protein loads and composition in aging oocytes depend to some extent on proper access to yolk during the reproductive period, reinforcing that some of the specific spectral differences in the Amide bands observed between young and old wild-type oocytes may indeed come about because of differences in yolk content inside these cells.

3.2.3 Yolk visualization in *rme-2* oocytes via BODIPY staining

Finally, the FTIR and *vit-2*::GFP analyses were validated by probing the total neutral lipid content in *rme-2* oocytes using the vital dye BODIPY 493/503. Consistent with FTIR spectra (Figure 3.9), young *rme-2* oocytes start up with much reduced lipid stores than the wild-type (compared Figure 3.8 with Figure 3.15). Nevertheless, as demonstrated by FTIR spectra of *rme-2* mutants (Figure 3.11), these cells are able to accumulate lipids as they advanced through reproductive life, since old *rme-2* -1 oocytes do show an overall increase in BODIPY fluorescence signals as compared to young cells (Figure 3.15), though this effect appears less accentuated than observed in the wild-type (compare Figure 3.8b with 3.15b). Together, these results are consistent with the FTIR analysis for *rme-2* oocytes and support the interpretation that yolk depletion substantially limits, but not entirely prevents, the normal lipid accumulation that characterizes post-reproductive oocytes.

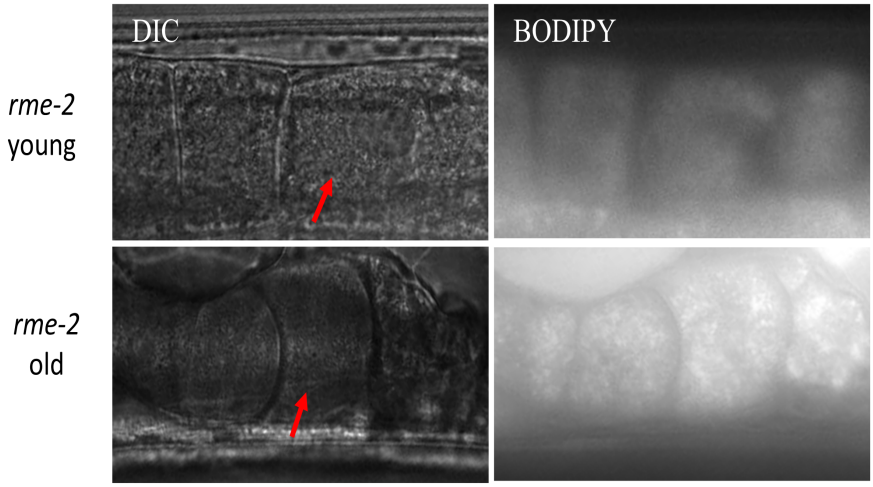

(a)

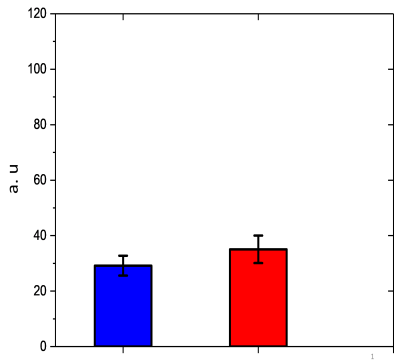

(b)

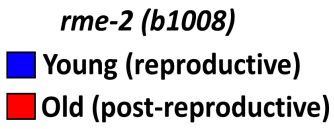

Figure 3.15: Neutral lipid stores in *rme-2(b1008)* oocytes revealed by BODIPY 493/503 staining. (a) DIC and fluorescence images of the proximal gonad regions from intact *rme-2(b1008)* worms fed BODIPY 493/503. The -1 oocyte position is indicated by a red arrow. (b) Relative fluorescence intensity values extracted from -1 oocytes. Blue-young oocytes; red-old oocytes. Data are presented as mean ± SE.

Chapter 4

DISCUSSION AND FUTURE WORK

The use of the *C. elegans* reproductive system as a model to address questions relevant to human reproductive aging has established several parameters with which to study the decline in oocyte quality overtime. The main purpose of this work was to extend the technical and experimental toolkit available for these studies by introducing FTIR microspectroscopy as a useful analytical method for the detection and quantification of the changes in the molecular composition of live oocytes undergoing normal aging. During this process, several technical improvements and new protocols required to reproducibly extract biologically relevant spectral information from *C. elegans* oocytes were established that will be no doubt useful in future research in this field. Finally, the analysis presented in this thesis introduces several lines of investigation aimed at exploring potential molecular signatures of aging oocytes that may be one day translate in a better understanding of the events that lead to germ cell aging in humans.

The accumulation of yolk in the body cavity of older worms and its involvement in aging has been previously reported (Ackerman & Gems, 2012; Herndon et al., 2002; McGee et al., 2012). In this thesis, yolk deposition was shown to also occur inside older oocytes. Yolk is a complex association of different protein and lipid forms and as such should contribute heterogeneously to several bands in a FTIR spectrum. Taking advantage of yolk-depleted oocytes from *rme-2* mutants, the specific changes in FTIR spectra attributed to yolk could be mapped. Thus, age-dependent yolk accumulation in oocytes can now be quantitatively measured in FTIR spectra using protein bands (1690 cm^{-1} - assigned to β-turn structures) and lipid bands (2925, 2956 and 1754 cm^{-1} - assigned to CH_2 asymmetric and symmetric stretching and ester carbonyl, respectively). Assuming that in oocytes, as in somatic tissues, the accumulation of yolk hinders the normal physiology of

these cells, it is reasonable to assume that these molecules also contribute to the deterioration in oocyte quality overtime. It is also possible, however, that the yolk accumulation observed is a by-product of other cellular events that regulate the aging process in germ cells, and as such it may not be a trigger for reproductive aging, but one of the downstream processes set in motion by earlier events. Either way, if lipid deposition is a conserved cellular characteristic of aging oocytes, this may represent a useful molecular marker with which to diagnose oocyte fertilizability, for example. To test that possibility, it will be important to transgenic manipulate yolk content in oocytes and directly measure the impact in fertilizability, for example. Because FTIR microspectroscopy can be used for quantifying several biomolecules, it is also possible that other spectral bands unrelated to yolk and not analyzed here in detail carry information relevant to changes occurring in aging oocytes.

How does FTIR spectra compare with existing biochemical and transgenic tools in detecting yolk stores in live animals? An important aspect of this work was validating the spectral information obtained from oocytes with data from lipid staining and *vit*::GFP fusion protein, two widely used tracers of yolk. Indeed, the age-dependent increased yolk signatures in older oocyte described above are paralleled by lipid staining (BODIPY) and by tracking vitellogenin deposition in live animals (VIT-2::GFP), consistent with a previous report (Chen et al., 2016; Grant & Hirsh, 1999).

Why do lipids accumulate inside oocytes? In theory, the accumulation of lipid content in post-reproductive oocytes may be a natural consequence of the longer residence of these cells in the gonad. The ovulation cycle in actively reproducing animals limits the window of time in which oocytes can take up yolk before being fertilized and the egg shell secreted, blocking further import. In post-reproductive stages, these constrains do not play a role and mature oocytes linger in the gonad for much longer. However, spectra collected from oocytes of feminized animals that are never fertilized (not shown in this thesis) and therefore remain in the gonads do not support this interpretation. It appears that residence time in the -1 position of the gonad does not per se explain the accumulation of lipids observed in post-reproductive oocytes. As such, and similar to other aging paradigms in the soma of *C. elegans*, yolk deposition in aging oocytes is likely not a stochastic event but

responds to some sort of genetic regulation.

Dissecting the genetic program behind yolk deposition will require examining mutant backgrounds in which yolk production, import and metabolism are affected. *rme-2*, in which yolk intake by oocytes is mostly abolished, provided a convenient platform to validate the ability of FTIR microspectroscopy to measure dynamic changes in yolk mobilization in live oocytes. The analysis of the FTIR lipid band confirmed the reduction of lipid levels in *rme-2* oocytes as compared to wild-type cells. In addition, β-sheet/turn structure at 1690 cm^{-1} in oocytes from both reproductive and post-reproductive *rme-2* mutants were reduced when compare to wild-type cells. Interestingly, significant differences in the Amide I band of FTIR spectra were previously reported between different body parts of adult worms. The sub-band Amide I at 1690 cm^{-1} assigned to β-sheet/turn structures was almost negligible in the tail region compared to the pharynx and intestine (Ami et al., 2004; Garigan et al., 2002). Perhaps not surprisingly, these last two anatomical regions are sources of yolk synthesis, as compared to the tail. Thus, changes in the Amide I bands provide an important comparative readout to asses yolk contents in *C. elegans*. Consistent with the FTIR spectra, results from lipid staining with BODIPY 493/503 and a *vit-2*::GFP reporter support a reduction in yolk loads in these cells, though a slow accumulation of lipids did take place in aging *rme-2* oocytes. Indeed, older *rme-2* oocytes have also been shown to accumulate cholesterol which was correlated with FTIR results by using C=O band analysis (Matyash et al., 2001). What could be the consequence of this altered lipid content to *rme-2* oocytes? Under the prevalent interpretation that associates lipid accumulation with cellular degradation, the loss of yolk in *rme-2* oocyte may slow aging in these cells, though this may not be functionally important when compared to the deleterious consequences caused by lack of yolk to oogenesis and fertilization. Conversely, *rme-2* worms may have normal reproductive aging. In this case, these findings would suggest that yolk contribution to oocyte aging is not dependent on the total lipid stores in these cells but the continuous deposition of lipids during reproductive life. The results from *rme-2* mutants thus highlight unanswered questions regarding the link between yolk accumulation in oocytes and cellular aging.

Lipids are a potent source of energy in oocytes and alterations in lipid stores affect

oocyte physiology and maturation. For instance, elevated lipid contents in mammalian oocytes have been associated with impaired developmental competence after cryopreservation (Prates et al., 2014). Furthermore, Dunning et al (2012) showed that promoting lipid utilization improves oocyte quality and oocyte developmental competence. The developmental potential of mammalian oocytes, a measure of cellular quality, is also decreased by normal aging and correlates with higher rates of meiotic errors that lead to aneuploid gametes, the major driver of infertility in older women. At the molecular level, aging is often accompanied by damage to macromolecules such as proteins, DNA, and lipids. It is possible, therefore, that increased loads of lipids and proteins provide substrates for the accumulation of damaged by-products that can be toxic to oocytes (Ackerman & Gems, 2012). For instance, lipids are one of the intracellular components of oocytes that are targeted by Reactive Oxygen Species (ROS) causing oxidative damage and cellular deterioration (Tarín, 1995, 1996).

In *C. elegans*, vitellogenins are also targeted by ROS and act as oxidants that drive tissue deterioration (Seehuus et al., 2006). During reproductive life, yolk uptake by oocytes and usage by embryos are balanced processes driven by continuous oocyte maturation, ovulation and fertilization. As previously mentioned, this coordinated series of events in the proximal gonad moves the oocyte production pipeline forward at such a rate that mature oocytes have time to import just enough yolk before being ovulated and newer developing oocytes take their place. The presence of sperm serves as the catalyzing force that prevents the stalling of oocytes in the proximal gonad where they age. Thus, reproduction itself may deter oocyte aging for as long as sperm repository is available. After all sperm is used up, reproduction ends and oocytes consequently stall. With ongoing yolk production and export, vitellogenins accumulate in the body cavity likely contributing to tissue degradation. FTIR analysis indicated these proteins also accumulate in aged oocytes from wild-type nematodes, where they potentially contribute to the loss of cell quality.

Increasing lipid and protein loads in yolk-accumulating oocytes could overwhelm the oocyte's ability to turn over these molecules after a threshold of toxicity is reached, triggering stress response pathways. For instance, lipotoxicity mediated by ROS generation can lead to significant damage to cellular organelles like the endoplasmic reticulum (ER)

(Igosheva et al., 2010; Wu et al., 2012). The ER is a multifunctional organelle responsible for synthesizing proteins and packaging triglycerides into lipid droplets to serve as energy stores. In states of energy imbalance such as in post-reproductive oocytes, surplus charge on the ER may lead to dysfunction in protein folding, triggering the unfolded protein response (UPR). If ER stress cannot be stabilized, UPR-mediated apoptosis can ensue due to protein aggregation. Evidence for UPR triggers in older wild-type oocytes may be extrapolated from the sub-Amide I band at 1630 cm^{-1} (β-sheet structure). In *C. elegans*, aging is also marked by an increase in intracellular levels of protein aggregation which contributes to tissue degradation (Ayyadevara et al., 2016; Taylor & Dillin, 2011). Consistent with lipid accumulation feeding proteotoxicity via ROS-mediated damage, old *rme-2* oocytes, which accumulate very little yolk, exhibited a dramatic decrease in β-sheet structure at 1630 cm^{-1} content relative to age-matched wild-type cells. One interpretation for these results is that the continuous accumulation of vitellogenins and yolk lipids saturates the oocyte with ROS-producing molecules that eventually overcome the cell's ability to process protein aggregates triggering cellular damage and death (Ben-Zvi et al., 2009). Paradoxically, these results also suggest that decreased yolk content may be advantageous insofar as delaying reproductive senescence, even though certain amount of yolk is required for reproduction. In that respect, *rme-2* oocytes that cannot sufficiently import yolk to fuel reproductive processes may be ultimately protected from the damaging consequences of yolk accumulation. This is indeed the paradigm reported for DAF-16-dependent lifespan extension via suppression of vitellogenesis in the intestine. In these animals, impaired yolk synthesis correlates with increased lifespan (DePina et al., 2011). Importantly *rme-2* mutants have been shown to have a normal lifespan (Seah et al., 2015), suggesting that the impact on longevity relies on a yolk-free soma. As suggested above, a more thorough functional investigation of the impact of RME-2 depletion in oocyte fertilizability is required to assess the true consequent of yolk depletion in *rme-2* mutant oocytes.

Aside from yolk-derived molecular signatures, FTIR spectra indicate possible changes in glycogen and phosphate content in aging oocytes. Glycogen is the principal energy storage molecule in nematodes and may serve a critical role in providing energy for

protein phosphorylation necessary for several signaling events during oocyte maturation and fertilization. Indeed, post-reproductive oocytes appear to generate ATP via glycogen hydrolysis at a higher rate than younger cells, presumably to support phosphorylative processes (Braeckman & Dhondt, 2017; Gazi et al., 2004).

The work presented in this thesis supports a role for yolk, as identified by its lipid and protein contributions, as a molecular marker for aging oocytes. However, yolk is prevalent only in vertebrates with exterior embryonic development, and mammalian oocytes do not undergo vitellogenesis which has been evolutionary substituted by lactation and placentation (Brawand et al., 2008). If oogenesis in mammals occurs in the absence of yolk storage, how relevant are the results shown here to humans? As it turns out, mammalian oocytes also contain substantial lipid stores made of phospholipids, triglycerides and polyunsaturated fatty acids (PUFAs), reflecting their ancestral amniotic egg (McEvoy et al., 2000). PUFAs, in particular, are essential lipid precursors for the production of steroid ligands (prostaglandins) involved in several conserved signaling pathways controlling growth, development and reproduction (Vrablik & Watts, 2013). In mammals, PUFA-rich diets increase mitochondrial dysfunction and elevate ROS levels in oocytes resulting in reduced fertilization capacity (Gu et al., 2015). Thus, unbalanced endogenous lipid stores in oocytes, in particular PUFAs, can significantly impact oocyte quality. It is possible, therefore, that mammalian reproductive aging is also characterized by increased lipid-mediated toxicity.

In the last half century, improvements in life standards and medicine have greatly extended life expectancy (Finch & Crimmins, 2004). However, reproductive life with respect, in particular, to women's fertility, did not accompany such increase in lifespan. Female reproductive aging poses a serious challenge to present and future health care systems and family planning in aging populations across the world. This thesis research highlighted potential molecular indicators of reproductive aging in oocytes of *C. elegans*. Reproductive aging is normally coupled to somatic aging as evident by many lifespan mutants with altered fertility and by the antagonizing relationship between germ line proliferation and lifespan (Flatt et al., 2008; Hsin & Kenyon, 1999). However, the question of why do worms and humans both have long post-reproductive lifespans if reproductive

and somatic aging are coupled (Aguilaniu, 2015; Flatt et al., 2008; Hsin & Kenyon, 1999) still poses some difficulties. Presumably, genes that influence reproductive lifespan but not longevity should also exist. Indeed, Luo et al (2009) identified a new pathway that regulates reproductive aging independently of somatic aging in worms. Reduced TGF-β Sma/Mab signaling significantly extends reproductive lifespan in *C. elegans*, at times doubling the progeny generation period, without slowing aging. As with genes integrating dietary restriction signalling (DR), future experiments addressing the contributions of IIS and TGF-β Sma/Mab pathway genes in the FTIR spectra of aging oocytes will be essential to dissect the genetic underpinning of the molecular changes described in this thesis.

References

[1] Aardema, H., Vos, P. L. A. M., Lolicato, F., Roelen, B. A. J., Knijn, H. M., Vaandrager, A. B., ... Gadella, B. M. (2011). Oleic acid prevents detrimental effects of saturated fatty acids on bovine oocyte developmental competence. *Biology of Reproduction*, 85(1), 62–69. https://doi.org/10.1095/biolreprod.110.088815

[2] Abma, J. C., Chandra, A., Mosher, W. D., Peterson, L. S., & Piccinino, L. J. (1997). Fertility, family planning, and women's health: new data from the 1995 National Survey of Family Growth. *Vital and Health Statistics. Series 23, Data from the National Survey of Family Growth*, (19), 1–114.

[3] Ackerman, D., & Gems, D. (2012). The mystery of *C.elegans* aging: An emerging role for fat. *BioEssays*, 34(6), 466–471. https://doi.org/10.1002/bies.201100189

[4] Aguilaniu, H. (2015). The mysterious relationship between reproduction and longevity. *Worm*, 4(2). https://doi.org/10.1080/21624054.2015.1020276

[5] Alberman, E., Elliott, M., Creasy, M., & Dhadial, R. (1975). Previous reproductive history in mothers presenting with spontaneous abortions . *BJOG: An International Journal of Obstetrics & Gynaecology*, 82(5), 366–373. https://doi.org/10.1111/j.1471-0528.1975. tb00651.x

[6] Ami, D., Mereghetti, P., Natalello, A., Doglia, S. M., Zanoni, M., Redi, C. A., & Monti, M. (2011). FTIR spectral signatures of mouse antral oocytes: Molecular markers of oocyte maturation and developmental competence. *Biochimica et Biophysica Acta (BBA) - Molecular Cell Research*, 1813(6), 1220–1229. https://doi.org/10.1016/j.bbamcr.2011.03.009

[7] Ami, D., Natalello, A., Zullini, A., & Doglia, S. M. (2004). Fourier transform infrared microspectroscopy as a new tool for nematode studies. *FEBSLetters*, 576(3), 297–300. https://doi.org/10.1016/j.febslet.2004.09.022

[8] Andrus, P. G. L., & Strickland, R. D. (1998). Cancer grading by Fourier transform infrared spectroscopy. *Biospectroscopy*, 4(1), 37–46. https://doi.org/10.1002/(SICI)1520-6343(1998)4:1<37::AID-BSPY4>3.0.CO;2-P

[9] Andux, S., & Ellis, R. E. (2008). Apoptosis maintains oocyte quality in aging *Caenorhabditis elegans* females. *PLOS Genetics*, 4(12), e1000295. https://doi.org/10.1371/journal.pgen.1000295

[10] Arrondo, J. L. R., & Goñi, F. M. (1999). Structure and dynamics of membrane proteins as studied by infrared spectroscopy. *Progress in Biophysics and Molecular Biology*, 72(4), 367–405. https://doi.org/10.1016/S0079-6107(99)00007-3

[11] Arrondo, J. L. R., Goñi, F. M., & Macarulla, J. M. (1984). Infrared spectroscopy of phosphatidylcholines in aqueous suspension a study of the phosphate group vibrations. *Biochimica et Biophysica Acta (BBA) - Lipids and Lipid Metabolism*, 794(1), 165–168. https://doi.org/10.1016/0005-2760(84)90310-2

[12] Austin, J., & Kimble, J. (1987). *glp-1* is required in the germ line for regulation of the decision between mitosis and meiosis in *C. elegans. Cell*, 51(4), 589–599.

[13] Ayyadevara, S., Balasubramaniam, M., Suri, P., Mackintosh, S. G., Tackett, A. J., Sullivan, D. H., ... Dennis, R. A. (2016). Proteins that accumulate with age in human skeletal-muscle aggregates contribute to declines in muscle mass and function in *Caenorhabditis elegans*. *Aging* (*Albany NY*), 8(12), 3486. https://doi.org/10.18632/aging.101141

[14] Baker, D. (2000). A surprising simplicity to protein folding. *Nature*, 405(6782), 39–42. https://doi.org/10.1038/35011000

[15] Baker, M. J., Trevisan, J., Bassan, P., Bhargava, R., Butler, H. J., Dorling, K. M., ... Martin, F. L. (2014). Using Fourier transform IR spectroscopy to analyze biological materials. *Nature Protocols*, 9(8), 1771–1791. https://doi.org/10.1038/nprot.2014.110

[16] Balasch, J. (2010). Ageing and infertility: an overview. *Gynecological Endocrinology*, 26(12), 855–860. https://doi.org/10.3109/09513590.2010.501889

[17] Barth, A. (2007). Infrared spectroscopy of proteins. *Biochimica et Biophysica Acta (BBA) - Bioenergetics*, 1767(9), 1073–1101. https://doi.org/10.1016/j.bbabio.2007.06.004

[18] Barth, A., & Zscherp, C. (2002). What vibrations tell us about proteins. *Quarterly Reviews of Biophysics*, 35(4), 369–430.

[19] Barton, G. J. (1995). Protein secondary structure prediction. *Current Opinion in Structural Biology*, 5(3), 372–376. https://doi.org/10.1016/0959-440X(95)80099-9

[20] Baxi, K., Ghavidel, A., Waddell, B., Harkness, T. A., & de Carvalho, C. E. (2017). Regulation of lysosomal function by the DAF-16 Forkhead Transcription Factor couples reproduction to aging in *Caenorhabditis elegans*. *Genetics*, 207(1), 83–101. https://doi.org/10.1534/genetics.117.204222

[21] Bellisola, G., & Sorio, C. (2012). Infrared spectroscopy and microscopy in cancer research and diagnosis. *American Journal of Cancer Research*, 2(1), 1–21.

[22] Bembenek, J. N., Richie, C. T., Squirrell, J. M., Campbell, J. M., Eliceiri, K. W., Poteryaev, D., ... White, J. G. (2007). Cortical granule exocytosis in *C. elegans* is regulated by cell cycle components including separase. *Development*, Vol. 134, H. 21, S. 3837-3848.

[23] Ben-Zvi, A., Miller, E. A., & Morimoto, R. I. (2009). Collapse of proteostasis represents an early molecular event in *Caenorhabditis elegans* aging. *Proceedings of the National Academy of Sciences of the United States of America*, 106(35), 14914–14919. https://doi.org/10.1073/pnas.0902882106

[24] Berg, J. M., Tymoczko, J. L., & Stryer, L. (2002). Triacylglycerols are highly concentrated energy stores. *Biochemistry. 5th Edition*. Retrieved from https://www.ncbi.nlm.nih.gov/books/NBK22369/

[25] Berman, J. R., & Kenyon, C. (2006). Germ-cell loss extends *C. elegans* lifespan through regulation of DAF-16 by *kri-1* and Lipophilic-hormone signaling. *Cell*, 124(5), 1055–1068. https://doi.org/10.1016/j.cell.2006.01.039

[26] Bertie, J. E., Ahmed, M. K., & Eysel, H. H. (1989). Infrared intensities of liquids. 5. Optical and dielectric constants, integrated intensities, and dipole moment derivatives of water and water-d2 at 22.degree.C. *The Journal of Physical Chemistry*, 93(6), 2210–2218. https://doi.org/10.1021/j100343a008

[27] Bertie, J. E., & Lan, Z. (1996). Infrared intensities of liquids XX: the Intensity of the OH stretching band of liquid water revisited, and the best current values of the optical constants of H_2O(l) at 25^0C between 15,000 and 1 cm^{-1}. *Applied Spectroscopy*,50(8), 1047–1057. https://doi.org/10.1366/0003702963905385

[28] Bhatt, R. I., Brown, M. D., Hart, C. A., Gilmore, P., Ramani, V. A. C., George, N. J., & Clarke, N. W. (2003). Novel method for the isolation and characterisation of the putative prostatic stem cell. *Cytometry Part A*, 54(2), 89–99. https://doi.org/10.1002/cyto.a.10058

[29] Blagosklonny, M. V. (2008). Aging: ROS or TOR. *Cell Cycle (Georgetown, Tex.)*, 7(21), 3344–3354. https://doi.org/10.4161/cc.7.21.6965

[30] Blasiole, D. A., Davis, R. A., & Attie, A. D. (2007). The physiological and molecular regulation of lipoprotein assembly and secretion. *Molecular BioSystems*, 3(9), 608–619. https://doi.org/10.1039/B700706J

[31] Blout, E. R., De Loze, C., & Asadourian, A. (1961). The deuterium exchange of water-soluble polypeptides and proteins as measured by Infrared Spectroscopy. *Journal of the American Chemical Society*, 83(8), 1895–1900. https://doi.org/10.1021/ja01469a028

[32] Bonda, M., Perrin, V., Vileno, B., Runne, H., Kretlow, A., Forró, L., ... Jeney, S. (2011). Synchrotron infrared micro-spectroscopy detects the evolution of Huntington's disease

neuropathology and suggests unique correlates of dysfunction in white versus grey brain matter. *Analytical Chemistry*, 83(20), 7712–7720. https://doi.org/10.1021/ac201102p

[33] Boulekbache, H. (1981). Energy Metabolism in Fish Development. *American Zoologist*, 21(2), 377–389.

[34] Bozkurt, O., Severcan, M., & Severcan, F. (2010). Diabetes induces compositional, structural and functional alterations on rat skeletal soleus muscle revealed by FTIR spectroscopy: a comparative study with EDL muscle. *The Analyst*, 135(12), 3110–3119. https://doi.org/10.1039/c0an00542h

[35] Braeckman, B., & Dhondt, I. (2017). Lifespan extension in *Caenorhabditis elegans* insulin/IGF-1 signalling mutants is supported by non-vertebrate physiological traits. *NEMATOLOGY*, 19(5), 499–508. https://doi.org/http://dx.doi.org/10.1163/15685411-00003060

[36] Brahms, S., & Brahms, J. (1980). Determination of protein secondary structure in solution by vacuum ultraviolet circular dichroism. *Journal of Molecular Biology*, 138(2), 149–178. https://doi.org/10.1016/0022-2836(80)90282-X

[37] Brawand, D., Wahli, W., & Kaessmann, H. (2008). Loss of egg yolk genes in mammals and the origin of lactation and placentation. *PLOS Biology*, 6(3), e63. https://doi.org/10.1371/journal.pbio.0060063

[38] Brenner, S. (1974). The Genetics of *Caenorhabditis elegans*. Genetics, 77(1), 71–94.

[39] Cakmak, G., Miller, L. M., Zorlu, F., & Severcan, F. (2012). Amifostine, a radioprotectant agent, protects rat brain tissue lipids against ionizing radiation induced damage: an FTIR microspectroscopic imaging study. *Archives of Biochemistry and Biophysics*, 520(2), 67–73. https://doi.org/10.1016/j.abb.2012.02.012

[40] Cakmak, G., Zorlu, F., Severcan, M., & Severcan, F. (2011). Screening of protective effect of amifostine on radiation-induced structural and functional variations in rat liver microsomal membranes by FT-IR spectroscopy. *Analytical Chemistry*, 83(7), 2438–2444. https://doi.org/10.1021/ac102043p

[41] Cant, M. A., & Johnstone, R. A. (2008). Reproductive conflict and the separation of reproductive generations in humans. *Proceedings of the National Academy of Sciences*, 105(14), 5332–5336. https://doi.org/10.1073/pnas.0711911105

[42] Carnevali, O., Mosconi, G., Ridolfi, S., & Polzonetti-Magni, A. M. (1998). Growth hormone and insulin-like growth factor-I in inducing vitellogenin synthesis by frog hepatocytesa. *Annals of the New York Academy of Sciences*, 839(1), 556–557. https://doi.org/10.1111/j.1749-6632.1998.tb10871.x

[43] Carugo, O. (2007). Recent progress in measuring structural similarity between proteins. *Current Protein and Peptide Science*, 8(3), 219–241.

[44] Casal, H. L., & Mantsch, H. H. (1984). Polymorphic phase behaviour of phospholipid membranes studied by infrared spectroscopy. *Biochimica et Biophysica Acta (BBA) - Reviews on Biomembranes*, 779(4), 381–401. https://doi.org/10.1016/0304-4157(84)90017-0

[45] Caughey, B., & Lansbury, P. T. (2003). Protofibrils, pores, fibrils, and neurodegeneration: separating the responsible protein aggregates from the innocent bystanders. *Annual Review of Neuroscience*, 26, 267–298. https://doi.org/10.1146/annurev.neuro.26.010302.081142

[46] Chen, W.-W., Yi, Y.-H., Chien, C.-H., Hsiung, K.-C., Ma, T.-H., Lin, Y.-C., ... Chang, T.-C. (2016). Specific polyunsaturated fatty acids modulate lipid delivery and oocyte development in *C. elegans* revealed by molecular-selective label-free imaging. *Scientific Reports*, 6. https://doi.org/10.1038/srep32021

[47] Choo, L. P., Wetzel, D. L., Halliday, W. C., Jackson, M., LeVine, S. M., & Mantsch, H. H. (1996). In situ characterization of beta-amyloid in Alzheimer's diseased tissue by synchrotron Fourier transform infrared microspectroscopy. *Biophysical Journal*, 71(4), 1672–1679.

[48] Chung, E., Ko, C., Kang, H., Choi, K., & Jun, J. (2008). Ultrastructure of oocytes during oogenesis and oocyte degeneration associated with follicle cells in female

Sinonovacula constricta (Bivalvia: Pharidae) in Western Korea. *Animal Cells and Systems*. https://doi.org/10.1080/19768354.2008.9647187

[49] Church, D. L., Guan, K. L., & Lambie, E. J. (1995). Three genes of the MAP kinase cascade, *mek-2*, *mpk-1/sur-1* and *let-60* ras, are required for meiotic cell cycle progression in *Caenorhabditis elegans*. Development, 121(8), 2525–2535.

[50] Coleman, P. B. (Ed.). (1993). Practical sampling techniques for infrared analysis. Boca Raton, FL: CRC Press.

[51] Colthup, N. B., Wiberley, S. E., & Daly, L. H. (1990). Introduction to infrared and Raman spectroscopy (3rd ed). Boston: *Academic Press*. Retrieved from https://trove.nla.gov.au/version/6574354

[52] Conti, C., Ferraris, P., Garavaglia, M., Giorgini, E., Rubini, C., Sabbatini, S., & Tosi, G. (2009). Microimaging FTIR of head and neck tumors. IV. *Microscopy Research and Technique*, 72(2), 67–75. https://doi.org/10.1002/jemt.20644

[53] Corona, M., Velarde, R. A., Remolina, S., Moran-Lauter, A., Wang, Y., Hughes, K. A., & Robinson, G. E. (2007). Vitellogenin, juvenile hormone, insulin signaling, and queen honey bee longevity. *Proceedings of the National Academy of Sciences*, 104(17), 7128–7133. https://doi.org/10.1073/pnas.0701909104

[54] Danielsson Jens, Andersson August, Jarvet Jüri, & Graslund Astrid. (2006). 15N relaxation study of the amyloid β-peptide: structural propensities and persistence length. *Magnetic Resonance in Chemistry*, 44(S1), S114–S121. https://doi.org/10.1002/mrc.1814

[55] David, D. C., Ollikainen, N., Trinidad, J. C., Cary, M. P., Burlingame, A. L., & Kenyon, C. (2010). Widespread Protein Aggregation as an Inherent Part of Aging in *C. elegans*. *PLoS Biology*, 8(8). https://doi.org/10.1371/journal.pbio.1000450

[56] Depuydt, G., Xie, F., Petyuk, V. A., Smolders, A., Brewer, H. M., Camp, D. G., ... Braeckman, B. P. (2014). LC–MS proteomics analysis of the insulin/IGF-1-deficient *Caenorhabditis elegans daf-2(e1370)* mutant reveals extensive restructuring

of intermediary metabolism. *Journal of Proteome Research*, 13(4), 1938–1956. https://doi.org/10.1021/pr401081b

[57] Dernburg, A. F., McDonald, K., Moulder, G., Barstead, R., Dresser, M., & Villeneuve, A. M. (1998). Meiotic recombination in *C. elegans* initiates by a conserved mechanism and is dispensable for homologous chromosome synapsis. *Cell*, 94(3), 387–398.

[58] Dillin, A., Crawford, D. K., & Kenyon, C. (2002). Timing requirements for insulin/IGF-1 signaling in *C. elegans. Science (New York, N.Y.)*, 298(5594), 830–834. https://doi.org/10.1126/science.1074240

[59] Dobson, C. M. (1999). Protein misfolding, evolution and disease. *Trends in Biochemical Sciences*, 24(9), 329–332.

[60] Dobson, C. M. (2002). Getting out of shape. *Nature*, 418(6899), 729–730. https://doi.org/10.1038/418729a

[61] Dogan, A., Ergen, K., Budak, F., & Severcan, F. (2007). Evaluation of disseminated candidiasis on an experimental animal model: a Fourier transform infrared study. *Applied Spectroscopy*, 61(2), 199–203. https://doi.org/10.1366/000370207779947459

[62] Dong, M.-Q., Venable, J. D., Au, N., Xu, T., Park, S. K., Cociorva, D., ... Yates, J. R. (2007). Quantitative mass spectrometry identifies insulin signaling targets in *C. elegans. Science*, 317(5838), 660–663. https://doi.org/10.1126/science.1139952

[63] Dougherty, E. C., & Calhoun, H. G. (1948). Possible significance of free-living nematodes in genetic research. *Nature*, 161(4079), 29.

[64] Dousseau, F., & Pezolet, M. (1990). Determination of the secondary structure content of proteins in aqueous solutions from their amide I and amide II infrared bands. Comparison between classical and partial least-squares methods. *Biochemistry*, 29(37), 8771–8779. https://doi.org/10.1021/bi00489a038

[65] Dumont, J., & Desai, A. (2012). Acentrosomal spindle assembly & chromosome segregation during oocyte meiosis. *Trends in Cell Biology*, 22(5), 241–249. https://doi.org/10.1016/j.tcb.2012.02.007

[66] Dunning, K. R., & Robker, R. L. (2012). Promoting lipid utilization with l-carnitine to improve oocyte quality. *Animal Reproduction Science*, 134(1), 69–75. https://doi.org/10.1016/j.anireprosci.2012.08.013

[67] Dunning, K. R., Russell, D. L., & Robker, R. L. (2014). Lipids and oocyte developmental competence: the role of fatty acids and β-oxidation. *Reproduction*, 148(1), R15–R27. https://doi.org/10.1530/REP-13-0251

[68] Eckel, R., Huo, H., Guan, H.-W., Hu, X., Che, X., & Huang, W.-D. (2001). Characteristic infrared spectroscopic patterns in the protein bands of human breast cancer tissue. *Vibrational Spectroscopy*, 27(2), 165–173. https://doi.org/10.1016/S0924-2031(01)00134-5

[69] Elibol-Can, B., Jakubowska-Dogru, E., Severcan, M., & Severcan, F. (2011). The effects of short-term chronic ethanol intoxication and ethanol withdrawal on the molecular cComposition of the rat hippocampus by FT-IR Spectroscopy. *Alcoholism: Clinical and Experimental Research*, 35(11), 2050–2062. https://doi.org/10.1111/j.1530-0277.2011.01556.x

[70] Erickson, J. D. (1978). Down syndrome, paternal age, maternal age and birth order. *Annals of Human Genetics*, 41(3), 289–298.

[71] Ermonval, M., Duvet, S., Zonneveld, D., Cacan, R., Buttin, G., & Braakman, I. (2000). Truncated N-glycans affect protein folding in the ER of CHO-derived mutant cell lines without preventing calnexin binding. *Glycobiology*, 10(1), 77–87.

[72] Fabian, H., Jackson, M., Murphy, L., Watson, P. H., Fichtner, I., & Mantsch, H. H. (1995). A comparative infrared spectroscopic study of human breast tumors and breast tumor cell xenografts. *Biospectroscopy*, 1(1), 37–45. https://doi.org/10.1002/bspy.350010106

[73] Fabian, H., & Schultz, C. P. (2006). Fourier Transform Infrared Spectroscopy in peptide and protein analysis. In *Encyclopedia of Analytical Chemistry. American Cancer Society.* https://doi.org/10.1002/9780470027318.a1612

[74] Faddy, M. J., Gosden, R. G., Gougeon, A., Richardson, S. J., & Nelson, J. F. (1992). Accelerated disappearance of ovarian follicles in mid-life: implications for forecasting menopause. *Human Reproduction (Oxford, England)*, 7(10), 1342–1346.

[75] Fahy, E., Cotter, D., Sud, M., & Subramaniam, S. (2011). Lipid classification, structures and tools. *Biochimica et Biophysica Acta*, 1811(11), 637–647. https://doi.org/10.1016/j.bbalip.2011.06.009

[76] Finch, C. E., & Crimmins, E. M. (2004). Inflammatory exposure and historical changes in human life-spans. *Science (New York, N.Y.)*, 305(5691), 1736–1739. https://doi.org/10.1126/science.1092556

[77] Fink, A. L. (1998). Protein aggregation: folding aggregates, inclusion bodies and amyloid. *Folding and Design*, 3(1), R9–R23. https://doi.org/10.1016/S1359-0278(98)00002-9

[78] Flatt, T., Min, K.-J., D'Alterio, C., Villa-Cuesta, E., Cumbers, J., Lehmann, R., ... Tatar, M. (2008). *Drosophila* germ-line modulation of insulin signaling and lifespan. *Proceedings of the National Academy of Sciences of the United States of America*, 105(17), 6368–6373. https://doi.org/10.1073/pnas.0709128105

[79] Flatt, T., Tu, M.-P., & Tatar, M. (2005). Hormonal pleiotropy and the juvenile hormone regulation of *Drosophila* development and life history. *BioEssays*, 27(10), 999–1010. https://doi.org/10.1002/bies.20290

[80] Folick, A., Min, W., & Wang, M. C. (2011). Label-free imaging of lipid dynamics using Coherent Anti-stokes Raman Scattering (CARS) and Stimulated Raman Scattering (SRS) microscopy. *Current Opinion in Genetics & Development*, 21(5), 585–590. https://doi.org/10.1016/j.gde.2011.09.003

[81] Forfang, K., Zimmermann, B., Kosa, G., Kohler, A., & Shapaval, V. (2017). FTIR Spectroscopy for evaluation and monitoring of lipid extraction efficiency for *Oleaginous Fungi*. *PLoS ONE*, 12(1). https://doi.org/10.1371/journal.pone.0170611

[82] Francis, R., Barton, M. K., Kimble, J., & Schedl, T. (1995). *gld-1*, a tumor suppressor gene required for oocyte development in *Caenorhabditis elegans. Genetics*, 139(2), 579–606.

[83] Frazier, H. N., & Roth, M. B. (2009). Adaptive Sugar Provisioning Controls Survival of *C. elegans* Embryos in Adverse Environments. *Current Biology*, 19(10), 859–863. https://doi.org/10.1016/j.cub.2009.03.066

[84] Fung, M. F. K., Senterman, M. K., Mikhael, N. Z., Lacelle, S., & Wong, P. T. T. (1996). Pressure-tuning fourier transform infrared spectroscopic study of carcinogenesis in human endometrium. *Biospectroscopy*, 2(3), 155–165. https://doi.org/10.1002/(SICI)1520-6343(1996)2:3<155::AID-BSPY2>3.0.CO;2-7

[85] Garigan, D., Hsu, A.-L., Fraser, A. G., Kamath, R. S., Ahringer, J., & Kenyon, C. (2002). Genetic analysis of tissue aging in *Caenorhabditis elegans*: a role for heat-shock factor and bacterial proliferation. *Genetics*, 161(3), 1101–1112.

[86] Gasper, R., Dewelle, J., Kiss, R., Mijatovic, T., & Goormaghtigh, E. (2009). IR spectroscopy as a new tool for evidencing antitumor drug signatures. *Biochimica et Biophysica Acta (BBA) - Biomembranes*, 1788(6), 1263–1270. https://doi.org/10.1016/j.bbamem.2009.02.016

[87] Gazi, E., Dwyer, J., Lockyer, N., Gardner, P., Vickerman, J. C., Miyan, J., ... Clarke, N. (2004). The combined application of FTIR microspectroscopy and ToF-SIMS imaging in the study of prostate cancer. *Faraday Discussions*, 126(0), 41–59. https://doi.org/10.1039/B304883G

[88] Gazi, E., Dwyer, J., Lockyer, N., Miyan, J., Gardner, P., Hart, C., ... Clarke, N. (2005). Fixation protocols for subcellular imaging by synchrotron-based Fourier transform infrared microspectroscopy. *Biopolymers*, 77, 18–30. https://doi.org/10.1002/bip.20167

[89] Gems, D., & Riddle, D. L. (1996). Longevity in *Caenorhabditis elegans* reduced by mating but not gamete production. *Nature*, 379(6567), 723–725. https://doi.org/10.1038/379723a0

[90] Gioacchini, G., Giorgini, E., Vaccari, L., Ferraris, P., Sabbatini, S., Bianchi, V., ... Carnevali, O. (2014). A new approach to evaluate aging effects on human oocytes: Fourier transform infrared imaging spectroscopy study. *Fertility and Sterility*, 101(1), 120–127. https://doi.org/10.1016/j.fertnstert.2013.09.012

[91] Gorbenko, G., & Trusova, V. (2011). Protein aggregation in a membrane environment. In R. Donev (Ed.), *Advances in Protein Chemistry and Structural Biology* (Vol. 84, pp. 113–142). Academic Press. https://doi.org/10.1016/B978-0-12-386483-3.00002-1

[92] Goud, P., Goud, A., Van Oostveldt, P., Van der Elst, J., & Dhont, M. (1999). Fertilization abnormalities and pronucleus size asynchrony after intracytoplasmic sperm injection are related to oocyte postmaturity. *Fertility and Sterility*, 72(2), 245–252.

[93] Government of Canada, S. C. (2013, July 9). Fertility: Overview, 2009 to 2011. Retrieved April 24, 2018, from https://www.statcan.gc.ca/pub/91-209-x/2013001/article/11784-eng.html

[94] Grant, B. (2006). Intracellular trafficking. *WormBook*. https://doi.org/10.1895/wormbook.1.77.1

[95] Grant, B., & Hirsh, D. (1999). Receptor-mediated Endocytosis in the *Caenorhabditis elegans* Oocyte. Molecular Biology of the Cell, 10(12), 4311–4326. https://doi.org/10.1091/mbc.10.12.4311

[96] Greenspan, P., Mayer, E. P., & Fowler, S. D. (1985). Nile red: a selective fluorescent stain for intracellular lipid droplets. *The Journal of Cell Biology*, 100(3), 965–973.

[97] Gregoire, F. M., Chomiki, N., Kachinskas, D., & Warden, C. H. (1998). Cloning and developmental regulation of a novel member of the insulin-like gene family in *Caenorhabditis elegans*. *Biochemical and Biophysical Research Communications*, 249(2), 385–390. https://doi.org/10.1006/bbrc.1998.9164

[98] Griffiths, P. R., & Griffiths, P. R. (2006). Introduction to Vibrational Spectroscopy. In *Handbook of Vibrational Spectroscopy. American Cancer Society.* https://doi.org/10.1002/0470027320.s0102

[99] Gu, L., Liu, H., Gu, X., Boots, C., Moley, K. H., & Wang, Q. (2015). Metabolic control of oocyte development: linking maternal nutrition and reproductive outcomes. *Cellular and Molecular Life Sciences*: CMLS, 72(2), 251–271. https://doi.org/10.1007/s00018-014-1739-4

[100] Gulia-Nuss, M., Robertson, A. E., Brown, M. R., & Strand, M. R. (2011). Insulin-Like peptides and the target of rapamycin pathway coordinately regulate blood digestion and egg maturation in the mosquito *Aedes aegypti*. *PLOS ONE*, 6(5), e20401. https://doi.org/10.1371/journal.pone.0020401

[101] Gumienny, T. L., Lambie, E., Hartwieg, E., Horvitz, H. R., & Hengartner, M. O. (1999). Genetic control of programmed cell death in the *Caenorhabditis elegans* hermaphrodite germline. Development (Cambridge, England), 126(5), 1011–1022.

[102] Hands, J. R., Clemens, G., Stables, R., Ashton, K., Brodbelt, A., Davis, C., ... Baker, M. J. (2016). Brain tumour differentiation: rapid stratified serum diagnostics via attenuated total reflection Fourier-transform infrared spectroscopy. *Journal of Neuro-Oncology*, 127(3), 463–472. https://doi.org/10.1007/s11060-016-2060-x

[103] Haris, P. I., & Severcan, F. (1999). FTIR spectroscopic characterization of protein structure in aqueous and non-aqueous media. *Journal of Molecular Catalysis B: Enzymatic*, 7(1), 207–221. https://doi.org/10.1016/S1381-1177(99)00030-2

[104] Hassold, T., & Chiu, D. (1985). Maternal age-specific rates of numerical chromosome abnormalities with special reference to trisomy. *Human Genetics*, 70(1), 11–17.

[105] Hellerer, T., Axäng, C., Brackmann, C., Hillertz, P., Pilon, M., & Enejder, A. (2007). Monitoring of lipid storage in *Caenorhabditis elegans* using coherent anti-Stokes Raman scattering (CARS) microscopy. *Proceedings of the National Academy of Sciences of the United States of America*, 104(37), 14658–14663. https://doi.org/10.1073/pnas.0703594104

[106] Hellwig, P., Behr, J., Ostermeier, C., Richter, O. M., Pfitzner, U., Odenwald, A., ... Mäntele, W. (1998). Involvement of glutamic acid 278 in the redox reaction of the

cytochrome c oxidase from Paracoccus denitrificans investigated by FTIR spectroscopy. *Biochemistry*, 37(20), 7390–7399. https://doi.org/10.1021/bi9725576

[107] Hellwig, P., Mogi, T., Tomson, F. L., Gennis, R. B., Iwata, J., Miyoshi, H., & Mäntele, W. (1999). Vibrational modes of Ubiquinone in Cytochrome bo3 from *Escherichia coli* identified by Fourier Transform Infrared Difference Spectroscopy and specific 13C labeling. *Biochemistry*, 38(44),14683-14689. https://doi.org/10.1021/bi991267h

[108] Herman, R. (2005). Introduction to sex determination. WormBook. https://doi.org/10.1895/wormbook.1.71.1

[109] Herndon, L. A., Schmeissner, P. J., Dudaronek, J. M., Brown, P. A., Listner, K. M., Sakano, Y., ... Driscoll, M. (2002). Stochastic and genetic factors influence tissue-specific decline in ageing *C. elegans*. *Nature*, 419(6909), 808–814. https://doi.org/10.1038/nature01135

[110] Hertweck, M., Göbel, C., & Baumeister, R. (2004). *C. elegans* SGK-1 is the critical component in the Akt/PKB kinase complex to control stress response and life span. *Developmental Cell*, 6(4), 577–588.

[111] Hirsh, D., Oppenheim, D., & Klass, M. (1976). Development of the reproductive system of *Caenorhabditis elegans*. *Developmental Biology*, 49(1), 200–219. https://doi.org/10.1016/0012-1606(76)90267-0

[112] Hodgkin, J., Horvitz, H. R., & Brenner, S. (1979). Nondisjunction mutants of the nematode *Caenorhabditis elegans*. *Genetics*, 91(1), 67–94.

[113] Hong, D.-P., Fink, A. L., & Uversky, V. N. (2008). Structural Characteristics of α-Synuclein Oligomers Stabilized by the Flavonoid Baicalein. *Journal of Molecular Biology*, 383(1), 214–223. https://doi.org/10.1016/j.jmb.2008.08.039

[114] Hsin, H., & Kenyon, C. (1999). Signals from the reproductive system regulate the lifespan of *C. elegans*. Nature, 399(6734), 362–366. https://doi.org/10.1038/20694

[115] Hua, Q.-X., Nakagawa, S. H., Wilken, J., Ramos, R. R., Jia, W., Bass, J., & Weiss, M. A. (2003). A divergent INS protein in *Caenorhabditis elegans* structurally resembles human insulin and activates the human insulin receptor. *Genes & Development*, 17(7), 826–831. https://doi.org/10.1101/gad.1058003

[116] Hubbard, E. J. A., & Greenstein, D. (2000). The *Caenorhabditis elegans* gonad: A test tube for cell and developmental biology. *Developmental Dynamics*, 218(1), 2–22. https://doi.org/10.1002/(SICI)1097-0177(200005)218:1<2::AID-DVDY2>3.0.CO;2-W

[117] Huelgas-Morales, G., & Greenstein, D. (2018). Control of oocyte meiotic maturation in *C. elegans*. *Seminars in Cell & Developmental Biology*, 84, 90–9

[118] Hughes, S. E., Evason, K., Xiong, C., & Kornfeld, K. (2007). Genetic and pharmacological factors that influence reproductive aging in nematodes. *PLOS Genetics*, 3(2), e25. https://doi.org/10.1371/journal.pgen.0030025

[119] Huleihel, M., Salman, A., Erukhimovitch, V., Ramesh, J., Hammody, Z., & Mordechai, S. (2002). Novel spectral method for the study of viral carcinogenesis in vitro. *Journal of Biochemical and Biophysical Methods*, 50(2–3), 111–121.

[120] Hutt, K. J., & Albertini, D. F. (2007). An oocentric view of folliculogenesis and embryogenesis. *Reproductive Biomedicine Online*, 14(6), 758–764.

[121] Igosheva, N., Abramov, A. Y., Poston, L., Eckert, J. J., Fleming, T. P., Duchen, M. R., & McConnell, J. (2010). Maternal diet-induced obesity alters mitochondrial activity and redox status in mouse oocytes and zygotes. *PloS One*, 5(4), e10074. https://doi.org/10.1371/journal.pone.0010074

[122] Jackson, M., & Mantsch, H. H. (2006). Infrared Spectroscopy, Ex Vivo Tissue Analysis by. In *Encyclopedia of Analytical Chemistry. American Cancer Society.* https://doi.org/10.1002/9780470027318.a0107

[123] Jackson, M., Sowa, M. G., & Mantsch, H. H. (1997). Infrared spectroscopy: a new frontier in medicine. *Biophysical Chemistry*, 68(1), 109–125. https://doi.org/10.1016/S0301-4622(97)80555-8

[124] Jaramillo-Lambert, A., Ellefson, M., Villeneuve, A. M., & Engebrecht, J. (2007). Differential timing of S phases, X chromosome replication, and meiotic prophase in the *C. elegans* germ line. *Developmental Biology*, 308(1), 206–221. https://doi.org/10.1016/j.ydbio.2007.05.019

[125] Johnson, T. E. (1986). Molecular and genetic analyses of a multivariate system specifying behavior and life span. *Behavior Genetics*, 16(1), 221–235. https://doi.org/10.1007/BF01065487

[126] Kawano, T., Nagatomo, R., Kimura, Y., Gengyo-Ando, K., & Mitani, S. (2006). Disruption of *ins-11*, a *Caenorhabditis elegans* insulin-like gene, and phenotypic analyses of the gene-disrupted animal. *Bioscience, Biotechnology, and Biochemistry*, 70(12), 3084–3087. https://doi.org/10.1271/bbb.60472

[127] Kellner, R. A., & Mermet, J.-M. (2004). *Analytical chemistry: a modern approach to analytical science*. Weinheim: Wiley-Vch.

[128] Kelly, J. W. (1998). The alternative conformations of amyloidogenic proteins and their multi-step assembly pathways. *Current Opinion in Structural Biology*, 8(1), 101–106. https://doi.org/10.1016/S0959-440X(98)80016-X

[129] Kenyon, C., Chang, J., Gensch, E., Rudner, A., & Tabtiang, R. (1993). A *C. elegans* mutant that lives twice as long as wild-type. *Nature*, 366(6454), 461–464. https://doi.org/10.1038/366461a0

[130] Kenyon, C. J. (2010). The genetics of ageing. *Nature*, 464(7288), 504–512. https://doi.org/10.1038/nature08980

[131] Kiernan, J. A. (1981). Histological and histochemical methods: theory and practice.

[132] Kimble, J., & Crittenden, S. L. (2007). Controls of germline stem cells, entry into meiosis, and the sperm/oocyte decision in *Caenorhabditis elegans*. *Annual Review of Cell and Developmental Biology*, 23, 405–433. https://doi.org/10.1146/annurev.cellbio.23.090506.123326

[133] Kimble, J., & Sharrock, W. J. (1983). Tissue-specific synthesis of yolk proteins in *Caenorhabditis elegans*. *Developmental Biology*, 96(1), 189–196.

[134] Kimura, K. D., Tissenbaum, H. A., Liu, Y., & Ruvkun, G. (1997). *daf-2*, an insulin receptor-like gene that regulates longevity and diapause in *Caenorhabditis elegans*. *Science*, 277(5328), 942–946. https://doi.org/10.1126/science.277.5328.942

[135] Klapper, M., Ehmke, M., Palgunow, D., Böhme, M., Matthäus, C., Bergner, G., ... Döring, F. (2011). Fluorescence-based fixative and vital staining of lipid droplets in *Caenorhabditis elegans* reveal fat stores using microscopy and flow cytometry approaches. *Journal of Lipid Research*, 52(6), 1281–1293. https://doi.org/10.1194/jlr.D011940

[136] Klass, M., & Hirsh, D. (1976). Non-ageing developmental variant of *Caenorhabditis elegans*. *Nature*, 260(5551), 523–525. https://doi.org/10.1038/260523a0

[137] Klass, M. R. (1983). A method for the isolation of longevity mutants in the nematode *Caenorhabditis elegans* and initial results. *Mechanisms of Ageing and Development*, 22(3–4), 279–286.

[138] Kong, J., & Yu, S. (2007). Fourier transform infrared spectroscopic analysis of protein secondary structures. *Acta Biochimica et Biophysica Sinica*, 39(8), 549–559. https://doi.org/10.1111/j.1745-7270.2007.00320.x

[139] Krafft, C., Sobottka, S. B., Schackert, G., & Salzer, R. (2004). Analysis of human brain tissue, brain tumors and tumor cells by infrared spectroscopic mapping. *TheAnalyst*, 129(10), 921–925. https://doi.org/10.1039/b408934k

[140] Krilov, D., Balarin, M., Kosović, M., Gamulin, O., & Brnjas-Kraljević, J. (2009). FT-IR spectroscopy of lipoproteins—A comparative study. *Spectrochimica Acta Part A: Molecular and Biomolecular Spectroscopy*, 73(4), 701–706. https://doi.org/10.1016/j.saa.2009.03.015

[141] Krimm, S., & Bandekar, J. (1986). Vibrational spectroscopy and conformation of peptides, polypeptides, and proteins. In C. B. Anfinsen, J. T. Edsall, & F. M. Richards (Eds.), *Advances in Protein Chemistry* (Vol. 38, pp. 181–364). Academic Press. https://doi.org/10.1016/S0065-3233(08)60528-8

[142] Kubagawa, H. M., Watts, J. L., Corrigan, C., Edmonds, J. W., Sztul, E., Browse, J., & Miller, M. A. (2006). Oocyte signals derived from polyunsaturated fatty acids control sperm recruitment in vivo. *Nature Cell Biology*, 8(10), 1143–1148. https://doi.org/10.1038/ncb1476

[143] Kumar, S., Liu, X., Borondics, F., Xiao, Q., Feng, R., Goormaghtigh, E., & Nikolajeff, F. (2017). Insights into Biochemical Alteration in cancer-associated fibroblasts by using novel correlative spectroscopy. *ChemistryOpen*, 6(1), 149–157. https://doi.org/10.1002/open.201600102

[144] Lant, B., & Storey, K. B. (2010). An overview of stress response and hypometabolic strategies in *Caenorhabditis elegans*: conserved and contrasting signals with the mammalian system. *International Journal of Biological Sciences*, 9-50. https://doi.org/10.7150/ijbs.6.9

[145] LaRue, B. L., & Padilla, P. A. (2011). Environmental and genetic preconditioning for long-term anoxia responses requires AMPK in *Caenorhabditis elegans*. *PloS One*, 6(2), e16790. https://doi.org/10.1371/journal.pone.0016790

[146] Lewis, R. N. A. H., & McElhaney, R. N. (2006). Vibrational Spectroscopy of Lipids. In *Handbook of Vibrational Spectroscopy. American Cancer Society.* https://doi.org/10.1002/0470027320.s8203

[147] Lewis, R. N., McElhaney, R. N., Pohle, W., & Mantsch, H. H. (1994). Components of the carbonyl stretching band in the infrared spectra of hydrated 1,2-diacylglycerolipid bilayers: a reevaluation. *Biophysical Journal*, 67(6), 2367–2375. https://doi.org/10.1016/S0006-3495(94)80723-4

[148] L'Hernault, S. W. (2006). *Spermatogenesis*. WormBook. Retrieved from https://www.ncbi.nlm.nih.gov/books/NBK19752/

[149] Li, Q., Hao, C., Kang, X., Zhang, J., Sun, X., Wang, W., & Zeng, H. (2017). Colorectal Cancer and Colitis Diagnosis Using Fourier Transform Infrared Spectroscopy

and an Improved K-Nearest-Neighbour Classifier. *Sensors (Basel, Switzerland)*, 17(12). https://doi.org/10.3390/s17122739

[150] Li, S., Xu, S., Ma, Y., Wu, S., Feng, Y., Cui, Q., ... Zhang, S. O. (2016). A Genetic Screen for Mutants with Supersized Lipid Droplets in *Caenorhabditis elegans*. *G3: Genes, Genomes, Genetics*, 6(8), 2407–2419. https://doi.org/10.1534/g3.116.030866

[151] Libina, N., Berman, J. R., & Kenyon, C. (2003). Tissue-specific activities of *C. elegans* DAF-16 in the regulation of lifespan. *Cell*, 115(4), 489–502. https://doi.org/10.1016/S0092-8674(03)00889-4

[152] Li-Chan, E. C. Y., Griffiths, P. R., & Chalmers, J. M. (2010). Applications of vibrational spectroscopy in food science: Volume I: Instrumentation and fundamental applications. *Applications of Vibrational Spectroscopy in Food Science: Volume I: Instrumentation and Fundamental Applications*. Retrieved from https://www.cabdirect.org/cabdirect/abstract/20113051329

[153] Lin, K., Dorman, J. B., Rodan, A., & Kenyon, C. (1997). *daf-16*: An HNF-3/forkhead family member that can function to double the life-span of *Caenorhabditis elegans*. Science, 278(5341), 1319–1322. https://doi.org/10.1126/science.278.5341.1319

[154] Lipiec, E., Bambery, K. R., Heraud, P., Hirschmugl, C., Lekki, J., Kwiatek, W. M., ... Wood, B. R. (2014). Synchrotron FTIR shows evidence of DNA damage and lipid accumulation in prostate adenocarcinoma PC-3 cells following proton irradiation. *Journal of Molecular Structure*, 1073, 134–141. https://doi.org/10.1016/j.molstruc.2014.04.056

[155] Liu, K.-Z., Jackson, M., Sowa, M. G., Ju, H., Dixon, I. M. C., & Mantsch, H. H. (1996). Modification of the extracellular matrix following myocardial infarction monitored by FTIR spectroscopy. *Biochimica et Biophysica Acta (BBA) - Molecular Basis of Disease*, 1315(2), 73–77. https://doi.org/10.1016/0925-4439(95)00118-2

[156] Luo, S., Kleemann, G. A., Ashraf, J. M., Shaw, W. M., & Murphy, C. T. (2010). TGF-β and insulin signaling regulate reproductive aging via oocyte and germline quality maintenance. *Cell*, 143(2), 299–312. https://doi.org/10.1016/j.cell.2010.09.013

[157] Luo, S., & Murphy, C. T. (2011). *Caenorhabditis elegans* reproductive aging: Regulation and underlying mechanisms. *Genesis (New York, N.Y.: 2000)*, 49(2), 53–65. https://doi.org/10.1002/dvg.20694

[158] Luo, S., Shaw, W. M., Ashraf, J., & Murphy, C. T. (2009). TGF-ß Sma/Mab Signaling Mutations Uncouple Reproductive Aging from Somatic Aging. *PLOS Genetics*, 5(12), e1000789. https://doi.org/10.1371/journal.pgen.1000789

[159] Mantsch, H. H. (1984). Biological applications of Fourier transform infrared spectroscopy: a study of phase transitions in biomembranes. *Journal of Molecular Structure*, 113, 201–212. https://doi.org/10.1016/0022-2860(84)80145-3

[160] Mari, M., Filippidis, G., Palikaras, K., Petanidou, B., Fotakis, C., & Tavernarakis, N. (2015). Imaging ectopic fat deposition in *Caenorhabditis elegans* muscles using nonlinear microscopy. Microscopy Research and Technique, 78(6), 523–528. https://doi.org/10.1002/jemt.22504

[161] Marteil, G., Richard-Parpaillon, L., & Kubiak, J. Z. (2009). Role of oocyte quality in meiotic maturation and embryonic development. *Reproductive Biology*, 9(3), 203–224. https://doi.org/10.1016/S1642-431X(12)60027-8

[162] Matyash, V., Geier, C., Henske, A., Mukherjee, S., Hirsh, D., Thiele, C., ... Kurzchalia, T. V. (2001). Distribution and transport of cholesterol in *Caenorhabditis elegans. Molecular Biology of the Cell*, 12(6), 1725–1736. https://doi.org/10.1091/mbc.12.6.1725

[163] McEvoy, T. G., Coull, G. D., Broadbent, P. J., Hutchinson, J. S., & Speake, B. K. (2000). Fatty acid composition of lipids in immature cattle, pig and sheep oocytes with intact zona pellucida. *Journal of Reproduction and Fertility*, 118(1), 163–170.

[164] McGee, M. D., Day, N., Graham, J., & Melov, S. (2012). cep-1/p53-dependent dysplastic pathology of the aging *C. elegans* gonad. *Aging (Albany NY)*, 4(4), 256–269.

[165] Mendelsohn, R., Anderle, G., Jaworsky, M., Mantsch, H. H., & Dluhy, R. A. (1984). Fourier transform infrared spectroscopic studies of lipid-protein interaction in native and reconstituted sarcoplasmic reticulum. *Biochimica Et Biophysica Acta*, 775(2), 215–224.

[166] Miller, L. M., & Dumas, P. (2006). Chemical imaging of biological tissue with synchrotron infrared light. *Biochimica et Biophysica Acta (BBA) - Biomembranes*, 1758(7), 846–857. https://doi.org/10.1016/j.bbamem.2006.04.010

[167] Miller, L. M., Wang, Q., Telivala, T. P., Smith, R. J., Lanzirotti, A., & Miklossy, J. (2006). Synchrotron-based infrared and X-ray imaging shows focalized accumulation of Cu and Zn co-localized with β-amyloid deposits in Alzheimer's disease. *Journal of Structural Biology*, 155(1), 30–37. https://doi.org/10.1016/j.jsb.2005.09.004

[168] Miller, M. A., Nguyen, V. Q., Lee, M.-H., Kosinski, M., Schedl, T., Caprioli, R. M., & Greenstein, D. (2001). A sperm cytoskeletal protein that signals oocyte meiotic maturation and ovulation. *Science*, 291(5511), 2144–2147. https://doi.org/10.1126/science.1057586

[169] Mordechai, S., Sahu, R. K., Hammody, Z., Mark, S., Kantarovich, K., Guterman, H., ... Argov, S. (2004). Possible common biomarkers from FTIR microspectroscopy of cervical cancer and melanoma. *Journal of Microscopy*, 215(Pt 1), 86–91. https://doi.org/10.1111/j.0022-2720.2004.01356.x

[170] Moss, D. A., Keese, M., & Pepperkok, R. (2005). IR microspectroscopy of live cells. *Vibrational Spectroscopy*, 38(1), 185–191. https://doi.org/10.1016/j.vibspec.2005.04.004

[171] Müller U. (2010). M. Diem: Introduction to modern vibrational spectroscopy, J. Wiley, New York, Chichester, 1993, ISBN 0-471- 59584-5, 285 Seiten, Preis: £ 49.50. *Berichte Der Bunsengesellschaft Für Physikalische Chemie*, 98(10), 1347–1348. https://doi.org/10.1002/bbpc.19940981029

[172] Murphy, C. T., Lee, S.-J., & Kenyon, C. (2007). Tissue entrainment by feedback regulation of insulin gene expression in the endoderm of *Caenorhabditis elegans*. *Proceedings of the National Academy of Sciences*, 104(48), 19046–19050. https://doi.org/10.1073/pnas.0709613104

[173] Murphy, C. T., McCarroll, S. A., Bargmann, C. I., Fraser, A., Kamath, R. S., Ahringer, J., ... Kenyon, C. (2003). Genes that act downstream of DAF-16 to influence the lifespan of *Caenorhabditis elegans*. *Nature*, 424(6946), 277–283. https://doi.org/10.1038/nature01789

[174] Mushayakarara, E., & Levin, I. W. (1982). Determination of acyl chain conformation at the lipid interface region: Raman spectroscopic study of the carbonyl stretching mode region of dipalmitoyl phosphatidylcholine and structurally related molecules. *The Journal of Physical Chemistry*, 86(13), 2324–2327. https://doi.org/10.1021/j100210a016

[175] Naik, P. (2011). *Essentials of Biochemistry (for Medical Students)*. JP Medical Ltd.

[176] Oberg, K., Chrunyk, B. A., Wetzel, R., & Fink, A. L. (1994). Native-like secondary structure in Interleukin-1.beta. Inclusion bodies by Attenuated Total Reflectance FTIR. *Biochemistry*, 33(9), 2628–2634. https://doi.org/10.1021/bi00175a035

[177] Ogg, S., Paradis, S., Gottlieb, S., Patterson, G. I., Lee, L., Tissenbaum, H. A., & Ruvkun, G. (1997). The Fork head transcription factor DAF-16 transduces insulin-like metabolic and longevity signals in C. elegans. *Nature*, 389(6654), 994–999. https://doi.org/10.1038/40194

[178] Ohnishi, S., & Takano, K. (2004). Amyloid fibrils from the viewpoint of protein folding. *Cellular and Molecular Life Sciences*: CMLS, 61(5), 511–524. https://doi.org/10.1007/s00018-003-3264-8

[179] O'Rourke, E. J., Soukas, A. A., Carr, C. E., & Ruvkun, G. (2009). *C. elegans* Major fats are stored in vesicles distinct from lysosome-related organelles. *Cell Metabolism*, 10(5), 430–435. https://doi.org/10.1016/j.cmet.2009.10.002

[180] Paradis, S., Ailion, M., Toker, A., Thomas, J. H., & Ruvkun, G. (1999). A PDK1 homolog is necessary and sufficient to transduce AGE-1 PI3 kinase signals that regulate diapause in *Caenorhabditis elegans*. *Genes & Development*, 13(11), 1438–1452.

[181] Paradis, S., & Ruvkun, G. (1998). *Caenorhabditis elegans* Akt/PKB transduces insulin receptor-like signals from AGE-1 PI3 kinase to the DAF-16 transcription factor. *Genes & Development*, 12(16), 2488–2498. https://doi.org/10.1101/gad.12.16.2488

[182] Paupard, M. C., Miller, A., Grant, B., Hirsh, D., & Hall, D. H. (2001). Immuno-EM localization of GFP-tagged yolk proteins in *C. elegans* Using microwave fixation. *Journal of Histochemistry and Cytochemistry*, 49(8), 949–956.

[183] Pavia, D. L., Lampman, G. M., & Kriz, G. S. (2001). *Introduction to spectroscopy a guide for students of organic chemistry* (3rd ed). Fort Worth Harcourt College Publishers. Retrieved from https://trove.nla.gov.au/work/8687496

[184] Petibois, C., & Déléris, G. (2005). Evidence that erythrocytes are highly susceptible to exercise oxidative stress: FT-IR spectrometric studies at the molecular level. *Cell Biology International*, 29(8), 709–716. https://doi.org/10.1016/j.cellbi.2005.04.007

[185] Petibois, C., & Déléris, G. (2006). Chemical mapping of tumor progression by FT-IR imaging: towards molecular histopathology. *Trends in Biotechnology*, 24(10), 455–462. https://doi.org/10.1016/j.tibtech.2006.08.005

[186] Pierce, S. B., Costa, M., Wisotzkey, R., Devadhar, S., Homburger, S. A., Buchman, A. R., ... Ruvkun, G. (2001). Regulation of DAF-2 receptor signaling by human insulin and ins-1, a member of the unusually large and diverse *C. elegans* insulin gene family. *Genes & Development*, 15(6), 672–686. https://doi.org/10.1101/gad.867301

[187] Popham, J. D., & Webster, J. M. (1979). Aspects of the fine structure of the dauer larva of the nematode *Caenorhabditis elegans*. *Canadian Journal of Zoology*, 57(4), 794–800. https://doi.org/10.1139/z79-098

[188] Porte, D., Baskin, D. G., & Schwartz, M. W. (2005). Insulin signaling in the central cervous system: a critical role in metabolic homeostasis and disease from *C. elegans* to humans. *Diabetes*, 54(5), 1264–1276. https://doi.org/10.2337/diabetes.54.5.1264

[189] Prates, E. G., Nunes, J. T., & Pereira, R. M. (2014). A role of lipid metabolism during cumulus-oocyte complex maturation: impact of lipid modulators to improve embryo production. https://doi.org/10.1155/2014/692067

[190] Raman, S., Lange, O. F., Rossi, P., Tyka, M., Wang, X., Aramini, J., ... Baker, D. (2010). NMR structure determination for larger proteins using Backbone-only data. *Science (New York, N.Y.)*, 327(5968), 1014–1018. https://doi.org/10.1126/science.1183649

[191] Reddy, P., Liu, L., Adhikari, D., Jagarlamudi, K., Rajareddy, S., Shen, Y., ... Liu, K. (2008). Oocyte-specific deletion of Pten causes premature activation

of the primordial follicle pool. *Science (New York, N.Y.)*, 319(5863), 611–613. https://doi.org/10.1126/science.1152257

[192] Reis-Rodrigues, P., Czerwieniec, G., Peters, T. W., Evani, U. S., Alavez, S., Gaman, E. A., ... Hughes, R. E. (2012). Proteomic analysis of age-dependent changes in protein solubility identifies genes that modulate lifespan. *Aging Cell*, 11(1), 120–127. https://doi.org/10.1111/j.1474-9726.2011.00765.x

[193] Richard, D. S., Rybczynski, R., Wilson, T. G., Wang, Y., Wayne, M. L., Zhou, Y., ... Harshman, L. G. (2005). Insulin signaling is necessary for vitellogenesis in *Drosophila melanogaster* independent of the roles of juvenile hormone and ecdysteroids: female sterility of the *chico1* insulin signaling mutation is autonomous to the ovary. *Journal of Insect Physiology*, 51(4), 455–464. https://doi.org/10.1016/j.jinsphys.2004.12.013

[194] Riddle, D. L., Swanson, M. M., & Albert, P. S. (1981). Interacting genes in nematode dauer larva formation. *Nature*, 290(5808), 668–671.

[195] Rikke, B. A., Murakami, S., & Johnson, T. E. (2000). Paralogy and orthology of tyrosine kinases that can extend the life span of *Caenorhabditis elegans. Molecular Biology and Evolution*, 17(5), 671–683. https://doi.org/10.1093/oxfordjournals.molbev.a026346

[196] Rinnan, Å., Berg, F. van den, & Engelsen, S. B. (2009). Review of the most common pre-processing techniques for near-infrared spectra. *TrAC Trends in Analytical Chemistry*, 28(10), 1201–1222. https://doi.org/10.1016/j.trac.2009.07.007

[197] Rompay, L. V., Borghgraef, C., Beets, I., Caers, J., & Temmerman, L. (2015). New genetic regulators question relevance of abundant yolk protein production in *C. elegans. Scientific Reports*, 5. https://doi.org/10.1038/srep16381

[198] Seah, N. E., de Magalhaes Filho, C. D., Petrashen, A. P., Henderson, H. R., Laguer, J., Gonzalez, J., ... Lapierre, L. R. (2015). Autophagy-mediated longevity is modulated by lipoprotein biogenesis. *Autophagy*, 12(2), 261–272. https://doi.org/10.1080/15548627.2015.1127464

[199] Seehuus, S.-C., Norberg, K., Gimsa, U., Krekling, T., & Amdam, G. V. (2006). Reproductive protein protects functionally sterile honey bee workers from oxidative stress. *Proceedings of the National Academy of Sciences of the United States of America*, 103(4), 962–967. https://doi.org/10.1073/pnas.0502681103

[200] Segrest, J. P., Jones, M. K., Mishra, V. K., Anantharamaiah, G. M., & Garber, D. W. (1994). apoB-100 has a pentapartite structure composed of three amphipathic alpha-helical domains alternating with two amphipathic beta-strand domains. Detection by the computer program LOCATE. *Arteriosclerosis, Thrombosis, and Vascular Biology*, 14(10), 1674–1685. https://doi.org/10.1161/01.ATV.14.10.1674

[201] Sharrock, W. J., Sutherlin, M. E., Leske, K., Cheng, T. K., & Kim, T. Y. (1990). Two distinct yolk lipoprotein complexes from *Caenorhabditis elegans. Journal of Biological Chemistry*, 265(24), 14422–14431.

[202] Shaw, R. A., Low-Ying, S., Leroux, M., & Mantsch, H. H. (2000). Toward reagent-free clinical analysis: quantitation of urine urea, creatinine, and total protein from the mid-infrared spectra of dried urine films. *Clinical Chemistry*, 46(9), 1493–1495.

[203] Siqueira, L. F. S., & Lima, K. M. G. (2016). A decade (2004 – 2014) of FTIR prostate cancer spectroscopy studies: An overview of recent advancements. *TrAC Trends in Analytical Chemistry*, 82, 208–221. https://doi.org/10.1016/j.trac.2016.05.028

[204] Smolenaars, M. M. W., Madsen, O., Rodenburg, K. W., & Horst, D. J. V. der. (2007). Molecular diversity and evolution of the large lipid transfer protein superfamily. *Journal of Lipid Research*, 48(3), 489–502. https://doi.org/10.1194/jlr.R600028-JLR200

[205] Sönnichsen, B., Koski, L. B., Walsh, A., Marschall, P., Neumann, B., Brehm, M., ... Echeverri, C. J. (2005). Full-genome RNAi profiling of early embryogenesis in *Caenorhabditis elegans*. Nature, 434(7032), 462–469. https://doi.org/10.1038/nature03353

[206] Spieth, J., & Blumenthal, T. (1985). The *Caenorhabditis elegans* vitellogenin gene family includes a gene encoding a distantly related protein. *Molecular and Cellular Biology*, 5(10), 2495–2501.

[207] Spira, A., & Lazar, P. (1979). Spontaneous abortions in sibship of children with congenital malformation or malignant disease. *European Journal of Obstetrics & Gynecology and Reproductive Biology*, 9(2), 89–95. https://doi.org/10.1016/0028-2243(79)90004-2

[208] Spiro, R. G. (2002). Protein glycosylation: nature, distribution, enzymatic formation, and disease implications of glycopeptide bonds. *Glycobiology*, 12(4), 43R–56R.

[209] Stuart Barbara H. (2006). Infrared Spectroscopy of Biological Applications: An Overview. *Encyclopedia of Analytical Chemistry*. https://doi.org/10.1002/9780470027318.a0208.pub2

[210] Subramanian, A., Harper, W. j., & Rodriguez-Saona, L. e. (2009). Rapid prediction of composition and flavor quality of cheddar cheese using ATR–FTIR spectroscopy. *Journal of Food Science*, 74(3), C292–C297. https://doi.org/10.1111/j.1750-3841.2009.01111.x

[211] Sunde, M., & Blake, C. (1997). The structure of amyloid fibrils by Electron microscopy and X-Ray diffraction. In F. M. Richards, D. S. Eisenberg, & P. S. Kim (Eds.), *Advances in Protein Chemistry (Vol. 50, pp. 123–159). Academic Press*. https://doi.org/10.1016/S0065-3233(08)60320-4

[212] Susi, H. (1972). Infrared spectroscopy-conformation. *In Methods in Enzymology (Vol. 26, pp. 455–472). Academic Press*. https://doi.org/10.1016/S0076-6879(72)26024-4

[213] Szczerbowska-Boruchowska, M., Dumas, P., Kastyak, M. Z., Chwiej, J., Lankosz, M., Adamek, D., & Krygowska-Wajs, A. (2007). Biomolecular investigation of human substantia nigra in Parkinson's disease by synchrotron radiation Fourier transform infrared microspectroscopy. *Archives of Biochemistry and Biophysics*, 459(2), 241–248. https://doi.org/10.1016/j.abb.2006.12.027

[214] Tanaka, T., Ikita, K., Ashida, T., Motoyama, Y., Yamaguchi, Y., & Satouchi, K. (1996). Effects of growth temperature on the fatty acid composition of the free-living nematode *Caenorhabditis elegans*. *Lipids*, 31(11), 1173–1178. https://doi.org/10.1007/BF02524292

[215] Tarín, J. J. (1995). Aetiology of age-associated aneuploidy: a mechanism based on the "free radical theory of ageing." *Human Reproduction (Oxford, England)*, 10(6), 1563–1565.

[216] Tarín, J. J. (1996). Potential effects of age-associated oxidative stress on mammalian oocytes/embryos. *Molecular Human Reproduction*, 2(10), 717–724.

[217] Tatar, M., Kopelman, A., Epstein, D., Tu, M.-P., Yin, C.-M., Garofalo, R. S. (2001). A Mutant *Drosophila* insulin receptor homolog that extends life-span and impairs neuroendocrine function. *Science*, 292(5514), 107–110. https://doi.org/10.1126/science.1057987

[218] Taylor, R. C., & Dillin, A. (2011). Aging as an event of proteostasis collapse. *Cold Spring Harbor Perspectives in Biology*, 3(5), a004440. https://doi.org/10.1101/cshperspect.a004440

[219] Templeman, N. M., Luo, S., Kaletsky, R., Shi, C., Ashraf, J., Keyes, W., & Murphy, C. T. (2018). Insulin signaling regulates oocyte quality maintenance with age via Cathepsin B Activity. *Current Biology*: CB, 28(5), 753–760.e4. https://doi.org/10.1016/j.cub.2018.01.052

[220] Tipler, M. (n.d.). *Physics For Scientists And Engineers Extended Edition 5 Tipler, Mosca*. http://archive.org/details/PhysicsForScientistsAndEngineersExtendedEdition5

[221] Tissenbaum, H. A. (2015). Using *C. elegans* for aging research. *Invertebrate Reproduction & Development*, 59(sup1), 59–63. https://doi.org/10.1080/07924259.2014.940470

[222] Tobin, M. J., Puskar, L., Barber, R. L., Harvey, E. C., Heraud, P., Wood, B. R., ... Munro, K. L. (2010). FTIR spectroscopy of single live cells in aqueous media by synchrotron IR microscopy using microfabricated sample holders. *Vibrational Spectroscopy*, 53(1), 34–38. https://doi.org/10.1016/j.vibspec.2010.02.005

[223] Uversky, V. N., & Fink, A. L. (2004). Conformational constraints for amyloid fibrillation: the importance of being unfolded. *Biochimica et Biophysica Acta (BBA) - Proteins and Proteomics*, 1698(2), 131–153. https://doi.org/10.1016/j.bbapap.2003.12.008

[224] van Balen, F., Verdurmen, J. E., & Ketting, E. (1995). Age, desire for children and probability of pregnancy in the Netherlands. *Nederlands Tijdschrift Voor Geneeskunde*, 139(15), 792–796.

[225] Vance, D. E., & Vance, J. E. (2002). *Biochemistry of lipids, lipoproteins, and membranes* (4th ed). Amsterdam; London: Elsevier. Retrieved from https://trove.nla.gov.au/version/20642295

[226] Velde, T., R, E., & Pearson, P. L. (2002). The variability of female reproductive ageing. *Human Reproduction Update*, 8(2), 141–154. https://doi.org/10.1093/humupd/8.2.141

[227] Vrablik, T. L., Petyuk, V. A., Larson, E. M., Smith, R. D., & Watts, J. L. (2015). Lipidomic and proteomic analysis of *Caenorhabditis elegans* lipid droplets and identification of ACS-4 as a lipid droplet-associated protein. *Biochimica Et Biophysica Acta*, 1851(10), 1337–1345. https://doi.org/10.1016/j.bbalip.2015.06.004

[228] Vrablik, T. L., & Watts, J. L. (2013). Polyunsaturated fatty acid derived signaling in reproduction and development: Insights from *Caenorhabditis elegans* and *Drosophila melanogaster*. *Molecular Reproduction and Development*, 80(4), 244–259. https://doi.org/10.1002/mrd.22167

[229] Wang, H. P., Wang, H. C., & Huang, Y. J. (1997). Microscopic FTIR studies of lung cancer cells in pleural fluid. *The Science of the Total Environment*, 204(3), 283–287.

[230] Ward, S., & Carrel, J. S. (1979). Fertilization and sperm competition in the nematode *Caenorhabditis elegans*. *Developmental Biology*, 73(2), 304–321. https://doi.org/10.1016/0012-1606(79)90069-1

[231] Watts, J. L., & Browse, J. (2002). Genetic dissection of polyunsaturated fatty acid synthesis in *Caenorhabditis elegans*. *Proceedings of the National Academy of Science*s, 99(9), 5854–5859. https://doi.org/10.1073/pnas.092064799

[232] Wolkers, W. F., Alberda, M., Koornneef, M., Léon-Kloosterziel, K. M., & Hoekstra, F. A. (1998). Properties of proteins and the glassy matrix in maturation-

defective mutant seeds of Arabidopsis thaliana. *The Plant Journal*, 16(2), 133–143. https://doi.org/10.1046/j.1365-313x.1998.00277.x

[233] Wolkow, C. A., Kimura, K. D., Lee, M. S., & Ruvkun, G. (2000). Regulation of *C. elegans* life-span by insulin-like signaling in the nervous system. *Science* (New York, N.Y.), 290(5489), 147–150.

[234] Wood, B. R., Chernenko, T., Matthäus, C., Diem, M., Chong, C., Bernhard, U., ... Lacham-Kaplan, O. (2008). Shedding new light on the molecular architecture of oocytes using a combination of synchrotron Fourier Transform-Infrared and Raman Spectroscopic mapping. *Analytical Chemistry*, 80(23), 9065–9072. https://doi.org/10.1021/ac8015483

[235] Wood, B. R., Quinn, M. A., Burden, F. R., & McNaughton, D. (1996). An investigation into FTIR spectroscopy as a biodiagnostic tool for cervical cancer. *Biospectroscopy*, 2(3), 143–153. https://doi.org/10.1002/(SICI)1520-6343(1996)2:3<143::AID-BSPY1>3.0.CO;2-9

[236] Wood, B. R., Quinn, M. A., Tait, B., Ashdown, M., Hislop, T., Romeo, M., & McNaughton, D. (1998). FTIR microspectroscopic study of cell types and potential confounding variables in screening for cervical malignancies. *Biospectroscopy*, 4(2), 75–91. https://doi.org/10.1002/(SICI)1520-6343(1998)4:2<75::AID-BSPY1>3.0.CO;2-R

[237] Wu, J.-G., Xu, Y.-Z., Sun, C.-W., Soloway, R. D., Xu, D.-F., Wu, Q.-G., ... Xu, G.-X. (2001). Distinguishing malignant from normal oral tissues using FTIR fiber-optic techniques. *Biopolymers*, 62(4), 185–192. https://doi.org/10.1002/bip.1013

[238] Wu, L. L., Russell, D. L., Norman, R. J., & Robker, R. L. (2012). Endoplasmic reticulum (ER) stress in cumulus-oocyte complexes impairs pentraxin-3 secretion, mitochondrial membrane potential ($\Delta\Psi$m) and Embryo Development. *Molecular Endocrinology*, 26(4), 562–573. https://doi.org/10.1210/me.2011-1362

[239] Wuertz, S., Nitsche, A., Jastroch, M., Gessner, J., Klingenspor, M., Kirschbaum, F., & Kloas, W. (2007). The role of the IGF-I system for vitellogenesis in maturing female

sterlet, Acipenser ruthenus Linnaeus, 1758. *General and Comparative Endocrinology*, 150(1), 140–150. https://doi.org/10.1016/j.ygcen.2006.07.005

[240] Yamawaki, T. M., Berman, J. R., Suchanek-Kavipurapu, M., McCormick, M., Gaglia, M. M., Lee, S.-J., & Kenyon, C. (2010). The somatic reproductive tissues of *C. elegans* promote longevity through steroid hormone signaling. *PLoS Biology*, 8(8). https://doi.org/10.1371/journal.pbio.1000468

[241] Yang, X., Dunning, K. R., Wu, L. L.-Y., Hickey, T. E., Norman, R. J., Russell, D. L., ... Robker, R. L. (2010). Identification of perilipin-2 as a lipid droplet protein regulated in oocytes during maturation. *Reproduction, Fertility, and Development*, 22(8), 1262–1271. https://doi.org/10.1071/RD10091

[242] Yen, K., Le, T. T., Bansal, A., Narasimhan, S. D., Cheng, J.-X., & Tissenbaum, H. A. (2010). A comparative study of fat storage quantitation in nematode *Caenorhabditis elegans* using label and label-free methods. *PLoS ONE*, 5(9). https://doi.org/10.1371/journal.pone.0012810

[243] Yoshida, S., Miyazaki, M., Sakai, K., Takeshita, M., Yuasa, S., Sato, A., ... Okuyama, H. (1997). Fourier transform infrared spectroscopic analysis of rat brain microsomal membranes modified by dietary fatty acids: Possible correlation with altered learning behavior. *Biospectroscopy*, 3(4), 281–290. https://doi.org/10.1002/(SICI)1520-6343(1997)3:4<281::AID-BSPY3>3.0.CO;2-7

[244] Zhang, P., Judy, M., Lee, S.-J., & Kenyon, C. (2013). Direct and indirect gene regulation by a life-extending FOXO protein in *C. elegans*: roles for GATA factors and lipid gene regulators. *Cell Metabolism*, 17(1), 85–100. https://doi.org/10.1016/j.cmet.2012.12.013

[245] Zhang, S. O., Trimble, R., Guo, F., & Mak, H. Y. (2010). Lipid droplets as ubiquitous fat storage organelles in *C. elegans*. *BMC Cell Biology*, 11(1), 96. https://doi.org/10.1186/1471-2121-11-96

From the web:

- Life cycle of a *C. elegans*: http://genomebiology.com/2010/11/2/105.
- The four levels of protein structure: https://en.wikibooks.org/wiki/Principles-of-Biochemistry/Amino-acids-and-proteins.
- YP170::GFP endocytosis by oocytes: https://dev.wormbook.org/chapters/www-intracellulartrafficking/Itrafig3.jpg.